Theses and Dissertations   Graduate School

2020

Reducing Material Attractiveness Utilizing Pu-238 and U-232

Cody Lloyd
Virginia Commonwealth University

REDUCING MATERIAL ATTRACTIVENESS UTILIZING ^{238}Pu AND ^{232}U

A Dissertation Presented in Partial Fulfillment of the Requirements for the Degree of

Doctor of Philosophy with a Major in Mechanical and Nuclear Engineering in the Graduate

School

Virginia Commonwealth University

By

Cody Lloyd

Dissertation Committee Chair: Braden Goddard

NOVEMBER 2020

ACKNOWLEDGEMENTS

TABLE OF CONTENTS

LIST OF TABLES

LIST OF FIGURES

LIST OF ABBREVIATIONS

AWCC   Active Well Coincidence Counter
BPE   Borate Polyethylene
CDC   Center for Disease Control
CNS   Central Nervous System
DPRK   Democratic People's Republic of Korea
FOM   Figure of Merit
GI   Gastrointestinal
HDPE   High Density Polyethylene
HNED   Hypothetical Nuclear Explosive Device
HEU   Highly Enriched Uranium
IAEA   International Atomic Energy Agency
INFCIRC   Information Circular
KAERI   Korean Atomic Energy Research Institute
LB   Lightbridge
LEU   Low Enriched Uranium
LWR   Light Water Reactor
MCNP   Monte Carlo N-Particle
MOX   Mixed Oxide
NNWS   Non-nuclear Weapons States
NPT   Treaty on the Non-Proliferation of Nuclear Weapons
NWS   Nuclear Weapons States
PRAETOR   Proliferation Resistance Analysis and Evaluation Tool for Observed Risk

GLOSSARY

Terms	Definitions
Criticality	The measure of the change in neutrons from one generation to the next.
Delayed neutron	A neutron that is released sometime after the fission event occurs.
Firewall	An intrinsic trait of a material that represents a barrier to proliferation.
Fission	An event in which a nucleus separates into multiple parts, releasing energy in the process.
Half-life	The amount of time in which half of the radionuclides in a sample have decayed.
HEU	Enriched uranium having a concentration of ^{235}U greater than 20%.
Induced fission	Fission event that is caused by an incident neutron.
k_{eff}	The ratio of the number of neutrons in one generation to the number of neutrons in the next.
LEU	Enriched uranium having a higher concentration of ^{235}U than natural, but less than 20% ^{235}U.
Material attractiveness	The attractiveness a particular material has for weapon's purposes.
Nuclear nonproliferation	The decrease in or spread of nuclear weapons technology or materials.
Nuclear proliferation	The increase in or spread of nuclear weapons technology or materials.
Predetonation	The detonation of a nuclear weapon before it has reached its optimal compression due to the amount of spontaneous fission neutrons produced by the material.
Proliferation resistance	The resistance an object (ex.: material, reactor design, fuel cycle, etc.) has to be utilized in a nuclear weapons program.
Prompt neutron	A neutron that is released at the moment of the fission event.
Self-explosion	The detonation of high explosives as a result of temperature increase above its "self-explosion temperature."
Spontaneous fission	Fission even that occurs suddenly due to the instability of the nucleus.
Tensile Strength	The amount of tensile stress a material can undergo before plastic deformation occurs.

Weaponization	The process by which a material is converted to a usable form for a nuclear weapon.
Yield	The expected amount of energy released from the detonation of a nuclear weapon.

Abstract

Decreasing the material attractiveness of uranium and plutonium materials is crucial to nuclear nonproliferation. The International Atomic Energy Agency (IAEA) implements safeguards across the world on a limited budget. Not only does decreasing material attractiveness reduce the possibility of proliferation, but also may lighten the financial burden on the IAEA if safeguards can be reduced. Two particular isotopes that have negative material attractiveness traits are ^{238}Pu and ^{232}U. Without isotopic separation technology, these isotopes cannot be removed from plutonium and uranium materials respectively. Both ^{238}Pu and ^{232}U produce large quantities of heat by alpha decay. High decay heat is considered one of the primary impacts on material attractiveness. This decay heat causes major issues during weaponization and can render the high explosives in a weapon useless and cause failure in the materials if high enough temperatures are reached. In addition to high alpha decay heat, ^{238}Pu has a high spontaneous fission neutron generation rate, which can lead to a reduction in the yield of a nuclear weapon. ^{232}U's daughter products give a relatively high dose rate over time. Both the dose rate and heat generation increase over time, reaching a maximum after 10 years. ^{232}U will also create difficulty during the enrichment process. Considering ^{232}U is lighter than ^{235}U, its concentration will increase at a higher rate during enrichment. The decay of ^{232}U in gaseous UF_6 can destroy UF_6 molecules creating a variety of lighter molecules that must be separated from the enrichment stream. This study will evaluate the effects of ^{238}Pu and ^{232}U on material attractiveness. The material attractiveness of these materials will be quantified using multiple methods in an attempt to make a broad statement about their attractiveness. In order to better understand the feasibility of the introduction of ^{232}U into a civilian nuclear fuel cycle, the effects on safety, security, and safeguards will also be explored.

1. INTRODUCTION

1.1. Motivation

Limiting the proliferation of nuclear material is crucial for the international use of nuclear energy for peaceful purposes. The utilization of nuclear energy is spreading internationally with several countries constructing or considering constructing their first commercial nuclear reactor, including Bangladesh, Belarus, Saudi Arabia, Turkey, and the United Arab Emirates (1). With the continuous expansion of nuclear energy internationally, the possible use of nuclear materials for weapons purposes remains a major concern. Although infrequent, this proliferation of nuclear materials has occurred historically such as in the case of Iran's enrichment program (2) or the Democratic People's Republic of Korea (DPRK) nuclear weapons program (3).

Increasing the difficulty of proliferation is a complex issue. Proliferation resistance is a commonly used term to describe the difficulty in proliferating nuclear technology or material. The term is broad and can be applied to anything from a specific nuclear material to an entire fuel cycle. Although useful in a qualitative sense, the term lacks the ability to be applied quantitatively. In order to limit ambiguity and foster a more quantitative analysis, a material's specific firewalls against proliferation are considered. These firewalls are intrinsic features of a material, such as decay heat, that make the material less attractive for weapons purposes. This falls within the scope of proliferation resistance and is narrow enough to analyze a particular nuclear material.

This increase in use of nuclear energy for peaceful purposes requires an increase in the international safeguards that ensure the material is not used for weapons purposes.

Implemented by the International Atomic Energy Agency (IAEA), international safeguards must cover nuclear fuel cycles across the world with limited resources. The use of these limited resources must be as efficient as possible, as to effectively safeguard nuclear material and deter proliferation. Decreasing a material's attractiveness may lead to a reduction in safeguards, allowing for resources to be reallocated to more essential tasks. Not only is this financially beneficial for the IAEA, but also decreasing material attractiveness creates significant obstacles with which a proliferant state must deal with in order to weaponize the material. These obstacles can limit a state's ability to proliferate both financially and technologically. Even in a breakout scenario in which a state has broken its safeguards agreement and decided to proliferate, decreased material attractiveness will slow the state's proliferation.

1.2. Objectives

The primary objective of this study is to understand the impact of elevated ^{238}Pu concentration in plutonium materials and ^{232}U concentration in uranium materials on material attractiveness. The impacts on critical mass, decay heat, spontaneous fission neutron generation rate, and dose rate from the addition of each isotope will be quantified and discussed within the scope of weapons usability. Considering ^{232}U does not occur naturally, additional impacts beyond those directly contributing to material attractiveness must be considered. In order for ^{232}U to be a realistic option for decreasing material attractiveness of uranium materials, the following issues must be explored. The effects on the gaseous centrifuge enrichment process from the addition of ^{232}U is evaluated. Also, possible issues with safeguards measurements of uranium materials containing ^{232}U is considered. From a safety perspective, the dose rate from these proposed uranium

materials is calculated and compared to safety standards. The detectability of these uranium materials is also simulated. Since ^{238}Pu is found in plutonium from used nuclear fuel, these additional issues need not be considered.

1.3. Background

1.3.1. Introduction to Nuclear Nonproliferation

1.3.1.1. Basics of Nuclear Proliferation

In order to understand nuclear nonproliferation, one must also understand nuclear proliferation. Nuclear proliferation is the increase in or spread of nuclear weapons technology or materials. The possession of nuclear weapons represents a certain amount of power and prestige for a state entity. Nuclear weapons are one of the most powerful weapons ever conceived and are capable of producing destruction on large scales. In 1945, the United States detonated the only two nuclear weapons ever used in warfare on the Japanese cities of Hiroshima and Nagasaki. The weapons had a yield equivalent to 21 and 15 kilotons of TNT (4). Although the exact estimates for those killed and wounded vary from source to source, an estimated 66,000 died in Hiroshima and 39,000 in Nagasaki. An estimated 69,000 were injured in Hiroshima and 25,000 in Nagasaki. These numbers are staggering considering the death toll for each was approximately one fourth of the cities' total populations, 255,000 and 195,000 (5).

The science behind nuclear energy is as follows. Although both the peaceful and weapons use of nuclear energy utilize the fission of fissile isotopes, the manner in which fission is utilized is slightly different. A fission event can be induced or spontaneous. An induced fission event occurs when the nucleus absorbs a neutron and splits. A spontaneous fission event occurs spontaneously without the need for neutron absorption. Induced

fission is far more probable in ^{235}U. However, ^{239}Pu has a notable probability of fissioning both spontaneously and induced. When a fission event occurs, fission fragments, neutrons, and gamma rays are released. Some of the neutrons released are released promptly at the moment of fission. These neutrons are called prompt neutrons. However, some neutrons are released slightly after. These neutrons are called delayed neutrons. The neutrons from one fission event may induce another fission which will release neutrons. The repetition of this process makes up a fission chain reaction. In a nuclear reactor, chain reactions are intended to be sustained by delayed neutrons. This allows for control by way of insertion or removal of control rods. A chain reaction made up of prompt neutrons within a reactor would be uncontrollable by human intervention. In a nuclear weapon, the chain reaction is intended to comprise solely of prompt neutrons. This allows for a rapid increase in power as the weapon is detonated. k_{eff} is important in understanding how the chain reactions will progress. k_{eff} is the ratio of the number of neutrons in a generation to the number of neutrons in the previous generation. If k_{eff} is less than one, the fissile material is subcritical and the chain reaction will eventually end as the number of neutrons are decreasing from one generation to the next. If k_{eff} is equal to one, the fissile material is critical and the chain reaction will continue with each generation having the same number of neutrons. If k_{eff} is greater than one, the chain reaction will continue with each generation of neutrons increasing in number (6). Fission type nuclear weapons are designed such that they're initially subcritical and will become super critical as the fissile material is compressed.

1.3.1.2. Nuclear Nonproliferation Policy

Nuclear nonproliferation is the decrease in or spread of nuclear weapons technology or materials. This field encompasses efforts around the world that seek to

prevent the spread of nuclear weapons. The Treaty on the Non-Proliferation of Nuclear

Weapons (NPT) was formed as a global effort to prevent the spread of nuclear weapons.

The treaty was opened for signatures in 1968 and entered into force in 1970. This treaty

creates two classifications of states: Nuclear Weapons States (NWS) and Non-nuclear

Weapons States (NNWS). The five NWS; the United States of America, the United Kingdom,

France, Russia, and China, were classified as such due to the fact that each state possessed

nuclear weapons at the time of the NPT's creation. The remaining signatories of the NPT

and presumably all future signatories are classified as NNWS. These NNWS agree to not

pursue nuclear weapons, including both receiving nuclear weapons from other states and

manufacturing them, in exchange for the ability to utilize nuclear energy for peaceful

purposes. In order to ensure each NNWS adheres to this agreement, the NPT requires

NNWS to agree to a nuclear safeguards agreement that is negotiated and monitored by the

IAEA (7).

Each safeguards agreement will be negotiated directly between the IAEA and the

member state in accordance with the Information Circular 153 (INFCIRC/153). This

document discusses the objectives of the safeguards agreement and lays the framework for

the agreement (8). Including the 5 NWS, 191 states have signed the NPT (9). Thus, the IAEA

is responsible for imposing safeguards on over 100 states across the world. This immense

responsibility, coupled with the limited budget of the IAEA, makes implementing

safeguards in the most efficient manner possible crucial. According to the IAEA Department

of Safeguards Long-Term Strategic Plan for 2012-2023, the IAEA desires to implement

"smarter" safeguards to reduce the overall burden of safeguards to where they're the most

needed (10). This is the major motivation for developing nuclear materials resistant to proliferation.

1.3.1.3. Direct Use Nuclear Materials

Proliferation resistance is especially of concern when considering direct use nuclear material. These materials contain fissile isotopes and have significant attractiveness for weapons purposes (11). The two most common of these materials are plutonium and highly enriched uranium (HEU). ^{233}U is also classified as a direct use nuclear material but is far less common in most nuclear fuel cycles across the world. However, with the significant research in thorium fuel cycles, ^{233}U may become more pertinent in the proliferation resistant conversation.

Plutonium is created through the burnup of uranium and is thus present in all used nuclear fuel. Although ^{239}Pu is the most attractive isotope of plutonium for weapons purposes, all plutonium is considered weapons usable. The only international safeguards exemption by the IAEA on plutonium is plutonium containing over 80% ^{238}Pu (11). This is primarily due to the high alpha decay heat of ^{238}Pu. This limit is well above the typical concentration of ^{238}Pu found in used nuclear fuel and doesn't exclude any plutonium found in used nuclear fuel.

HEU is uranium with a ^{235}U concentration ≥20% (11). HEU is obtained through the enrichment of natural uranium (0.711 wt. % ^{235}U). This material is not as fissile as plutonium, but is still a significant threat for weaponization. Although HEU is considered direct use nuclear material, an additional classification for uranium, weapons grade, is especially important when considering weaponization. Weapons grade uranium is uranium having approximately >90 wt. % ^{235}U.

1.3.2. Contributions to Material Attractiveness

Material attractiveness is constantly debated within the nuclear nonproliferation community. In simplistic terms, a material's attractiveness is a measure of how attractive that material is for weapons purposes. Several physical characteristics of a nuclear material contribute to the material's attractiveness.

This debate is often centered on plutonium. Although the proliferation of uranium is possible, a plutonium weapon requires less mass and plutonium can be found in all used nuclear fuel. The three main properties of plutonium that is of proliferation concern are the bare critical mass, spontaneous fission neutron rate, and heat generation (12). The bare critical mass is important as it is related to the amount of mass required to weaponized the material. The spontaneous fission neutron rate is important as it impacts the functionality of the weapon. As the implosion occurs, a higher neutron emission rate in the fissile material can stop the implosion before the optimal implosion has occurred thus reducing the yield of the weapon (13). The heat generation within a weapon can cause problems within the high explosives and other materials. An additional property that should be considered is the radiation dose from a material.

The radiation dose from the materials can have a negative impact on the high explosives within a weapon as well as anyone responsible for handling the material. In order to understand the effects of radiation dose, a brief summary of radiation dose units is needed. There are two main types of radiation doses typically discussed; absorbed dose and dose equivalent. Absorbed dose quantifies the amount of radiation absorbed within the matter. The units used for this type of dose are gray (Gy) and rad. One Gy is equivalent to 100 rad. In terms of energy deposition, one gray is equivalent to one J/kg. Dose equivalent

incorporates the biological effects of each radiation type through weighting factors. The units used for this type of dose are Sievery (Sy) and rem. One Sv is equivalent to 100 rem (6). For the sake of simplicity, this study will focus on absorbed dose.

The explosives within a nuclear weapon will begin to degrade once a high enough dose has been given. This degradation will reduce the effectiveness of the high explosives by reducing the detonation velocity (14). This reduction in the explosive potential of the high explosives will lead to a reduced yield in the weapon.

The effect of the dose rate on humans can be best understood in terms of whole body dose. The whole body dose is the dose to the entire body without considering a specific section of the body. When the dose rate is relatively high, lethal acute syndromes can be considered. Three of these syndromes to be used in this study are central nervous system (CNS) syndrome, gastrointestinal (GI) syndrome, and Haemopoietic syndrome. CNS syndrome progresses from drowsiness to lethargy. After several hours, seizures begin and eventually loss of control of bodily movements occur. Death occurs within 2-3 days. GI syndrome consists of severe vomiting and diarrhea. This leads to serious dehydration. GI syndrome typically leads to death within 2-3 weeks. Haemopoietic syndrome is the slowest progress of the three. Initially slight nausea, vomiting, and diarrhea may occur within the first 6-12 hours after exposure. However, these symptoms may subside for up to three weeks. The patient may feel healthy until headache, fever, and fatigue begin. This worsens until the condition proves lethal after 1-2 months (15). Table 1.1 shows the minimum dose thresholds for the three acute radiation syndromes.

*Table 1.1: Minimum Dose for Acute Radiation Syndromes (15) * (16)*

Syndrome	Minimum Dose Required [Gy]
CNS	50
GI	5
Haemopoietic	0.7*

A more general method to determine the lethality of a dose is to consider the mean lethal dose. The lethal dose required for death in 50% of exposed individuals is represented as the LD_{50}. Various time intervals can be related to this dose such as 15, 30, and 60 days. This will utilize the 60-day time interval. This is represented as the $LD_{50/60}$. According to the Center for Disease Control, the $LD_{50/60}$ is approximately 2.5 to 5 Gy (16).

In addition to the $LD_{50/60}$ other dose thresholds can be considered. The radiation safety standards in the United States are set by the United States Nuclear Regulatory Commission (NRC). For simplicity, the doses considered in this study are total effective dose equivalent. The NRC's annual limit for the occupational dose of an adult is 5 rem (17). An additional safety limit is the "self-protecting" dose rate of 500 rad/h at 1 meter (18). This dose rate limit represents a threshold above which the material is considered practically unusable for any purpose. This limit is often referred to in terms of material attractiveness for weapon's purposes, rather than within the scope of the material's use in a civilian nuclear fuel cycle.

1.4. ^{238}Pu Unattractive Features

Elevating the concentration of ^{238}Pu will decrease the material attractiveness of the plutonium material. This strategy takes advantage of the high alpha decay heat if ^{238}Pu. Elevated decay heat introduces significant difficulties in handling and weaponizing the

material (19). Increased temperature within a hypothetical nuclear explosive device (HNED) can cause the high explosives to self-explode once a particular temperature is reached (20). As shown in Table 1.2, [238]Pu has a high decay heat per unit mass than the other plutonium isotopes. These values have been calculated using data from the Korean Atomic Energy Research Institute (KAERI) (21).

Table 1.2: Decay Heat Contributions of Pu Isotopes [W/kg]

Isotope	α	β
[238]Pu	557.43	-
[239]Pu	1.88	-
[240]Pu	6.94	-
[241]Pu	-	3.22
[242]Pu	0.11	-

In addition to the high alpha decay heat of [238]Pu, the spontaneous fission neutron generation rate is unattractive for weapons purposes. A high spontaneous fission neutron generation rate within an HNED can cause the HNED to detonate prematurely before maximum compression is achieved resulting in a lower yield (22). As shown in Table 1.3, the even numbered plutonium isotopes have higher spontaneous fission neutron generation rates with [238]Pu having the highest. Although not often mentioned when discussing plutonium, the dose rate from the elevated [238]Pu concentration may also contribute to its material attractiveness. This has not been thoroughly investigated and could play an important role in decreasing the material attractiveness of plutonium in used fuel.

Table 1.3: Spontaneous Fission Neutron Generation Rate of Pu Isotopes [n/s/g] (23)

Isotope	n/s/g
^{238}Pu	$2.59 \cdot 10^3$
^{239}Pu	$2.18 \cdot 10^{-2}$
^{240}Pu	$1.02 \cdot 10^3$
^{241}Pu	$5.00 \cdot 10^{-2}$
^{242}Pu	$1.72 \cdot 10^3$

1.5. Possible Production Routes for ^{238}Pu

Higher ^{238}Pu concentration in used nuclear fuel can be achieved using a few

methods. The most common is burning fuel with a higher concentration of ^{235}U than

typically in reactor grade uranium at a high burnup. Figure 1.1 shows the production route

of ^{238}Pu via ^{235}U.
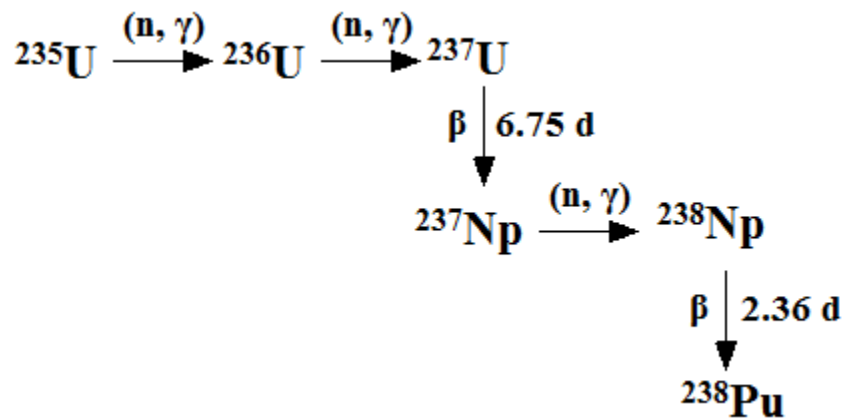
Figure 1.1: ^{238}Pu Production by way of ^{235}U

In addition to ^{235}U, ^{237}Np and ^{241}Am can also be used (24). These isotopes can be

mixed with fresh fuel and burned in a reactor to produce higher concentrations of ^{238}Pu in

used nuclear fuel. Figure 1 shows the production route using ^{237}Np. Figure 1.2 shows the

production route using ^{241}Am.

$^{241}Am \xrightarrow{\text{(n, }\gamma\text{)}} {}^{242}Am$

$\beta \mid 16.02 \text{ h}$

^{242}Cm

$\alpha \mid 162.8 \text{ d}$
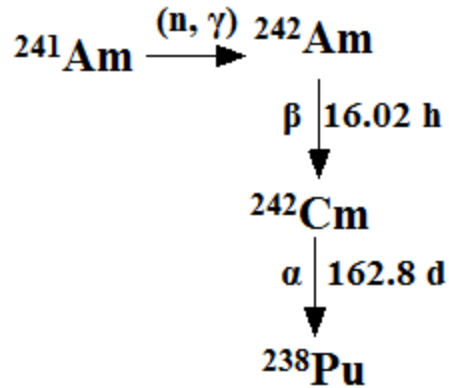
^{238}Pu

Figure 1.2: ^{238}Pu Production by way of ^{241}Am

1.6. ^{232}U Unattractive Features

Mixing ^{232}U with naturally occurring uranium isotopes can decrease the material

attractiveness. The unattractive features of ^{232}U are two-fold. The initial alpha decay of ^{232}U

is relatively high and over time the dose rate and decay heat of the material increases (25).

This increase in dose rate over time is due to the build-up of ^{208}Tl, which emits an energetic

gamma ray with energy of 2.615 MeV. Not only is the dose rate a danger to anyone who

may handle the material, but also can damage the high explosives of a weapon. Over time,

energy deposition by gamma radiation within the high explosives may cause them to

degrade leading to reduced effectiveness (14). Table 4 shows the decay heat contributions

and half-lives of the uranium isotopes (21). The decay heat of ^{232}U is notable in comparison

to the naturally occurring uranium isotopes. Also, worth noting is the half-life of ^{232}U, which

is several orders of magnitude shorter than that of the naturally occurring uranium

isotopes.

Table 1.4: Decay Heat Contribution and Half-lives of U Isotopes

Isotope	α-Decay Heat [W/kg]	Half-life [years]
^{232}U	703	68.9
^{234}U	0.176	$2.45 \cdot 10^5$
^{235}U	$5.63 \cdot 10^{-5}$	$7.04 \cdot 10^8$
^{238}U	$8.35 \cdot 10^{-6}$	$4.47 \cdot 10^9$

In order to understand how the decay heat and dose rate change over time, the decay chain of ^{232}U must be considered. As shown in Figure 1.3, the daughter products of ^{232}U have relatively short half-lives and ^{208}Tl builds up rapidly. The decay chain progresses rapidly upon the decay of ^{228}Th.
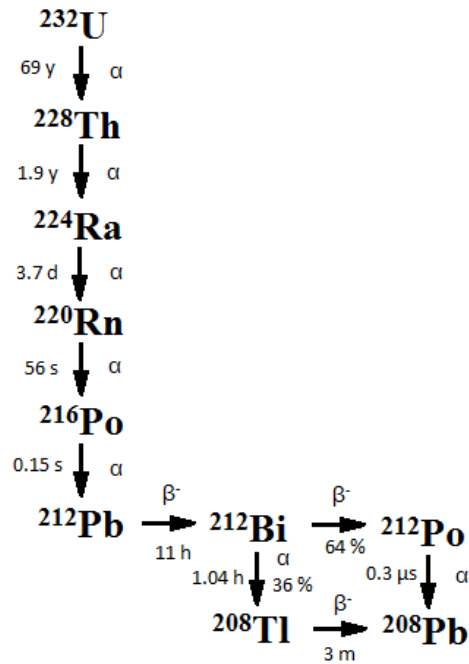
Figure 1.3: ^{232}U Decay Chain

Table 1.5 shows the decay heat per unit mass of ^{232}U's daughter products. Although the daughter products are present in fractional amounts, they produce high enough decay

13

heat to greatly increase the total decay heat of the material over time. Both the decay heat

and dose rate reach a maximum after approximately 10 years (25).

Table 1.5: ^{232}U Daughter Products Decay Heat

Isotope	W/kg
^{228}Th	$2.63 \cdot 10^4$
^{224}Ra	$5.36 \cdot 10^6$
^{220}Rn	$3.44 \cdot 10^{10}$
^{216}Po	$1.45 \cdot 10^{13}$
^{212}Pb	$8.25 \cdot 10^5$
^{212}Bi	$2.32 \cdot 10^8$
^{208}Tl	$9.82 \cdot 10^8$
^{212}Po	$9.27 \cdot 10^{18}$

In addition to the decay heat and dose rate, ^{232}U poses a significant obstacle for the

enrichment process (26). Without utilizing isotopic separation technology, ^{232}U cannot be

separated from the uranium material. The main purpose of the enrichment of natural

uranium is to increase the concentration of ^{235}U and decrease the concentration of ^{238}U

making the material more fissile. Although the concentration of ^{234}U is also increased, the

initial concentration of ^{234}U is so low that it is not an impact. However, the significant mass

difference between ^{232}U and ^{235}U (three neutrons) would cause the concentration of ^{232}U to

greatly increase during the enrichment process. This would increase the effects of heat

generation and dose rate as the material is enriched. The emission of alpha particles in

gaseous UF_6 poses an additional threat to the enrichment process (26). When UF_6

molecules are irradiated with alpha particles, the molecules may decompose through the

creation of ion pairs. Historically, this issue was considered through the scope of the effects

of ^{234}U's alpha decay in gaseous UF_6 (27). ^{232}U's effects will be significantly more notable as

its alpha emission rate is higher than that of ^{234}U. Table 1.6 shows the alpha emission rates of ^{232}U and the naturally occurring uranium isotopes.

Table 1.6: Alpha Emission Rate of U Isotopes

Isotope	Alpha Emission Rate [α/s/g]
^{232}U	$8.28 \cdot 10^{11}$
^{234}U	$2.31 \cdot 10^{8}$
^{235}U	$8.00 \cdot 10^{4}$
^{238}U	$1.24 \cdot 10^{4}$

Although not typically mentioned when referencing uranium, the spontaneous fission neutron rate of ^{232}U may increase the detectability of uranium materials containing ^{232}U. Neutrons are often more difficult to shield than gamma rays and may allow for the detection of these materials in situations where gamma ray measurements may not. Table 1.7 shows the spontaneous fission neutron generation rate of ^{232}U and the naturally occurring uranium isotopes. Although these values are smaller than that of the even numbered plutonium isotopes, the spontaneous fission neutron generation rate of ^{232}U is notable as it would allow for increased detection ability.

Table 1.7: Spontaneous Fission Neutron Generation Rate of U Isotopes (23)

Isotope	Spontaneous Fission Neutron Rate [n/(s·kg)]
^{232}U	1300
^{234}U	5.02
^{235}U	0.299
^{238}U	13.6

In addition to spontaneous fission neutrons, uranium materials that include ^{232}U in an oxide matrix (such as UO$_2$) will release a higher number of (α,n) neutrons. (α,n) neutrons are produced when an alpha particle reacts with an atom (such as oxygen) and releases a neutron. Table 1.8 shows the (α,n) neutron generation rate of ^{232}U and the naturally occurring uranium isotopes. Considering ^{232}U's high alpha particle emission rate, its presence in UO$_2$ creates orders of magnitude more (α,n) neutrons than naturally occurring uranium isotopes.

Table 1.8: (α,n) Neutron Generation Rate of U Isotopes (23)

Isotope	(α,n) Neutron Rate [n/(s·kg)]
^{232}U	$1.49 \cdot 10^7$
^{234}U	$3.00 \cdot 10^3$
^{235}U	$7.10 \cdot 10^{-1}$
^{238}U	$8.30 \cdot 10^{-2}$

1.7. Possible Production Routes for ^{232}U

Although this study will not focus specifically on producing ^{232}U, proposing and highlighting possible production routes is essential to understanding the feasibility of the proposed use of ^{232}U. Historically, ^{232}U has been discussed as it relates to thorium fuel cycles. When natural thorium, containing mostly ^{232}Th, is irradiated by neutrons, ^{233}U is produced containing fractional amounts of ^{232}U. ^{232}Th absorbs a neutron producing ^{233}Th, which then beta decays to ^{233}Pa. ^{233}Pa then beta decays to ^{233}U, an isotope whose fissile capabilities are more like plutonium than ^{235}U. An (n,2n) reaction with ^{233}Th, ^{233}Pa, or ^{233}U, will lead to the production of ^{232}U (28). This production route is not useful for the method proposed in this study. Only fractional amounts of ^{232}U are produced with most of the uranium produced being ^{233}U. These isotopes would be difficult to separate as doing so

16

would require isotopic separation technology. The production route needed here should produce mainly ^{232}U.

Producing ^{232}U specifically can be done by utilizing ^{230}Th and ^{231}Pa (29). ^{230}Th and ^{231}Pa are both found in nature in fractional amounts. Figure 1.4 show the production route for ^{232}U.

$$^{230}\text{Th} \xrightarrow{(\text{n}, \gamma)} {}^{231}\text{Th}$$
$$\beta^- \downarrow 25.5 \text{ h}$$
$$^{231}\text{Pa} \xrightarrow{(\text{n}, \gamma)} {}^{232}\text{Pa}$$
$$\beta^- \downarrow 1.31 \text{ d}$$
$$^{232}\text{U}$$
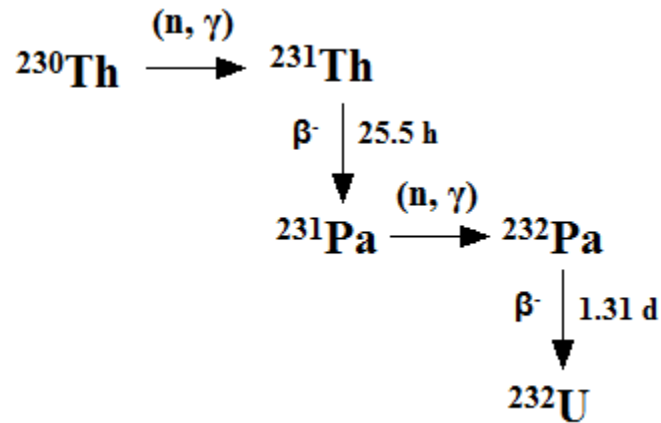
Figure 1.4: Production Route for ^{232}U

1.8. Material Properties

This section will discuss the material properties of both plutonium and uranium.

1.8.1. Plutonium Material Properties

This study will analyze plutonium in metallic form as this is the most attractive for weapons purposes. Plutonium has a several solid phases with various densities. Figure 1.5 shows the solid phases of plutonium as a function of density and temperature.
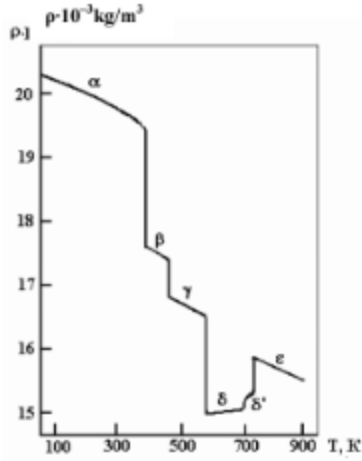
Figure 1.5: Plutonium phases (30)

The delta phase is most attractive for weapons purposes (20), but is not stable at room temperature. In order to stabilize delta phase plutonium at room temperature and across a wide range of temperatures, a small percentage (5 at.%) of gallium can be added. Figure 1.6 shows the plutonium-gallium phase diagram (31).
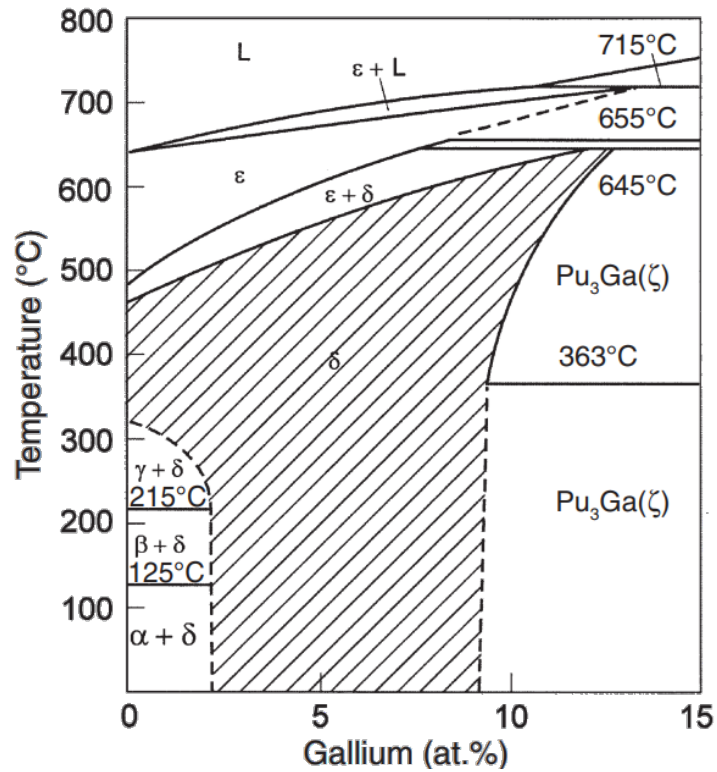
Figure 1.6: Plutonium-Gallium Phase Diagram (31)

18

The crystal structure of delta phase plutonium is a face-centered cubic. Delta phase plutonium has a density of 15.8 g/cm^3. Table 1.9 shows the thermophysical properties of plutonium used in this study.

Table 1.9: Thermophysical Properties of Plutonium (30) (31)

Thermal Conductivity [W/m·K]	Heat Capacity [J/g·K]	Modulus of Elasticity [GPa]	Thermal Expansion [1/K]	Tensile Strength [GPa]
10.97	0.13	68	$3.00 \cdot 10^{-6}$	$1.00 \cdot 10^{-1}$

1.8.2. Uranium Material Properties

Uranium will be considered in several material form; metallic, UO_2 powder, and sintered UO_2. The metallic form is considerably less complicated than in the case of plutonium. Metallic uranium has three solid phases; α, β, and γ. α phase is stable under 669 °C so this is the phase considered here. α phase uranium has an orthorhombic crystal structure with a density of 19.05 g/cm^3.

Table 1.10: Thermophysical Properties of Uranium (30)

Thermal Conductivity [W/(m·K)]	Heat Capacity [J/(g·K)]	Modulus of Elasticity [GPa]	Thermal Expansion [1/K]	Tensile Strength [GPa]
28.9	0.1163	190	$1.39 \cdot 10^{-5}$	0.615

UO_2 is not attractive for weapons purposes but is found in nuclear fuel cycles as fuel. Initially, UO_2 may be stored as a powder and later sintered. Powder UO_2 has an approximate density of 2.5 g/cm^3. Sintered UO_2 has a density of 10.96 g/cm^3 (30). The thermophysical properties previously described are not needed for the analysis of UO_2 done here.

1.8.3. Additional Material Properties

In addition to the thermophysical properties of the fissile material, that of the other materials found in the HNED is also needed. The high explosives chosen to analyze is PBX 9502. PBX 9502 is a polymer bonded explosive that has a self-explosion temperature of 331 °C, starts pyrolysis at 395 °C, and melts at 448 °C. Table 1.11 shows the densities for the HNED materials.

*Table 1.11: HNED Material Densities ** (20)*

Material	Density (30) [g/cm^3]	References
Be	1.85	(30)
PBX 9502	1.90**	(20)
Al casing	2.7	(30)

Table 1.12 shows the thermophysical properties of the additional HNED materials.

Table 1.12: Thermophysical Properties of HNED Materials (30), (32), (33), (34), (35), (36)

Material	Thermal Conductivity [W/m·K]	Heat Capacity [J/g·K]	Modulus of Elasticity [GPa]	Thermal Expansion [1/K]	Tensile Strength [GPa]
Be	102	1.78	303	$1.60 \cdot 10^{-5}$	$1.90 \cdot 10^{-1}$
PBX 9502	0.5607	1.125	15.3	$4.01 \cdot 10^{-6}$	$3.23 \cdot 10^{-3}$
Al casing	98‡	1.177	17	$2.30 \cdot 10^{-5}$	$4.80 \cdot 10^{-1}$

The properties affecting the radiation and convective heat transfer at the surface of the models must be considered. The radiation heat transfer will be assumed to be that of a black body as this produces the best case for the heat transfer and is a limiting case. Table 1.13 shows the convective heat transfer coefficients for air and liquid nitrogen.

Table 1.13: Convective Heat Transfer Coefficients [W/cm²·K] (37) (38)

Fluid	Convective Heat Transfer Coefficient
Air	0.001
Liquid Nitrogen	0.01

1.9. Layout of Dissertation

This dissertation is made up of five chapters. The second chapter describes the previous studies that serve as the basis and background for this dissertation. These studies span several techniques for evaluating the attractiveness of both plutonium and uranium materials for weapons purposes. The third chapter describes the methodology used in this study. This methodology consists of a model based approach and figure of merit approach for both plutonium and uranium materials. In addition, an analysis to evaluate the practicality of the implementation of the uranium material in the civilian world. The fourth chapter reports and discusses the results from the methods described in Chapter 3. The fifth chapter concludes the dissertation. This chapter not only summarizes and concludes the plutonium and uranium analyses, but also elaborates on the scope of the final conclusions and describes possible future works.

2. LITERATURE REVIEW

Quantifying proliferation resistance is a complex task. In particular, when referencing the proliferation resistance of a specific material, making an accurate assessment can be open to interpretation. Historically, proliferation resistance assessments have varied greatly. This section will discuss three specific analyses used to assess proliferation resistance of nuclear materials.

2.1. Modeling Based Analysis

This section shall describe the use of a specific model in order to assess the material attractiveness and proliferation resistance of the fissile material. These studies investigated plutonium vectors with elevated ^{238}Pu content. Two similar studies are worth discussing to illustrate their methodology and possible shortfalls.

Dr. Kessler of the Technical University of Karlsruhe in Germany has published his work in regards to denaturing plutonium using ^{238}Pu. Kessler analyzed 8 plutonium vectors having ^{238}Pu concentrations ranging from 1.6% to 24.5%. He created three simple hypothetical spherical fission type nuclear weapon models representing high, medium, and low technology. Each model had varying thicknesses of high explosives and reflectors, with the high technology having the thinnest and the low technology having the thickest. Figure 2.1 shows the three simplistic models. Each model is spherically symmetric.

22
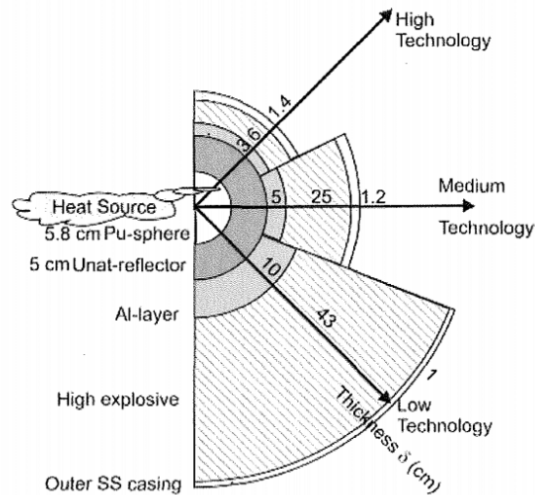
Figure 2.1: Kessler's Models (20)

The plutonium masses for each vector were chosen in order to give the model a k_{eff} of 0.98. Using steady state heat transfer through the model, the temperature throughout each layer was determined. The temperature within the high explosives were compared to the "self-explosion" temperature of the high explosives to determine if the weapon would self-explode. Kessler concluded that plutonium vectors containing approximately 6% [238]Pu or more would result in the self-explosion temperature being reached even in the high technology case (20).

Using the models shown in Figure 2.1, a group from the Research Laboratory from Nuclear Reactors at the Tokyo Institute of Technology analyzed the temperature within the high explosives as a function of [238]Pu concentration. Rather than analyze a few specific plutonium vectors, they sought to relate the maximum temperature in the high explosives to the concentration of [238]Pu. Their final conclusion was that [238]Pu above 15% would be infeasible in the high technology case, above 6% in the medium technology case, and above 2% in the low technology case (19). The 15% is a significantly higher concentration of [238]Pu than that the 6% proposed by Kessler.

Although these studies were able to make conclusions regarding how the ^{238}Pu concentration impacts the three models, the scope of these studies are narrow and only draw conclusions in regards to those specific models. These studies fail to make a more broad assessment of material attractiveness. The plutonium vectors analyzed by Kessler aren't necessarily realistic. These vectors were obtained at high burnups that do not represent what is currently standard in the nuclear fuel cycle. Another major issue is that the results are heavily dependent on the models. Any deviation in the models (ex. changes in the high explosives type or thickness) will change the results. Also, these models do not represent a limiting case. A k_{eff} of 0.98 is close to critical (k_{eff}=1) and the weapon essentially has nearly a maximal plutonium mass without being critical. A nearly maximal plutonium mass would then produce a nearly maximal heat generation. In order for the model to be a limiting case, the k_{eff} must be minimal in order to minimize the mass and heat generation while still being a functional HNED.

2.2. Figure of Merit Analysis

In order to broaden the assessment of material attractiveness, a Figure of Merit (FOM) analysis is useful. A group led by Charles Bathke at Lawrence Livermore National Laboratory developed a FOM that serves as a metric for attractiveness (18). An important note of this study is its definition of proliferation resistance. Proliferation resistance is defined as the characteristics of a material to impeded diversion of nuclear material by a state. This definition excluded any non-state entities such as terrorist organization. Non-state entities are not considered in the analysis. The state entities considered in this study are separated into two categories: technically advanced states and less technically advanced states.

This analysis uses physical characteristics of a material as inputs and output a FOM value that measures the material's attractiveness. These physical characteristics are the bare critical mass, the heat generation, the spontaneous fission neutron generation rate, and the dose rate. These are seen as the four main properties of a material that determine its attractiveness for weapons purposes. Each characteristic is represented by a factor that is normalized to accepted standards. The bare critical mass factor is normalized to the threshold for low enriched uranium (<20% ^{235}U). The heat generation factor is normalized to the international safeguards limit for ^{238}Pu concentration (80% ^{238}Pu). The spontaneous fission neutron generation rate factor is normalized to reactor grade plutonium (≥20% ^{240}Pu). The dose rate factor is normalized to a "self-protecting" dose rate of 500 rad/h at 1 meter. For technically advanced states, the spontaneous fission neutron generation rate factor is excluded as a technically advanced state can handle a high neutron generation rate within a weapon and avoid pre-detonation. All four factors are included in the case of less technically advanced states. Equation 2.1 shows the FOM for less technically advanced states (FOM$_1$). Equation 2.2 shows the FOM for technically advanced states (FOM$_2$). In these equations the FOM is related to the bare critical mass in units of kg (M), the heat generation in units of W/kg (h), the spontaneous fission neutron rate in units of neutrons/s/kg (S), and the dose rate in units of rad/h (D).

Equation 2.1

$$FOM_1 = 1 - \log_{10}\left(\frac{M}{800} + \frac{Mh}{4500} + \frac{MS}{6.8(10)^6} + \frac{M}{50}\left[\frac{D}{500}\right]^{\frac{1}{\log_{10}2}}\right)$$

Equation 2.2

$$FOM_2 = 1 - \log_{10}\left(\frac{M}{800} + \frac{Mh}{4500} + \frac{M}{50}\left[\frac{D}{500}\right]^{\frac{1}{\log_{10} 2}}\right)$$

The FOM is separated into ranges that relate the value to the material's weapons utility and attractiveness. Table 2.1 shows these ranges.

Table 2.1: FOM Ranges and Material Attractiveness

FOM	Weapons Utility	Attractiveness
> 2	Preferred	High
1-2	Attractive	Medium
0-1	Unattractive	Low
< 0	Unattractive	Very Low

Bathke applies this FOM to a variety of materials to quantify their attractiveness (18). The FOM analysis makes a broader statement about material attractiveness than the model based analysis as it doesn't apply to a specific situation but rather the material in any situation. However, this analysis is only useful for direct use material in a weapon's usable form (i.e. metal). Any potential process such as conversion from one chemical form to another or enrichment is excluded from this analysis. For example, if considering a uranium vector, the FOM would result in unattractive if the ^{235}U enrichment were below 20%. However, if the same material were enriched, the FOM would change. The infrastructure required to convert an unattractive material to an attractive one is not possessed by every state and should be accounted for. Also, how the material might affect these processes is important when determining the material's attractiveness.

2.3. Broader Approaches

In the case of ^{232}U proliferation resistance analyses, studies have been broad and somewhat ambiguous. Considering ^{232}U is currently found in thorium fuel cycles, previous studies were done on ^{232}U/^{233}U mixtures. As natural thorium is irradiated with neutrons, ^{233}U is created with fractional amount of ^{232}U as a result of (n,2n) reactions.

A study done at Lawrence Livermore National Laboratory by Dr. Moir attempted to analyze the proliferation resistant features of ^{232}U/^{233}U mixtures. The study shows the major increase in heat generation and dose rate over time from the daughter products of ^{232}U. Both reaching a maximum after approximately 10 years. This study also introduces the impact of radiation damage to high explosives. A high explosive can withstand 100 MR, equivalent to 0.877 Mrads and 0.00877 MGy, before degrading (14). However, the study only evaluates the dose rate from 1 meter rather than analyzing the dose given to high explosive within a realistic model. Without a realistic model, the study ignores the photon attenuation that would occur within the layers of the model.

Another study evaluates denaturing 20% ^{235}U uranium materials with ^{232}U (26). This study mentions the increase in dose rate, but focuses mostly on the increase in the neutron yield. The neutron yield is significantly larger than that of a uranium material containing natural uranium isotopes and would allow for detection via neutron detectors. This study also mentions the effect of alpha decay within gaseous UF_6. UF_6 molecules are destroyed by the irradiation of alpha particles. The study concludes that 48% of UF_6 molecules are destroyed in one tenth of a year. However, the analysis is difficult to follow and not rigorous. A considerable percentage of UF_6 molecules being destroyed would pose a serious barrier to uranium enrichment. Since the separation of isotopes are driven by

mass differences, the lighter molecules created from the destruction of UF_6 molecules

would be counterproductive to the enrichment process.

3. METHODOLOGY

3.1. Heat Transfer Theory

This study analyzes conductive heat transfer throughout multiple shells of several spherically symmetric HNED models in   order to calculate the temperature profiles throughout each shell. Equation 3.1 shows the complete conductive heat transfer equation in spherical coordinates (37). In this equation, the temperature in units of K (T) is related to the radius in units of m (r), time in units of s (t), the angle with respect to the x-axis in units of radian (θ), the angle with respect to the z-axis in units of radian (ϕ), the thermal conductivity in units of W/(m·K) (k), the density in units of kg/m³ (ρ), the heat capacity in units of J/K (C_p), and the heat generation in units of W ($\dot{g}$).

Equation 3.1

$$\frac{1}{r^2}\frac{\partial}{\partial r}\left(kr^2\frac{\partial T}{\partial r}\right) + \frac{1}{r^2\sin^2\theta}\frac{\partial}{\partial \phi}\left(k\frac{\partial T}{\partial \phi}\right) + \frac{1}{r^2\sin\theta}\frac{\partial}{\partial \theta}\left(k\sin\theta\frac{\partial T}{\partial \theta}\right) + \dot{g} = \rho C_p\frac{\partial T}{\partial t}$$

Considering all of the models considered here are spherically symmetric, all partial derivatives with respect to θ and ϕ are equal to 0. The simplified version of the heat equation is shown in Equation 3.2.

Equation 3.2

$$\frac{1}{r^2}\frac{\partial}{\partial r}\left(kr^2\frac{\partial T}{\partial r}\right) + \dot{g} = \rho C_p\frac{\partial T}{\partial t}$$

3.1.1. Steady State Conductive Heat Transfer

In the steady state case (no time dependence), Equation 3.2 is simplified to Equation 3.3.

Equation 3.3

$$\frac{1}{r^2}\frac{\partial}{\partial r}\left(kr^2\frac{\partial T}{\partial r}\right) + \dot{g} = 0$$

Equation 3.3 is solved analytically for two cases; with heat generation ($\dot{g} \neq 0$) and without heat generation ($\dot{g} = 0$). Equation 3.4 shows the temperature profile within a shell that is generating heat. This equation relates the temperature (T) with the outer temperature (T_o), the inner radius (r_i), the outer radius (r_o), the heat generation ($\dot{g}$), the thermal conductivity (k), and the radius (r).

Equation 3.4

$$T(r) = -\frac{\dot{g}r^2}{6k} - \frac{\dot{g}r_i^3}{3kr} + \frac{\dot{g}r_o^2}{6k} + \frac{\dot{g}r_i^3}{3kr_o} + T_o$$

Equation 3.5 shows the temperature profile with a shell that is not generating heat.

Equation 3.5

$$T(r) = \frac{r_o r_i (T_i - T_o)}{r(r_o - r_i)} - \frac{r_i(T_i - T_o)}{r_o - r_i} + T_o$$

3.1.2. Transient Conductive Heat Transfer

Considering the complexity in attempting to solve Equation 3.2 analytically, discretizing the equation is a simpler way to analyze the transient conductive heat transfer. In to discretize, the partial derivate with respect to the radius must be expanded. Equation 3.6 shows the expanded equation.

Equation 3.6

$$\frac{2k}{r}\frac{\partial T}{\partial r} + k\frac{\partial^2 T}{\partial r^2} + \dot{g} = \rho C_p \frac{\partial T}{\partial t}$$

Each term is discretized using a forward finite difference discretization (39). Equation 3.7 and Equation 3.8 show the forward finite difference discretization of the first derivative with respect to r and t. Equation 3.9 shows the central forward difference discretization of the second derivative with respect to r. i corresponds to the ith node. j

30

corresponds to the jth node. *Δr* is the step size in the radial direction. *Δt* is the step size in time.

Equation 3.7

$$\frac{\partial T}{\partial r} = \frac{T_{i+1}^{j} - T_{i}^{j}}{\Delta r}$$

Equation 3.8

$$\frac{\partial T}{\partial t} = \frac{T_{i}^{j+1} - T_{i}^{j}}{\Delta t}$$

Equation 3.9

$$\frac{\partial^2 T}{\partial r^2} = \frac{T_{i+1}^{j} - 2T_{i}^{j} + T_{i-1}^{j}}{\Delta r^2}$$

Equation 3.10 shows Equation 3.6 with Equation 3.7, Equation 3.8, and Equation 3.9 substituted for each of the derivative terms. This equation is solved for the temperature at the j+1 time step. Matlab will be used to model this equation.

Equation 3.10

$$T_{i}^{j+1} = \frac{k\Delta t}{\rho C_p \Delta r}\left[\frac{2}{r}\left(T_{i+1}^{j} - T_{i}^{j}\right) + \frac{1}{\Delta r}\left(T_{i+1}^{j} - 2T_{i}^{j} + T_{i-1}^{j}\right)\right] + T_{i}^{j} + \frac{\dot{g}\Delta t}{\rho C_p}$$

Equation 3.11 shows the only stability criteria for Equation 3.10.

Equation 3.11

$$\frac{k\Delta t}{\rho C_p \Delta r^2} < \frac{1}{2}$$

3.1.3. Boundary Conditions

In order to analyze the heat transfer throughout the entire models, the boundary conditions must be used. The first boundary condition is the thermal energy transferred at each boundary is the same, because only the inner most shell is generating heat. At the outermost layer, the thermal energy is transferred via natural convection and radiation.

31

Equation 3.12 shows the relationship between the thermal energy in units of W ($\dot{Q}$) and the surface temperature in units of K (T_s), the temperature of the surroundings in units of K (T_{surr}), the temperature of the surrounding wall in units of K (T_∞), the surface area in units of m^2 (A), the convective heat transfer coefficient in units of W/(m^2·K) (h), the radiative heat transfer coefficient (ε), and the Stefan-Boltzmann constant in units of W/(m^2·K^4) (σ).

Equation 3.12

$$\dot{Q} = \varepsilon\sigma A(T_s^4 - T_{surr}^4) + hA(T_s - T_\infty)$$

In addition to the first boundary condition, the temperature throughout the model is assumed continuous. Although in reality slight air gaps between the shells may be present, these air gaps would raise the temperature in the outer shells. Therefor assuming perfect heat conduction between each shell is the best case for heat transfer and would yield the lowest temperature profile. This serves as the limiting case for this analysis. Since the models are spherically symmetric, the shells are treated as parts of a thermal resistance circuit. Equation 3.13 shows the expression of the thermal energy. Since the temperature profile is continuous, the outer temperature of a shell is equal to the inner temperature of the next shell.

Equation 3.13

$$\dot{Q} = \frac{4\pi r_o r_i k(T_i - T_o)}{r_o - r_i}$$

When considering time dependence, the boundary conditions are the same. However, the shells are not treated as parts of a thermal circuit, but rather Fourier's law is used as an additional boundary condition. Equation 3.14 shows the convective and radiation boundary condition at the outermost boundary of the model.

Equation 3.14

$$\frac{\delta T}{\delta r} = \varepsilon\sigma(T_s^4 - T_{surr}^4) + h(T_s - T_\infty)$$

Equation 3.15 shows Fourier's law at the interface. In this equation, k_m is the thermal conductivity of the mth shell, k_n is the thermal conductivity of the nth shell, T_m is the temperature profile within the mth shell, T_n is the temperature profile within the nth shell, and r_{int} is the radius at the interface.

Equation 3.15

$$k_m \frac{\delta T_m}{\delta r}\bigg|_{r_{int}} = k_n \frac{\delta T_n}{\delta r}\bigg|_{r_{int}}$$

3.1.4. Thermal Stress

Considering the temperature increases, thermal stresses will be experienced in the shells due to thermal expansion. As the temperature increases in the shells, they will expand. Since the shells are fixed and won't be allowed to expand, the shells will experience thermal stress. Equation 3.16 shows thermal stress (σ_T), Young's Modulus of Elasticity (E), the temperature difference (ΔT), and the linear thermal expansion coefficient (α).

Equation 3.16

$$\sigma_T = E \cdot \Delta T \cdot \alpha$$

3.2. Plutonium Analysis

3.2.1. Plutonium Vector

In order to obtain a realistic plutonium vector, a real world fuel design must be used. An innovative metallic fuel design from Lightbridge (40) will produce elevated ^{238}Pu content in its used fuel. Previously, the Lightbridge fuel has been referred to as "proliferation resistant" (41) and may achieve a significant concentration of ^{238}Pu to

decrease material attractiveness. Lightbridge fuel has an initial high ^{235}U enrichment (19.7% ^{235}U) and relatively high fuel burnup (191 MWd/kg).

Using ORIGEN2 software, the Lightbridge fuel was simulated for a pressurized water reactor. Table 3.1 shows the resulting plutonium vector (42).

Table 3.1: Plutonium Vector

Isotope	wt. %
^{238}Pu	18.14
^{239}Pu	35.66
^{240}Pu	21.08
^{241}Pu	13.54
^{242}Pu	11.58

The plutonium will be alloyed with 5 at. % gallium and has a density of 15.8 g/cm^3.

3.2.2. Modeling Based Analysis

3.2.2.1. Models

Kessler's high technology model will be used initially to redo Kessler's analysis using the plutonium vector in Table 3.2 and updated material properties. Updated decay heat contributions from each plutonium vector will be used to ensure the correct amount of heat generation is being analyzed. The results can then be compared to Kessler's.

Table 3.2: Kessler's Plutonium Vector

Isotope	wt. %
^{238}Pu	8.7
^{239}Pu	30.1
^{240}Pu	30.6
^{241}Pu	11.3
^{242}Pu	19.3

In addition, this analysis will use two models for the steady state heat transfer

analysis. The most realistic of these models will be used for the transient heat transfer

analysis. Each model will be slightly modified to maintain the k_{eff} when the plutonium

vector in Table 3.1 is used. The k_{eff} for each model is found using kcode within the software

MCNP (43).

Model One is based on Fat Man. Fat Man is the only plutonium based nuclear

weapon used in warfare and thus represents a logical realistic case to consider. The

geometry of the model is well known. The k_{eff} of the original design is 0.98. Table 3.3 shows

the radial thickness of each shell in the initial Fat Man geometry (4) and the updated

geometry (42). Pu is plutonium. U_{nat} is natural uranium. BPE is borated polyethylene. Al is

aluminum. PBX 9502 is the polymer bonded explosives. The updated geometry contains

more plutonium mass because the original geometry contained weapons grade plutonium

rather than the less fissile plutonium vector used in the updated geometry. The borated

polyethylene was removed from the updated geometry as the heat produced by the

plutonium would melt it.

Table 3.3: Model One Initial and Updated Geometries

Material	Radial Thickness [cm]	
	Initial	*Updated*
Neutron Initiator	1	-
Pu	3.6	5.105
U_{nat}	6.5	5
BPE	0.33	-
Al	12.07	12.40
PBX 9502	47	47
Steel casing	1	1

Although this design is relatively large, Model One represents a limiting case. The larger outer surface area of the geometry will lead to a reduction in the temperatures within the materials.

Model Two is considered to be the most realistic design. This model features a minimum amount of plutonium and has a significantly lower k_{eff} than Model One. The lower plutonium mass will generate less heat and represents an important limiting case. The k_{eff} of Model Two is 0.66. The only change between the initial and updated models is the expansion of the plutonium shell inward. Table 3.4 shows the radial thickness of each shell in the initial model (44) and the updated model (42).

Table 3.4: Model Two Initial and Updated Geometries

Material	Radial Thickness [cm]	
	Initial	*Updated*
Inner cavity	4.25	3.715
Pu	0.75	1.285
Be	2	2
U_{dep}	3	3
PBX 9502	10	10
Al casing	1	1

3.2.2.2. Steady State Heat Transfer

The temperature will be found analytically for each model using the theory described in the Steady State Conductive Heat Transfer section. The temperature within the high explosives will be compared to its self-explosion temperature to assess whether self-explosion will occur.

Although the α and β decay heat from each plutonium isotope has previously been assumed to be the main contributor to the heat generation, other decay heat contributor

36

will be considered. The heat generation due to gamma rays and spontaneous fission

(including gamma rays, neutrons, fission fragments, and induced fission) will be considered

in each layer. The gamma ray emissions from the plutonium will found using the software

RadSrc. RadSrc takes radionuclide content and age in years as inputs and outputs the

decayed content as an MCNP usable gamma ray emission spectrum (45). MCNP is then

used to find the energy deposition from the sources previously described with the

exception of the fission fragments. The energy deposition from the fission fragments is

found using the average energy of the fission fragments (46).

3.2.2.3. Transient Heat Transfer

Although a steady state transfer analysis will determine if the heat generation is

significant enough to cause the high explosives to reach its self-explosion temperature, this

analysis will not yield a time limit at which this temperature is met. This information is

crucial as it serves as a time window within which the model is usable even with the

increased heat generation. In order to find this limit, a transient heat transfer model must

be used.

Matlab is used to create a computational model of the most realistic model (Model

Two). The theory described in the Transient Conductive Heat Transfer section will be used

to "step" through time and space to create the temperature throughout the model over

time. The changes in temperature over time will also be used to calculate the maximum

thermal stress (Equation 3.16) in each of the shells to determine if any deformation or

failure will occur. Deformation or failure with an HNED would cause a nonuniform

implosion leading to a reduction in the overall yield and could possibly reduce the weapon

37

to a radiological dispersal device. The transient heat transfer will be considered for four

unique scenarios (42).

In the first scenario, the plutonium pit is inserted into the HNED. Prior to insertion,

the HNED is at room temperature and the plutonium pit is in thermal equilibrium with the

surrounding room. Post insertion, the HNED is stationary within a large room and the heat

is transferred at the surface of the HNED by way of natural convection and radiative heat

transfer.

In the second scenario, the plutonium pit is externally cooled in liquid nitrogen prior

to insertion. As in scenario 1, the HNED is at room temperature however the plutonium pit

is in thermal equilibrium with the liquid nitrogen. Post insertion, the HNED is again

stationary within a large room and the heat is transferred at the surface by way of natural

convection and radiative heat transfer.

In the third scenario, the plutonium pit is inserted into an externally cooled HNED.

Prior to insertion, the HNED is at thermal equilibrium with the liquid nitrogen surrounding

it and the plutonium pit is at thermal equilibrium with the surrounding room. Post

insertion, the HNED remains externally cooled by liquid nitrogen.

In the fourth scenario, the fully assembled, liquid nitrogen cooled HNED is removed

and place into a large room. The initial temperature profile of scenario 4 is the final

temperature profile of scenario 3. Once the HNED is removed, heat is transferred at its

surface by way of natural convection and radiative heat transfer.

3.2.3. Figure of Merit Analysis

In order to make a broader statement regarding the plutonium vector's material

attractiveness, the FOM described in Equation 2.1 and Equation 2.2 will be calculated for

this plutonium vector. The resulting FOM values will be compared to the ranges shown in

Table 2.1. In order to put the results in perspective, the FOM will be calculated for two

additional plutonium vectors; one from a typical light water reactor (LWR) used fuel and

the other from mixed oxide (MOX) used fuel. Table 3.5 shows these vectors (47).

Table 3.5: Addition Plutonium Vectors [wt. %]

Isotope	LWR	MOX
^{238}Pu	2.00	3.17
^{239}Pu	41.3	43.7
^{240}Pu	27.6	22.2
^{241}Pu	19.2	17.0
^{242}Pu	9.91	13.9

Each of the four components of the FOM equation: bare critical mass, dose rate, heat

generation, and spontaneous fission neutron generation rate must be calculated. The bare

critical mass will be found using kcode within MCNP. The geometry is a bare sphere of

metallic plutonium surrounded by air. The mass will be slightly modified until the mass is

critical (k_{eff}=1). The heat generation is found by combining the plutonium vectors with the

decay heat per unit mass of each plutonium isotope. Similarly, the spontaneous fission rate

is found by combining the plutonium vectors with the spontaneous fission neutron

generation rate per unit mass of each plutonium isotope. MCNP will be used to find the

dose rate of 0.2 the bare critical mass from 1 meter. Using the gamma ray spectrum from

RadSrc for each plutonium vector, MCNP will calculate the dose rate 1 meter from the

surface of a metallic plutonium sphere having 0.2 the bare critical mass.

In addition to calculating the FOM values, contributions from possible sources of

uncertainty must be accounted for. Although the bare critical mass is found

computationally using MCNP6, the result is dependent on the cross section libraries chosen

for each isotope. Using a technique previously used at Los Alamos National Laboratory (48), the bare critical mass will be calculated using several cross section libraries. The resulting masses will be averaged and their standard deviation is used as the uncertainty. The decay heat values are calculated using decay data from KAERI (21) and data used in plutonium denaturing studies done by a research groups in Tokyo (24). The spontaneous fission values are calculated by using the spontaneous fission rates from the book "Passive Nondestructive Assay of Nuclear Materials" (23) and from the studies from the Tokyo Institute of Technology mentioned previously (24). As with the bare critical mass values, the decay heat values and spontaneous fission values will be averaged and the standard deviation will be used as the uncertainty for each. The dose rate is calculated entirely computationally in MCNP6 such that the computational uncertainty is negligible.

3.3. Uranium Analysis

3.3.1. Uranium Vectors

Two unique sets of uranium vectors are used in the analysis. The first set is an initial mixture of ^{232}U and natural uranium enriched to various concentrations of ^{235}U for various applications. The second set are similar to the first set in terms of ^{235}U enrichment, but do not contain ^{232}U and have the same ^{235}U/^{238}U. The second set will be used to illustrate the effects of the introduction of ^{232}U on various safety, security and safeguards measurements.

For the first set, the initial mixture is 0.029 wt. % ^{232}U and natural uranium. This initial mixture was chosen because preliminary calculations concluded that the amount of ^{232}U when enriched to weapons grade from this initial mixture was sufficient to cause self-explosion in the high explosives of a HNED model. The mixture is enriched to approximately 3, 5, 20, 90 at. % ^{235}U. The 3 and 5 at. % vectors represent reactor grade

uranium. The 20 at. % vector represents the limit above which uranium is classified as HEU. The 90 at. % vector represents weapons grade uranium. The enrichment of the initial vector was simulated via MSTAR. MSTAR is a software program currently developed at Oak Ridge National Laboratory that takes an initial concentration of the various uranium isotope and a final concentration of ^{235}U and outputs the final concentration of the other uranium isotopes (49). Table 3.6 shows the uranium vectors that include ^{232}U.

Table 3.6: Uranium Vectors with ^{232}U [wt. %]

Isotope	Initial	3%	5%	20%	90%
^{232}U	0.029	0.179	0.310	1.330	6.241
^{234}U	0.005	0.028	0.043	0.180	0.930
^{235}U	0.702	2.940	4.741	19.805	89.844
^{238}U	99.263	96.853	94.706	78.714	2.985

Table 3.7 shows the uranium vectors that do not include ^{232}U.

Table 3.7: Uranium Vectors without ^{232}U [wt. %]

Isotope	Initial	3%	5%	20%	90%
^{234}U	0.005	0.028	0.044	0.183	0.992
^{235}U	0.702	2.945	4.956	20.066	95.824
^{238}U	99.292	97.027	95.027	79.751	3.184

Not only are these fresh uranium vectors to be considered, but also the vectors as they age. Considering the relative rapid increase in heat generation and dose rate over time, each uranium vector will be analyzed at three time intervals: 0 year, 0.5 year, and 10 years. The gamma ray spectrum and intensities as well as the isotopic composition of each vector is found using RadSrc (45).

3.3.2. Model Based Analysis

3.3.2.1. Model

The uranium model based analysis will only utilize one HNED model. This model is similar to Model Two in the plutonium analysis. The model is considered realistic as it has a minimal amount of uranium mass. Considering this is an HNED model, the "90%" uranium vector in Table 3.6 is used. Considering this uranium vector is different than the weapons grade uranium originally in the design, the model is slightly modified to maintain the k_{eff}. According to MCNP's kcode, the k_{eff} of this model is 0.69. Table 3.8 shows the initial (44) and update models. The inner cavity contains dry air. The U is the uranium weapons pit. The Be is the beryllium. The U_{dep} is depleted uranium. The PBX 9502 is the polymer bonded high explosives. The Al casing is the aluminum casing.

Table 3.8: Uranium HNED Initial and Updated Models

Material	Radial Thickness [cm]	
	Initial	*Updated*
Inner cavity	5.77	5.897
U	1.23	1.102
Be	2	2
U_{dep}	3	3
PBX 9502	10	10
Al casing	1	1

3.3.2.2. Steady State Heat Transfer

The temperature will be found analytically for the updated model in Table 3.8 using the theory described in the Steady State Conductive Heat Transfer section. The temperature within the high explosives will be compared to its self-explosion temperature to assess whether self-explosion will occur.

Considering the heat generation contributions for sources besides α and β decay are calculated in the plutonium steady state heat transfer analysis, these contributions will only be included in the uranium analysis if their contributions are significant in comparison to the heat generation from α and β decay. Otherwise, these contributions are considered negligible.

3.3.2.3. Transient Heat Transfer

As with the plutonium model based analysis, time dependent must also be considered in the case of uranium. Matlab is used to create a computational model of the model. This computational approach is the same as in the plutonium analysis with slightly different geometry and materials. The maximum thermal stress as a result in the changes in temperature is also calculated and compared to the material tensile strength in order to determine if deformation or failure will occur. The same four scenarios are considered here.

In the first scenario, the uranium pit is inserted into the HNED. Prior to insertion, the HNED is at room temperature and the uranium pit is in thermal equilibrium with the surrounding room. Post insertion, the HNED is stationary within a large room and the heat is transferred at the surface of the HNED by way of natural convection and radiative heat transfer.

In the second scenario, the uranium pit is externally cooled in liquid nitrogen prior to insertion. As in scenario 1, the HNED is at room temperature however the uranium pit is in thermal equilibrium with the liquid nitrogen. Post insertion, the HNED is again stationary within a large room and the heat is transferred at the surface by way of natural convection and radiative heat transfer.

In the third scenario, the uranium pit is inserted into an externally cooled HNED. Prior to insertion, the HNED is at thermal equilibrium with the liquid nitrogen surrounding it and the uranium pit is at thermal equilibrium with the surrounding room. Post insertion, the HNED remains externally cooled by liquid nitrogen.

In the fourth scenario, the fully assembled, liquid nitrogen cooled HNED is removed and placed into a large room. The initial temperature profile of scenario 4 is the final temperature profile of scenario 3. Once the HNED is removed, heat is transferred at its surface by way of natural convection and radiative heat transfer.

3.3.3. Figure of Merit Analysis

In order to make a broader statement regarding the material attractiveness with the addition ^{232}U in uranium materials, the FOM equations found in Equation 2.1 and Equation 2.2 are applied. Considering the FOM equations only apply to direct use nuclear materials, only the weapons grade uranium vector containing ^{232}U can be used. Since two components of the FOM equations (dose rate and heat generation) increase over time, the FOM values for the uranium vector will be calculated at 0 year, 0.5 year, and 10 years. This will illustrate how the material attractiveness changes over time and if/when the uranium materials will become unattractive for weapons purposes.

The methods used to calculate each of the four components of the FOM equation; bare critical mass, dose rate, heat generation, and spontaneous fission neutron generation rate, are as follows. The bare critical mass will be found using kcode within MCNP. The geometry is a bare sphere of metallic uranium surrounded by air. The mass will be slightly modified until the mass is critical (k_{eff}=1). The heat generation is found by combining the uranium vectors with the decay heat per unit mass of each uranium isotope. Similarly, the

heat generation is found by combining the uranium vectors with the spontaneous fission neutron generation rate per unit mass of each uranium isotope. MCNP will be used to find the dose rate of 0.2 the bare critical mass from 1 meter. Using the gamma ray spectrum from RadSrc for each uranium vector, MCNP will calculate the dose rate 1 meter from the surface of a metallic uranium sphere having 0.2 the bare critical mass.

As in the case of the plutonium analysis, the sources of uncertainties must be accounted for. For the bare critical mass, multiple cross section libraries within MCNP6 are used to calculate multiple bare critical mass values. The spontaneous fission rate is calculated using the values in the book "Passive Nondestructive Assay of Nuclear Materials" (23) and using the software Sources 4C (50). These values are averaged and the standard deviation is used as the uncertainty. Considering the decay heat includes ^{232}U daughter products, there is no easily assessable data to compare and include in the uncertainty. As with the plutonium analysis, the uncertainty from the dose rate is negligible. These values are averaged and the standard deviation is used as the uncertainty.

3.3.4. Enrichment Issues

The relatively large alpha emission of ^{232}U within gaseous UF$_6$ could cause major enrichment issues. Calculating the number of UF$_6$ molecules destroyed per time will gives insight into the magnitude of these issues. Approximately 9 UF$_6$ molecules are destroyed per every keV deposited. Combining this with the average alpha particle energy released by ^{232}U (5301.6 keV) (21) and the activity of ^{232}U in Becquerel will yield the rate of destruction of UF$_6$ molecules. Equation 3.17 shows the relationship between the number of UF$_6$ molecules destroyed per second (*U*) and the activity of the ^{232}U (*A*) and the average energy of the alpha particle emitted by ^{232}U (*E*) (51).

Equation 3.17

$$U = 9AE$$

Equation 3.17 will be applied to the uranium vectors shown in Table 3.6. This will show the effect of ^{232}U's alpha decay at various stages of the enrichment process.

3.3.5. Effects on Safety

Although the dose rate from ^{232}U is considered a proliferation resistant feature, elevated dose rate in materials used in a civilian nuclear fuel cycle pose operational challenges. Higher dose rates lead to higher and more expensive precautions to protect workers. In order to utilize ^{232}U in a fuel cycle for nonproliferation considerations, the safety aspects of such use must be considered.

Three basic models found in a nuclear fuel cycle will be used: a UO_2 fuel pellet, a UO_2 fuel rod, and a can of powdered UO_2. These models will contain the uranium vectors shown in Table 3.6 (excluding the weapons grade vector). The dose rate from each model with each vector at 1 m will be calculated using MCNP. As mentioned previously, the gamma ray emissions will change over time and will be considered at time intervals of 0 year, 0.5 year, and 10 years. These dose rates will then be compared to set standards.

For completeness, the dose rate from neutron emissions will also be included. Both spontaneous fission neutrons and (α,n) neutrons must be included. In the case of the spontaneous fission neutron emissions, the source definition parameter is set to SF (spontaneous fission) and MCNP will calculate the dose rate from 1 meter from spontaneous fission neutrons. Since the (α,n) neutron energy spectrum is unique to the specific isotopic and elemental composition of the material, the spectrum must first be generated and input into MCNP. Sources 4C is utilized to calculate the (α,n) neutron

46

spectrum. Sources 4C is a program that takes the elemental and actinide composition of the material and outputs the (α,n) energy spectrum and yield (50).

The fuel pellet model consists of solid UO_2 with a density of 10.96 g/cm^3 (30) surrounded by dry air. The model has a height of 1 cm and a diameter of 1 cm (52). Figure 3.1 shows the MCNP UO_2 fuel pellet geometry. The red is the UO_2. The yellow is dry air.
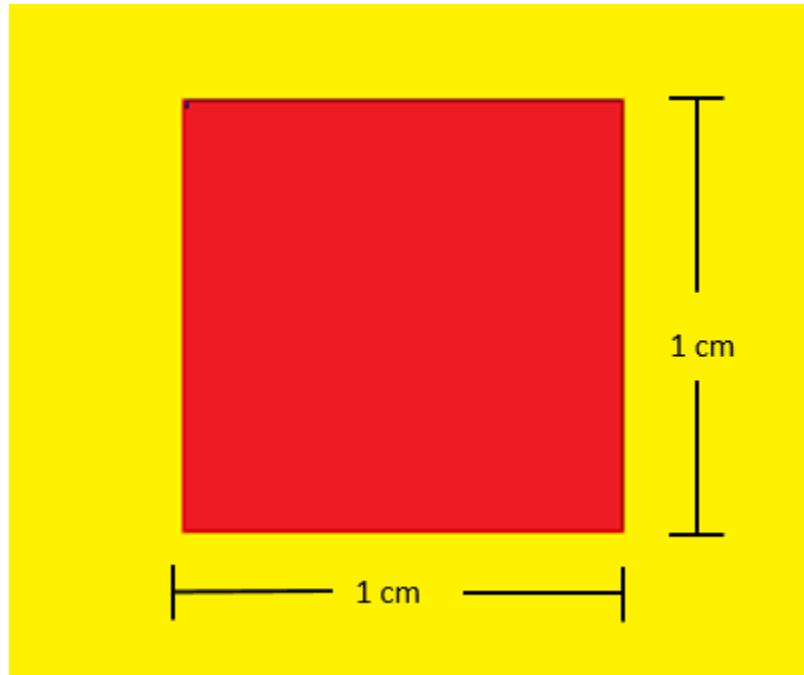
Figure 3.1: UO₂ Fuel Pellet Model

The fuel rod model consists of 400 fuel pellets stacked on one another surrounded by zirconium alloy cladding. The fuel pellets are identical to the one shown in Figure 3.1 with a density of 10.96 g/cm^3 and a radius and height of 1 cm. The total length of the fuel rod is 400 cm. The rod is surrounded by zirconium alloy cladding with a thickness of 0.06 cm (53) and a density of 6.5 g/cm^3 (30). Figure 3.2 shows a cross-sectional view of the MCNP UO_2 fuel rod geometry. The red is the UO_2. The yellow is dry air. The blue is the cladding.
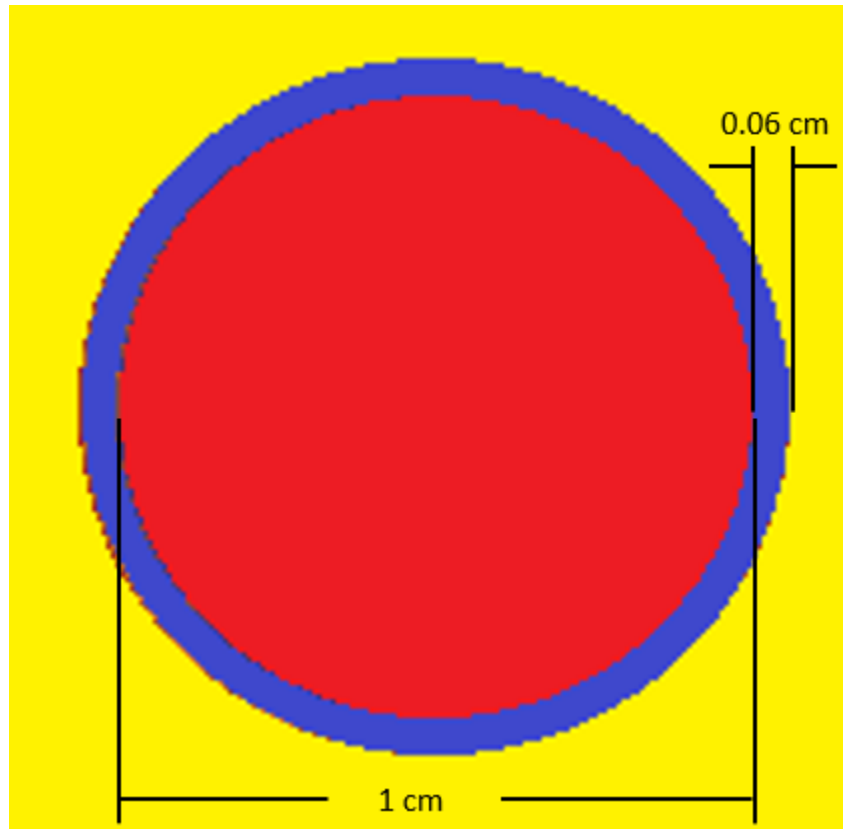
Figure 3.2: UO₂ Fuel Rod Model

The can of powdered UO_2 consists of UO_2 with a density of 2.5 g/cm^3. The outer

radius and height are 5.23 cm. The steel can is 0.39 cm thick and has a density of 7.8 g/cm^3.

These dimensions were chosen as they allow the can to contain approximately 990 g of

uranium and is consistent with UISO standards (54). Figure 3.3 shows the MCNP UO_2 can

geometry. The red is the UO_2. The yellow is dry air. The orange is the can.
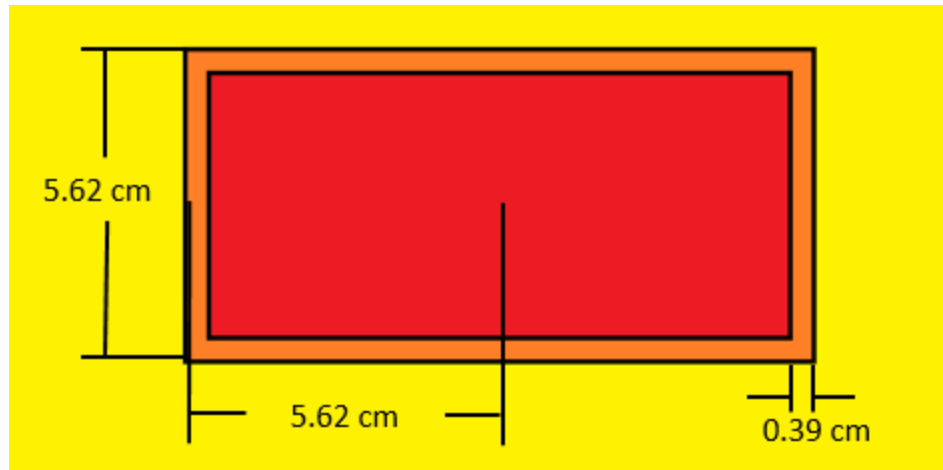
Figure 3.3: UO₂ Can Model

3.3.6. Effects on Security

The introduction of ^{232}U in uranium material will increase the detectability of the material and thus benefits security measures. Considering the energetic gamma rays of ^{232}U daughter products and the relatively high spontaneous fission neutron emission rate of ^{232}U, the presence of ^{232}U will increase the ability to detect the material by way of both gamma ray and neutron detectors.

The model used in the security analysis is a sphere of metallic uranium with a 5.39 cm radius. The security model has a density of 19.05 g/cm^3 and total uranium mass of 12.5 kg. This mas was chosen as it is similar to ½ of a significant quantity (12.5 kg) (11). The analysis will include the model unshielded and surrounded by 1 cm of lead shielding with a density of 11.3 g/cm^3. The model will be analyzed first with the weapons grade (90%) vector with ^{232}U. Then the analysis will be repeated for the weapons grade (90%) vector without ^{232}U in order to illustrate the effect the introduction of ^{232}U had on the overall detectability of the material. This model was chosen as the major focus of security to detect

covert smuggling of direct use materials. Figure 3.4 shows the shielded security model. The

red is the metallic uranium. The green is the lead. The yellow is dry air.
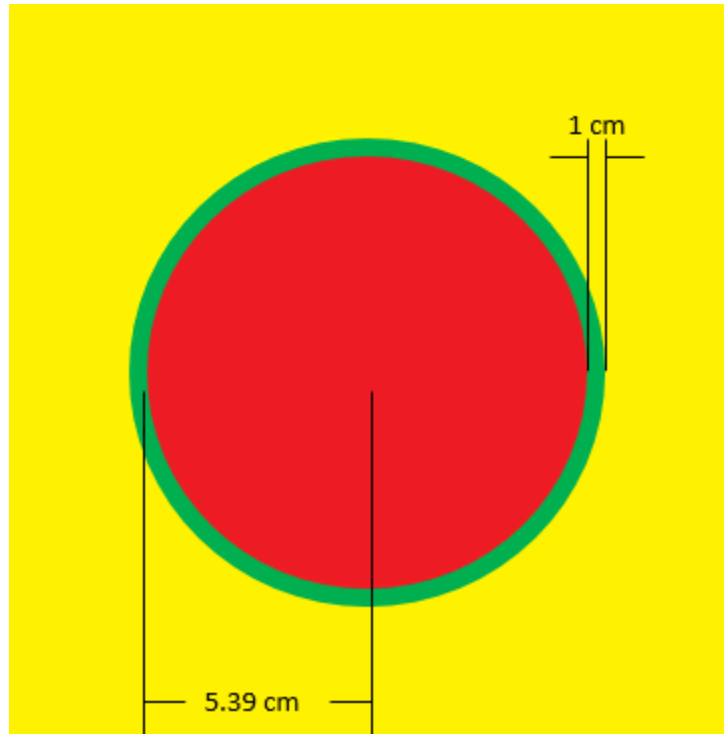
Figure 3.4: Security Model

The gamma detector chosen for this analysis is a NaI-Tl detector. This detector

consists of a solid 4"x4"x16" block of NaI-Tl with a density of 2.7 g/cm^3 incased in a 0.04"

shell of aluminum. It was chosen because its high-efficiency is more important for security

purposes than energy resolution. Figure 3.5 shows the gamma detector used here.

Figure 3.5: 4x4x16 NaI-Tl Detector

The gamma detector is 10 meters from the surface of the model and oriented such that the 4"x16" side faced the model. This configuration is simulated in MCNP6 using gamma ray spectra from RadSrc. The final spectrum will include a background spectrum taken by this detector within a concrete building at Virginia Commonwealth University in Richmond, Virginia. The measurement time for the spectra are 5 minutes.

The neutron detector utilized here has four ^{3}He tubes surrounded by high density polyethylene (HDPE). This detector will count the number of neutrons, rather than create an energy spectrum. Each ^{3}He tube has a height of 32" and a radius of 1" at a pressure of 4 atm. The outer dimensions of the HDPE are 7.22"x7.15"x47.5". The detector is 10 meters from the model and oriented such that the sides of the ^{3}He tubes face the model. Figure 3.6 shows the neutron security detector model in MCNP6. The purple is the ^{3}He. The green is the HDPE. The yellow is dry air.
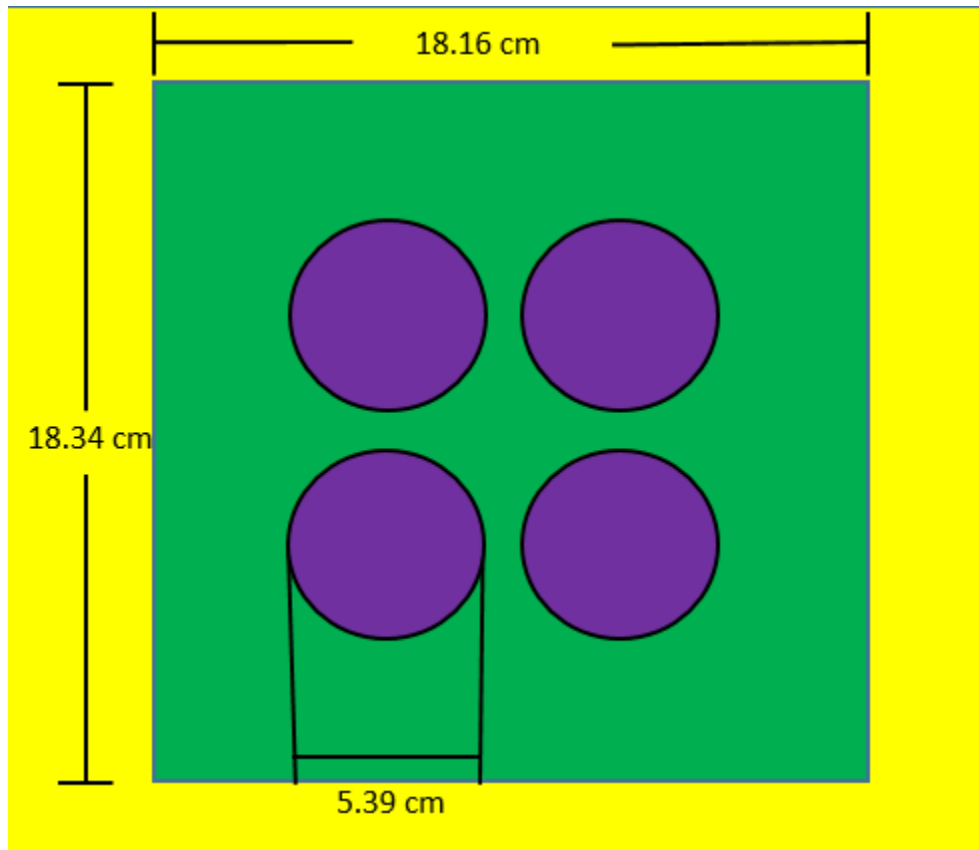
Figure 3.6: Neutron Security Detector

As with the gamma ray measurements, the model shown in Figure 3.4 will first be measured for 5 minutes with the weapons grade (90%) vector with ^{232}U. The results will then be compared to the results from the same 5-minute measurement interval with the weapons grade (90%) vector without ^{232}U. The total number of neutrons from each measurement plus the estimated background counts are compared to quantify the increase in neutron detectability from the introduction of ^{232}U.

3.3.7. Effects on Safeguards

In order to implement uranium materials containing ^{232}U into civilian nuclear fuel cycles, the effects on safeguards measurements must be explored. Basic nondestructive assay safeguards techniques of both gamma rays and neutrons are used to determine their

effectiveness on uranium materials containing ^{232}U. The can model in Figure 3.3 is used for this analysis.

The gamma ray technique used here is a method to calculate the enrichment of ^{235}U in the sample. This method compared the ratio of the intensity of the 185.7 keV ^{235}U peak to the 1001 keV ^{234m}Pa. The ^{234m}Pa peak can be used in place of a ^{238}U peak because ^{238}U is in secular equilibrium with ^{234m}Pa at the time intervals considered in this study (0.5 year and 10 years). Equation 3.10 shows the ratio of the peak areas of the ^{235}U and ^{238}U without ^{232}U to the ratio of the peak areas of the ^{235}U and ^{238}U with ^{232}U (23). This technique is applied to each of the pairs of uranium vectors shown in Table 3.6 and Table 3.7 excluding the 90% vectors.

Equation 3.18

$$1 = \frac{\frac{^{235}U_{without\ U-232}}{^{238}U_{without\ U-232}}}{\frac{^{235}U_{with\ U-232}}{^{238}U_{with\ U-232}}}$$

The intensity of each of the peaks is found via the three-window extraction technique. The three-window extraction technique calculates the net peak area by calculating and subtracting the continuum from the peak (55). The continuum is calculated by forming two windows on both sides of the peak. Equation 3.19 shows the continuum counts (B) as a function of the number of bins in the peak's region (N), the number of counts in the region to the left (B_1), the number of bins in the region to the left (n_1), the number of counts in the region to the right (B_2), and the number of bins in the region to the right (n_2).

Equation 3.19

$$B = N \frac{1}{2}\left(\frac{B_1}{n_1} + \frac{B_2}{n_2}\right)$$

As shown in Equation 3.20, the continuum counts calculated in Equation 3.19 (B) is

subtracted from the gross counts in the peak region (P), yielding the net peak area (S).

Equation 3.20

$$S = P - B$$

A 2"x2" HPGe detector is chosen for the safeguards measurements, because of its

high energy resolution which allows for easy identification and analysis of the ^{235}U and ^{238}U

peaks. MCNP6 is used to generate a gamma ray spectrum and the measurements are 5

minutes.

The neutron techniques chosen here are active and passive neutron

coincidence/multiplicity counting. Both techniques seek to quantify the mass of uranium in

the sample. An active measurement refers to a measurement in which the sample is being

irradiated by a source during the measurement, in this case with neutrons. A passive

measurement refers to a measurement in which the sample is being measured without an

external source of radiation. Typically, neutron measurements on uranium materials are

active because the spontaneous fission neutron generation rate of naturally occurring

uranium isotopes are relatively low. However, passive measurements of uranium materials

have been shown effective in calculating the ^{238}U$_{\text{eff}}$ mass (56).

A brief review neutron multiplicity basics is useful in understanding the analyses

used here. Considering neutrons are released in multiples from fission events, the detection

of these multiples can be related to the mass of material being measured. The detection of a

single neutron is known as a singles count (S). The detection of two neutrons closely

correlated in time is known as a doubles count (D). The detection of three neutrons closely correlated in time is known as a triples count (T).

Passive neutron measurements can be used to calculate an "effective" mass, typically of the isotope with a notable contribution to the neutron generation rate. In this analysis, the effective ^{238}U mass ($m_{238\,eff}$) and ^{232}U mass ($m_{232\,eff}$) are used. Equation 3.21 shows the relationship between the k value for the ^{23x}U isotope ($k_{23x}{}^{238}$) and the spontaneous fission rate per unit mass of the ^{23x}U isotope (F_{0_23x}), the second spontaneous fission factorial moment of the ^{23x}U isotope (v_{s2_23x}), the spontaneous fission rate per unit mass of ^{238}U (F_{0_238}), and the second spontaneous fission factorial moment of ^{238}U (v_{s2_238}).

Equation 3.21

$$k_{23x}^{238} = \frac{F_{0\_23x} v_{s2\_23x}}{F_{0\_238} v_{s2\_238}}$$

Equation 3.22 shows the relationship between the effective ^{238}U mass ($m_{238\,eff}$) and the k values of each uranium isotope and the mass of each uranium isotope.

Equation 3.22

$$m_{238\,eff} = k_{232}^{238} m_{232} + k_{234}^{238} m_{234} + k_{235}^{238} m_{235} + m_{238}$$

Equation 3.23 shows the relationship between the k value for the ^{23x}U isotope ($k_{23x}{}^{232}$) and the spontaneous fission rate per unit mass of the ^{23x}U isotope (F_{0_23x}), the second spontaneous fission factorial moment of the ^{23x}U isotope (v_{s2_23x}), the spontaneous fission rate per unit mass of ^{232}U (F_{0_232}), and the second spontaneous fission factorial moment of ^{232}U (v_{s2_232}).

Equation 3.23

$$k_{23x}^{232} = \frac{F_{0\_23x} v_{s2\_23x}}{F_{0\_232} v_{s2\_232}}$$

Equation 3.24 shows the relationship between the effective ^{232}U mass ($m_{232\,eff}$) and

the k values of each uranium isotope and the mass of each uranium isotope. The k^{232}_{23x} is

the ratio of the spontaneous fission rate per mass of ^{23x}U to the spontaneous fission rate

per mass of ^{232}U.

Equation 3.24

$$m_{232\,eff} = m_{232} + k^{232}_{234}m_{234} + k^{232}_{235}m_{235} + k^{232}_{238}m_{238}$$

Equation 3.25 shows the relationship between the effective ^{238}U mass ($m_{238\,eff}$) with

the singles counts (S), doubles counts (D), detector efficiency (ε), doubles gate fraction (f_d),

leakage multiplication factor (M_L), the first factorial induced fission multiplicity of ^{235}U (v_{i1}),

the second factorial induced fission multiplicity of ^{235}U (v_{i2}), the first factorial spontaneous

fission multiplicity of ^{238}U (v_{s2}), and the spontaneous fission yield of ^{238}U (F_0) (56).

Equation 3.25

$$m_{238\,eff} = \frac{\dfrac{2D}{\varepsilon f_d} - \dfrac{M_L(M_L - 1)v_{i2}S}{v_{i1} - 1}}{\varepsilon F_0 M_L^2 v_{s2}}$$

Equation 3.26 shows the relationship between the effective ^{232}U mass ($m_{232\,eff}$) with

the singles counts (S), doubles counts (D), detector efficiency (ε), doubles gate fraction (f_d),

leakage multiplication factor (M_L), the first factorial induced fission multiplicity of ^{235}U (v_{i1}),

the second factorial induced fission multiplicity of ^{235}U (v_{i2}), the first factorial spontaneous

fission multiplicity of ^{232}U (v_{s2}), and the spontaneous fission yield of ^{232}U (F_0).

Equation 3.26

$$m_{232\,eff} = \frac{\dfrac{2D}{\varepsilon f_d} - \dfrac{M_L(M_L - 1)v_{i2}S}{v_{i1} - 1}}{\varepsilon F_0 M_L^2 v_{s2}}$$

Equation 3.27 shows the relationship between the doubles gate fraction (f_d) as a function of the pre-delay gate width (P), the gate width (G), and the neutron die-away time (τ).

Equation 3.27

$$f_d = e^{-\frac{P}{\tau}}(1 - e^{-\frac{G}{\tau}})$$

The leakage multiplications (M_L) is calculated using three coefficients (a, b, c). Considering the coefficients contain values specific to the uranium isotope whose effective mass is being calculated, it must be calculated for both the ^{238}U and ^{232}U effective masses. Equation 3.28 shows the relationship between the leakage multiplication (M_L) and the coefficients (a, b, c).

Equation 3.28

$$a + bM_L + cM_L^2 + M_L^3 = 0$$

Equation 3.29 shows the relationship between a and the singles counts (S), the triples counts (T), the first factorial induced fission multiplicity (ν_{i1}), the second factorial induced fission multiplicity (ν_{i2}), the third factorial induced fission multiplicity (ν_{i3}), the second factorial spontaneous fission multiplicity (ν_{s2}), the third factorial spontaneous fission multiplicity (ν_{s3}), the efficiency of the detector (ε), and the triples gate fraction (f_t).

Equation 3.29

$$a = -\frac{6T\nu_{s2}(\nu_{i1} - 1)}{\varepsilon^2 f_t S(\nu_{s2}\nu_{i3} - \nu_{s3}\nu_{i2})}$$

Equation 3.30 shows the relationship between b and the singles counts (S), the doubles counts (D), the first factorial induced fission multiplicity (ν_{i1}), the second factorial induced fission multiplicity (ν_{i2}), the third factorial induced fission multiplicity (ν_{i13}), the

second factorial spontaneous fission multiplicity (v_{s2}), the third factorial spontaneous

fission multiplicity (v_{s3}), the efficiency of the detector (ε), and the doubles gate fraction (f_d).

Equation 3.30

$$b = \frac{2D[v_{s3}(v_{i1} - 1) - 3v_{s2}v_{i2}]}{\varepsilon f_d S(v_{s2}v_{i3} - v_{s3}v_{i2})}$$

Equation 3.31 shows the relationship between c and the singles counts (S), the

doubles counts (D), the first factorial induced fission multiplicity (v_{i1}), the second factorial

induced fission multiplicity (v_{i2}), the third factorial induced fission multiplicity (v_{i13}), the

second factorial spontaneous fission multiplicity (v_{s2}), the third factorial spontaneous

fission multiplicity (v_{s3}), the efficiency of the detector (ε), and the doubles gate fraction (f_d).

Equation 3.31

$$c = \frac{6Dv_{s2}v_{i2}}{\varepsilon f_d S(v_{s2}v_{i3} - v_{s3}v_{i2})} - 1$$

Table 3.9 shows the induced fission multiplicities of ^{235}U and the spontaneous

fission multiplicities of ^{238}U. These values for ^{232}U will be obtained using MCNP6.

Table 3.9: Induced and Spontaneous Fission Multiplicities

	v_{i1}	v_{i2}	v_{i3}	v_{s1}	v_{s2}	v_{s3}
^{235}U	2.69	6.17	11.57	-	-	-
^{238}U	-	-	-	1.99	2.87	2.82
^{232}U	-	-	-	1.71	2.34	2.33

The neutron die away time is related to the detector configuration and is often cited

from a known value. However, an MCNP output can also be used to calculate it. The doubles

counts from two gate widths (one is the standard gate width for that detector (G) and the

other is half the standard gate width) are used to calculate the neutron die away time.

Equation 3.32 shows the relationship between the neutron die away time (τ) to the shorter

gate width (G_1), the normalized doubles counts from the shorter gate (D_1), and the

normalized doubles counts from the longer gate (D_2).

Equation 3.32

$$\tau = \frac{G_1}{\ln\left(\frac{D_2}{D_1} - 1\right)}$$

Similarly, the efficiency can also be calculated via MCNP. Equation 3.33 shows the

relationship between the efficiency (ε) and the normalized singles counts (S_{norm}) and the

net multiplication (M_{net}).

Equation 3.33

$$\varepsilon = \frac{S_{norm}}{M_{net}}$$

The passive technique described here will first be used to calculate the effective ^{238}U

mass and then the effective ^{232}U mass. These masses will be compared to the known value.

The can model with the uranium vectors that do not include ^{232}U are simulated to calculate

an effective ^{238}U mass in each case. This will be repeated with the uranium vectors

including ^{232}U and both the ^{238}U and ^{232}U effective masses will be used.

Active neutron coincidence counting is a bit more simplistic. The doubles counts

from the same detector and sample configuration have a linear relationship to the ^{235}U

mass, for small multiplication values (56). Multiple samples having the same geometry and

mass but various ^{235}U concentrations can be measured and related to the ^{235}U mass.

Repeating this procedure for each of the uranium vectors containing ^{232}U in the can model

will illustrate the methods effectiveness at verifying ^{235}U mass despite the presence of ^{232}U.

The major source of uncertainty are the singles, doubles, and triples counts. The computational uncertainties from the MCNP6 simulations are not related to the uncertainties expected in a real world measurement. In order to estimate the uncertainties of a real world measurement, a technique developed by Dr. Croft will be used (57). Equation 3.34 shows the relationship between the singles count rate uncertainty (σ_s) and the singles count rate (S_r), the measurement time (t), the doubles count rate (D_r), and the doubles gate fraction (f_d).

Equation 3.34

$$\sigma_S = \sqrt{\frac{S_r}{t} + \frac{2D_r}{f_d t}}$$

Equation 3.35 shows the relationship between the doubles count rate uncertainty (σ_D) and the gate width (G), the doubles gate fraction (f_d), the neutron die away time (τ), the singles count rate (S_r), the doubles count rate (D_r), and the measurement time (t).

Equation 3.35

$$\sigma_D = \sqrt{(1 + 8(1 - \frac{1 - e^{-\frac{G}{\tau}}}{\frac{G}{\tau}})(\frac{D_r}{S_r f_d}))\frac{D_r + 2S_r^2 G}{t}}$$

Equation 3.36 shows the relationship between the triples count rate (σ_T), which is

Equation 3.36

$$\sigma_T = \sqrt{\left(\left(1 + 10\left(1 - \frac{1 - e^{-\frac{G}{\tau}}}{\frac{G}{\tau}}\right)\left(\frac{D}{f_d S}\right)\right)\left(\frac{1}{t}\right)\left(T + 2SG\left(\left(1 + \frac{D}{f_d}\left(1 - \frac{1 - e^{-\frac{G}{\tau}}}{\frac{G}{\tau}}\right)\right) + \frac{S^2 G}{2}\right)\right)\right)}$$

The Active Well Coincidence Counter (AWCC) is used for both the passive and active simulations. Although the AWCC has primarily an active configuration, the neutron sources can be removed making it a passive configuration. The AWCC has 42 ^{3}He tubes embedded in HDPE. The sample cavity is 20 cm in diameter and can be adjusted from 23 to 35 cm in height. In its active configuration, the AWCC has two AmLi neutron sources (58). The AWCC can be operated in two modes; thermal or fast mode. In fast mode, a cadmium sleeve is used to remove thermal neutrons thus preventing them from scattering back into the sample and inducing fission. The cadmium sleeve is removed in thermal mode (59). The MCNP6 model of the AWCC used for this analysis is in fast mode.

4. RESULTS AND DISCUSSIONS

4.1. Plutonium Analysis

4.1.1. Model Based Analysis

This section contains both the steady state and transient temperature profiles of the various models described earlier. The plutonium vector shown in Table 3.1 is utilized in the weapons pit of each model with the exception of the Kessler comparison.

Figure 4.1 shows the steady state temperature profile of Kessler's high technology model from Figure 2.1 with the plutonium vector shown in Table 3.2. The temperature within the high explosives does surpass the self-explosion temperature. This self-explosion would render the HNED useless. Kessler's plutonium vector has less than half the ^{238}Pu concentration as the plutonium vector from the Lightbridge fuel simulation. However, the temperature barely reaches the self-explosion temperature and as previously discussed, Kessler's model does not represent a limiting case. Therefore, the ^{238}Pu concentration in Kessler's plutonium vector would not be enough to reach the self-explosion temperature in the high explosive of a more limiting case HNED.
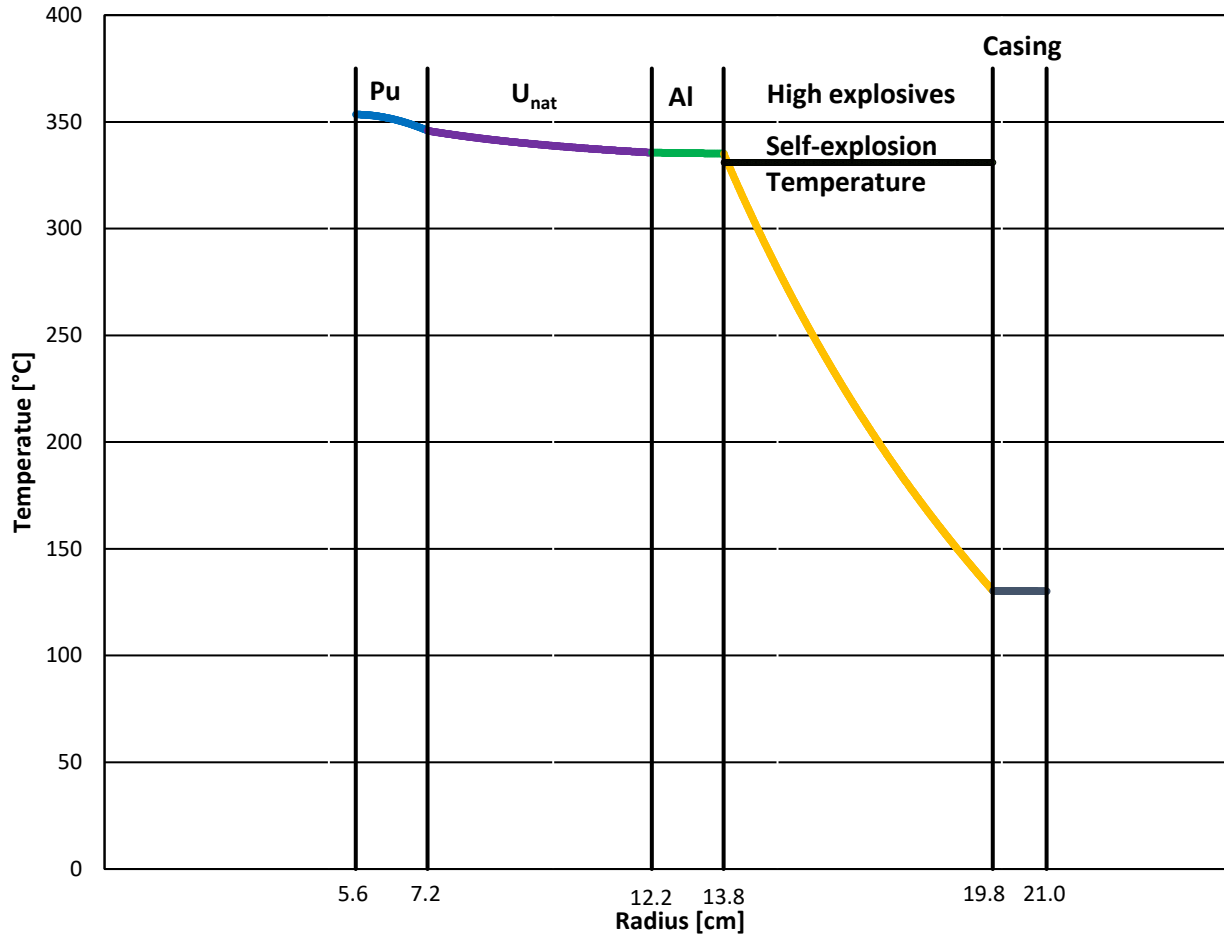
Figure 4.1: Steady State Temperature Profile of Kessler's Model (60)

The decay heat contribution from the plutonium vector in Table 4.1 in each layer of

Model One is shown Table 4.1. All decay heat contributions besides α and β decay within

the plutonium pit are negligible. Thus only the heat generation from α and β decay within

the plutonium pit will be included.

Table 4.1: Decay Heat Contribution within Model One [W] (60)

Material	α/β decay	γ	spontaneous fission					total
			γ	n	fission fragments	induced fission	total	
Pu	$8.71 \cdot 10^2$	$2.80 \cdot 10^{-1}$	$9.68 \cdot 10^{-4}$	$9.09 \cdot 10^{-4}$	$2.47 \cdot 10^{-3}$	$9.68 \cdot 10^{-4}$	$5.31 \cdot 10^{-3}$	$8.70 \cdot 10^2$
U_{nat}	$1.71 \cdot 10^{-3}$	$6.10 \cdot 10^{-5}$	$2.41 \cdot 10^{-4}$	$2.28 \cdot 10^{-4}$	$2.47 \cdot 10^{-3}$	$2.41 \cdot 10^{-4}$	$3.18 \cdot 10^{-3}$	$4.95 \cdot 10^{-3}$
Al	-	$1.17 \cdot 10^{-10}$	$5.94 \cdot 10^{-6}$	$2.81 \cdot 10^{-6}$	-	-	$8.75 \cdot 10^{-6}$	$8.75 \cdot 10^{-6}$
PBX 9502	-	$1.37 \cdot 10^{-11}$	$3.07 \cdot 10^{-5}$	$1.06 \cdot 10^{-5}$	-	-	$4.13 \cdot 10^{-5}$	$4.13 \cdot 10^{-5}$
Steel casing		$0.00 \cdot 10^0$	$2.94 \cdot 10^{-7}$	$3.53 \cdot 10^{-10}$	-	-	$2.95 \cdot 10^{-7}$	$2.95 \cdot 10^{-7}$

Figure 4.2 shows the steady state temperature profile of Model One. The temperature within the high explosives reaches the self-explosion temperature, rendering the HNED useless.
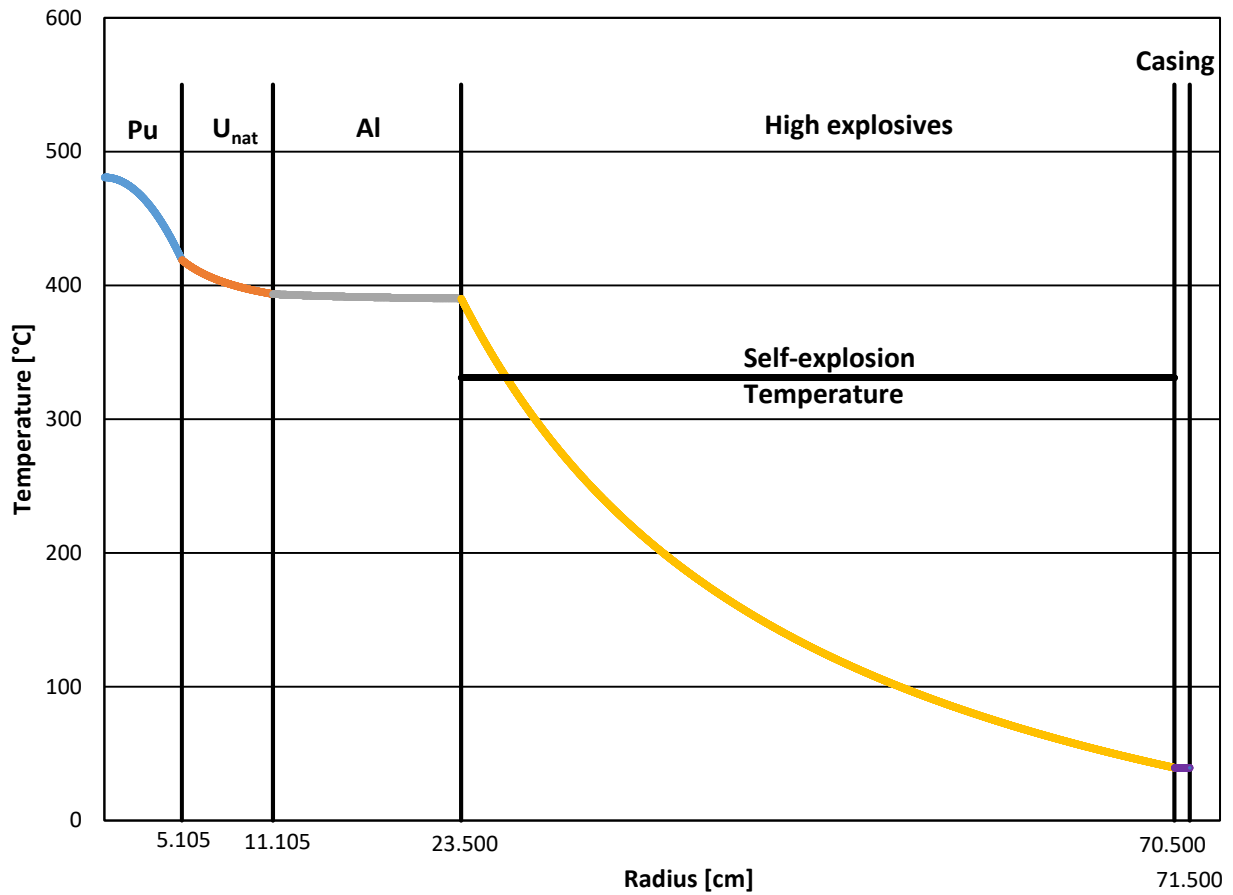
Figure 4.2: Model One Steady State Temperature Profile (60)

Table 4.2 shows each decay heat contribution within each layer of Model Two. As in Model One, only α and β decay within the plutonium is notable and all other decay heat contributions are considered negligible.

Table 4.2: Decay Heat Contributions within Model Two [W] (60)

Material	α/β decay	γ	spontaneous fission					total
			γ	n	fission fragments	induced fission	total	
Pu	$4.93\cdot10^2$	$1.58\cdot10^{-1}$	$2.14\cdot10^{-6}$	$3.23\cdot10^{-5}$	$1.41\cdot10^{-3}$	$3.44\cdot10^{-5}$	$1.48\cdot10^{-3}$	$4.94\cdot10^2$
Be	-	$1.91\cdot10^{-5}$	$9.21\cdot10^{-8}$	$2.67\cdot10^{-7}$	-	-	$3.59\cdot10^{-7}$	$1.94\cdot10^{-5}$
U_{dep}	$5.29\cdot10^{-4}$	$3.35\cdot10^{-5}$	$1.57\cdot10^{-6}$	$6.01\cdot10^{-6}$	$9.06\cdot10^{-9}$	$6.39\cdot10^{-6}$	$1.40\cdot10^{-5}$	$5.77\cdot10^{-4}$
PBX 9502	-	$1.15\cdot10^{-8}$	$1.12\cdot10^{-7}$	$5.11\cdot10^{-7}$	-	-	$6.23\cdot10^{-7}$	$6.34\cdot10^{-7}$
Al casing	-	$1.04\cdot10^{-9}$	$1.25\cdot10^{-8}$	$3.77\cdot10^{-9}$	-	-	$1.63\cdot10^{-8}$	$1.73\cdot10^{-8}$

Figure 4.3 shows the steady state temperature profile within Model Two. The temperature within the high explosives surpasses the self-explosion temperature by nearly 100 °C. Like Model One, Model Two would be rendered useless.
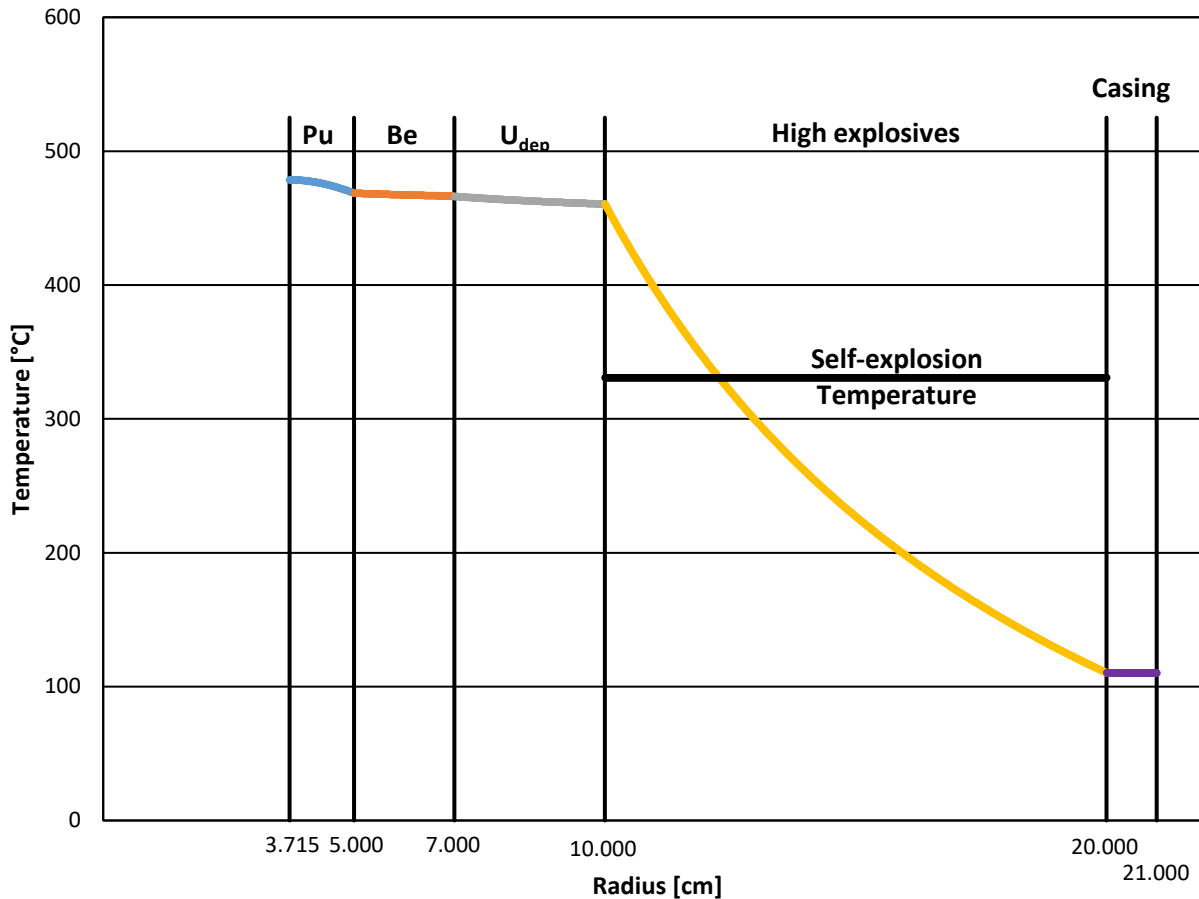
Figure 4.3: Model Two Steady State Temperature Profile (60)

The following discussion focusses on the transient heat transfer within Model Two as a result of four different scenarios. Below is a brief review of each scenario.

- Scenario 1: the plutonium pit reaches thermal equilibrium with surrounding room then inserted into Model Two

- Scenario 2: the plutonium pit is externally cooled in liquid nitrogen then inserted into Model Two

- Scenario 3: the plutonium pit is inserted into an externally cooled Model Two

- Scenario 4: the fully assembled Model Two in thermal equilibrium with liquid nitrogen is removed and placed into a large room

Figure 4.4 shows the transient temperature profile at various time intervals of Model Two from scenario 1. The temperature within the high explosives reaches the self-explosion temperature within 7.5 hours. In order to avoid premature detonation of Model Two, the HNED must be detonated less than 7.5 hours from the insertion of the plutonium pit. This time frame is relatively small and not useful for deterrence purposes. An HNED utilized for deterrence must be armed and ready quickly for an extended period of time (months to years).
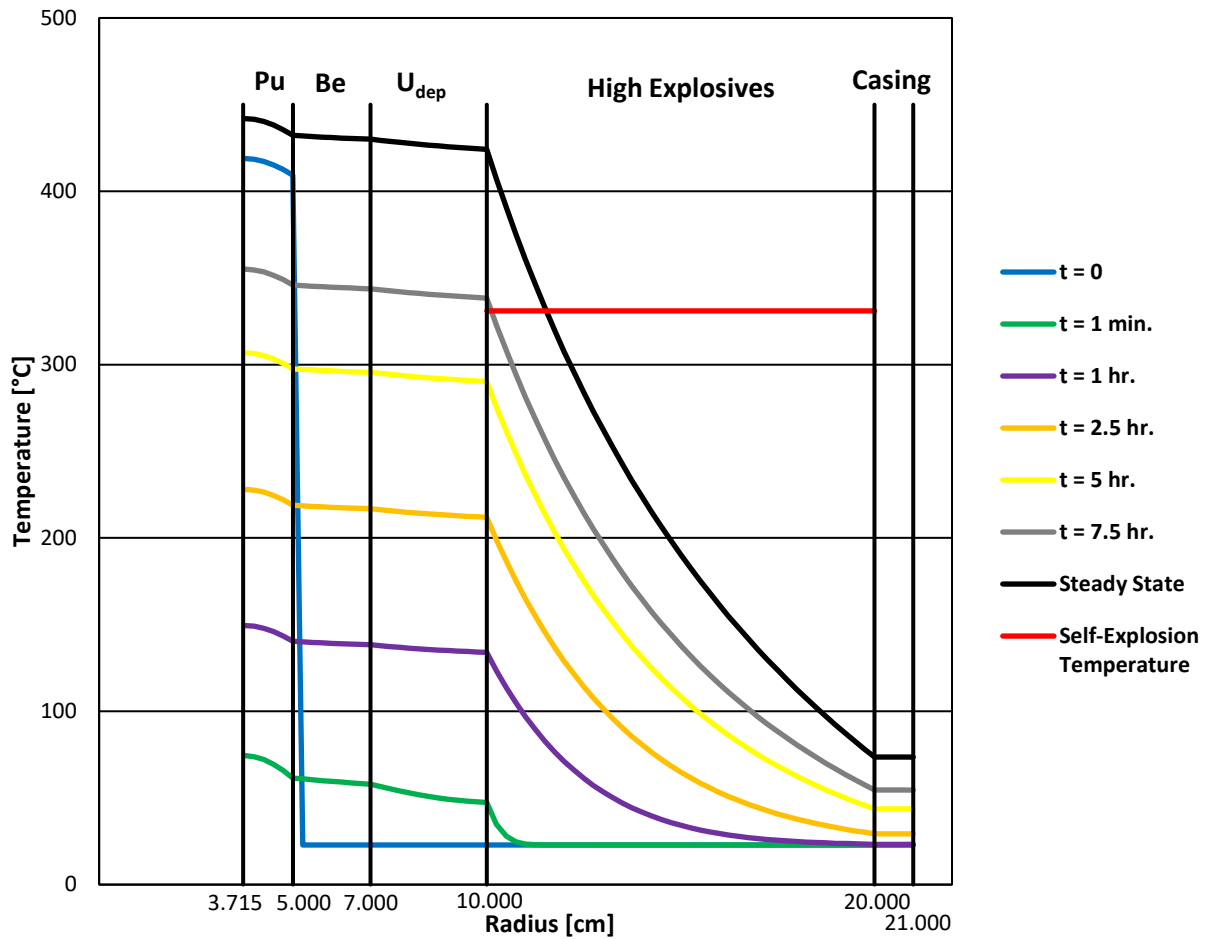

Figure 4.4: Transient Temperature Profile of Model One Scenario 1 (42)

Figure 4.5 shows the transient temperature profile at various time intervals of Model Two from scenario 2. As in scenario 1, the temperature within the high explosives

reaches the self-explosion temperature within 7.5 hours. As discussed above, this time frame is too short for deterrence purposes and would be significantly inconvenient.

Figure 4.5: Transient Temperature Profile of Model One Scenario 2 (42)

Figure 4.6 shows the transient temperature profile at various time intervals of Model Two from scenario 3. The external cooling keeps the temperature well below the high explosive temperature. Model Two could be stored externally cooled by liquid nitrogen for an indefinite amount of time. Although this would be useful for deterrence purposes, the costs of externally cooling Model Two for an extended period of time would be expensive and would likely cause other challenges that would need to be overcome.
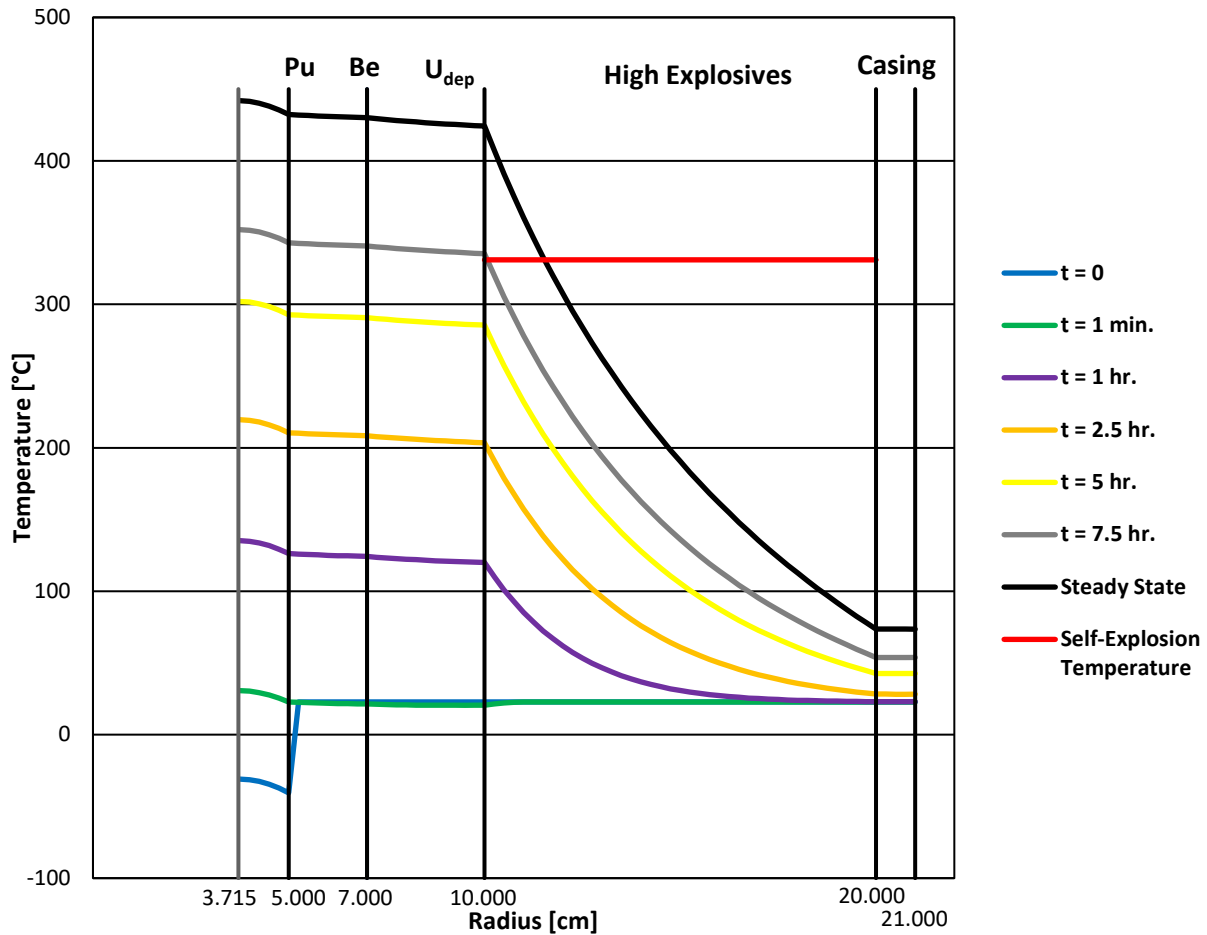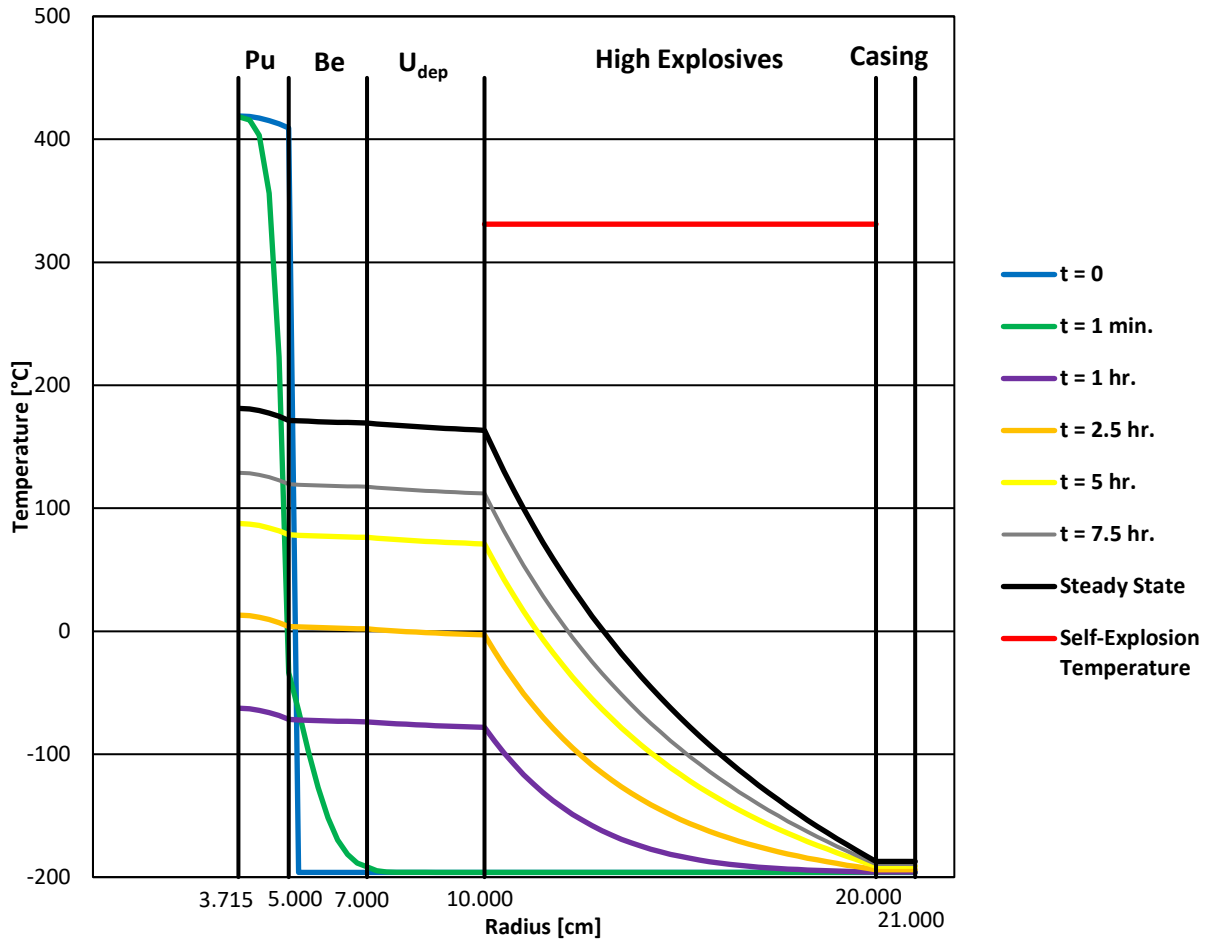
Figure 4.6: Transient Temperature Profile of Model One Scenario 3 (42)

Figure 4.7 shows the transient temperature profile at various time intervals of Model Two from scenario 4. Unlike in scenarios 1 and 2, the temperature reaches the self-explosion temperature within the high explosives in slightly longer than 7.5 hours. This scenario would also be impractical from a deterrence perspective. The results from scenarios 1, 2, and 4 show that regardless of how the pit or HNED is cooled, natural convective and radiative heat transfer within an empty room causes the temperature within the high explosives to reach the self-explosion temperature too quickly for the HNED to be useful for deterrence.
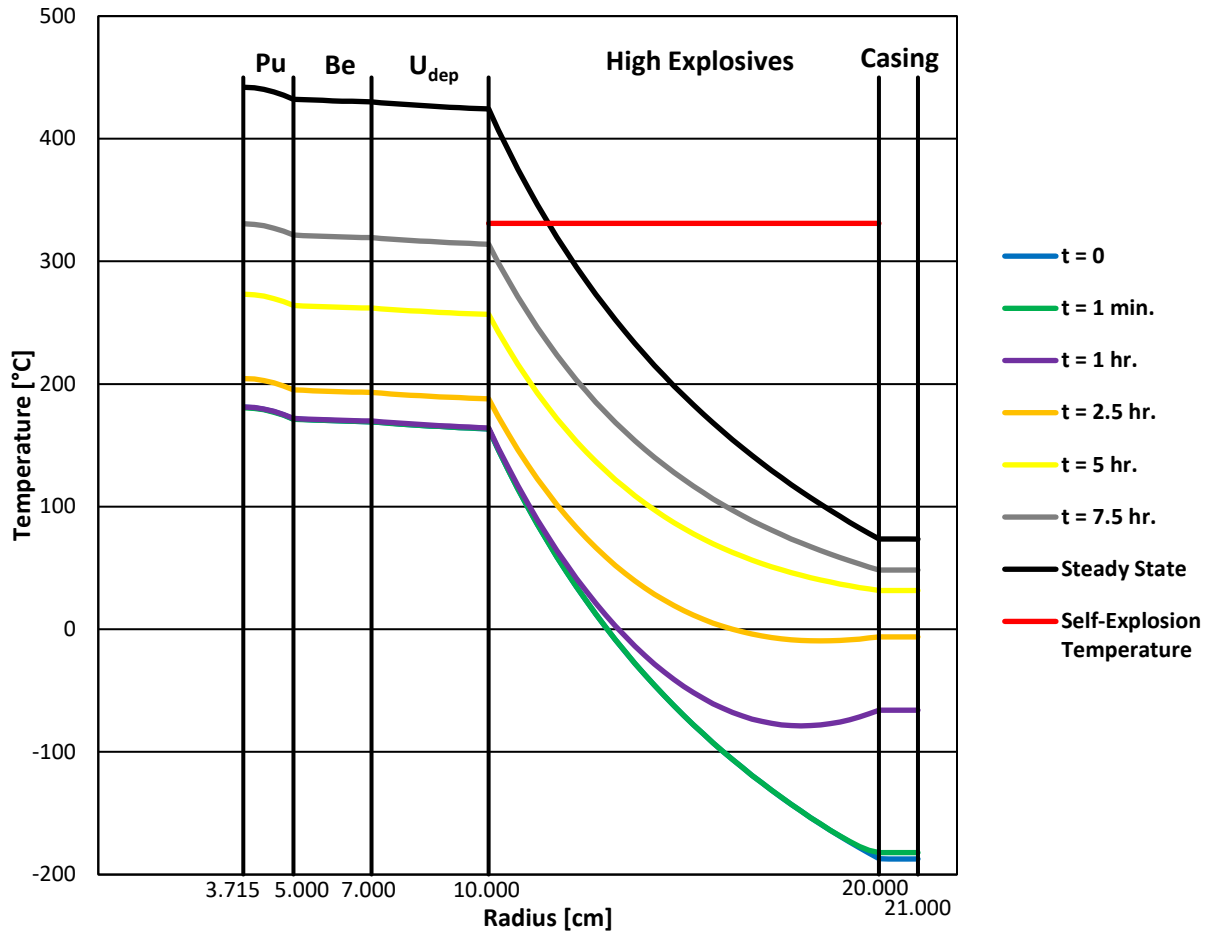
Figure 4.7: Transient Temperature Profile of Model One Scenario 4 (42)

Figure 4.8 through Figure 4.12 show the maximum thermal stress as a function of time within each layer of Model Two during each scenario and the tensile strength of that material. In the aluminum and plutonium layers, the maximum stress does not reach the tensile strength in any of the four scenarios. Thus, no plastic deformation will occur in the aluminum or plutonium layers as a result of thermal stress. In the uranium layer, the maximal thermal stress reaches the tensile strength in scenarios 1, 2, and 4 within approximately 200-300 minutes. Plastic deformation will occur within the uranium in 200-300 minutes in scenarios 1, 2, and 4, but no plastic deformation will occur in scenario 3. In the high explosives and beryllium layers, the maximum thermal stress reaches the tensile

strength in all 4 scenarios within 300 minutes. Plastic deformation will occur in the high

explosives and beryllium in all 4 scenarios. This deformation can decrease the overall

performance of Model Two by producing asymmetry within the layers. This asymmetry

will cause asymmetry within the implosion reducing the yield. Although Model Two would

likely somewhat function, the reduction of the yield may not be considered effective

depending on the adversary. In the case of a state entity, the use of a nuclear weapon that

underperforms could have dire consequences if used, because the other nuclear weapons

states will have weapons that almost certainly won't underperform. However, in the case of

a non-state entity, the use of a nuclear weapon with any notable yield may be considered
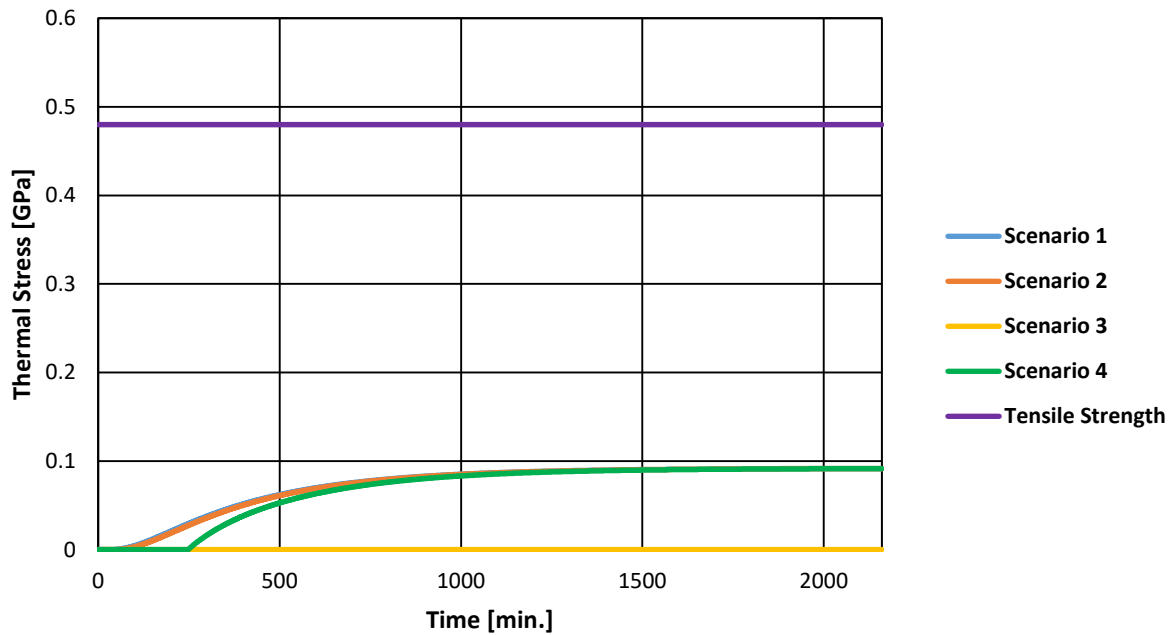
effective.

Figure 4.8: Maximum Thermal Stress within the Aluminum

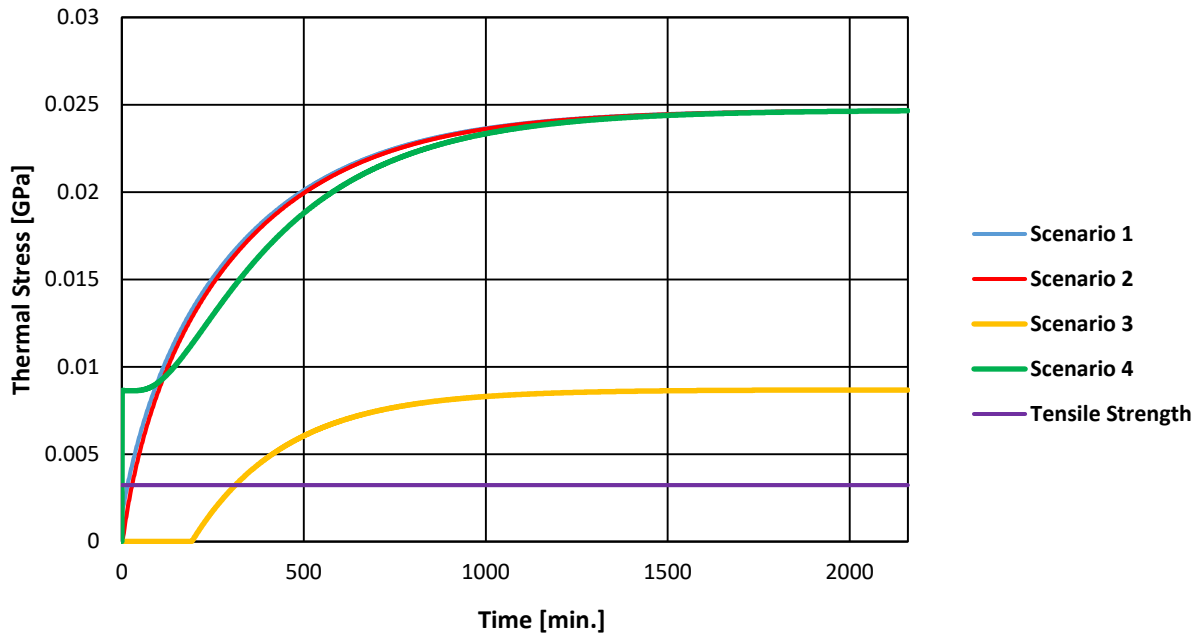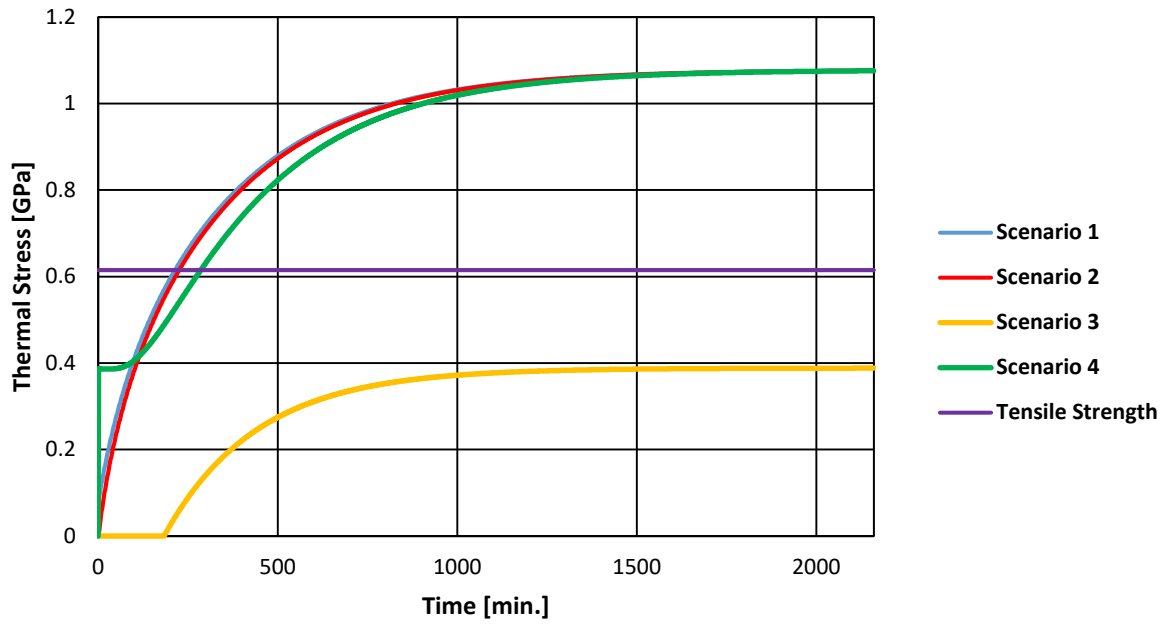*Figure 4.9: Maximum Thermal Stress within the High Explosives*
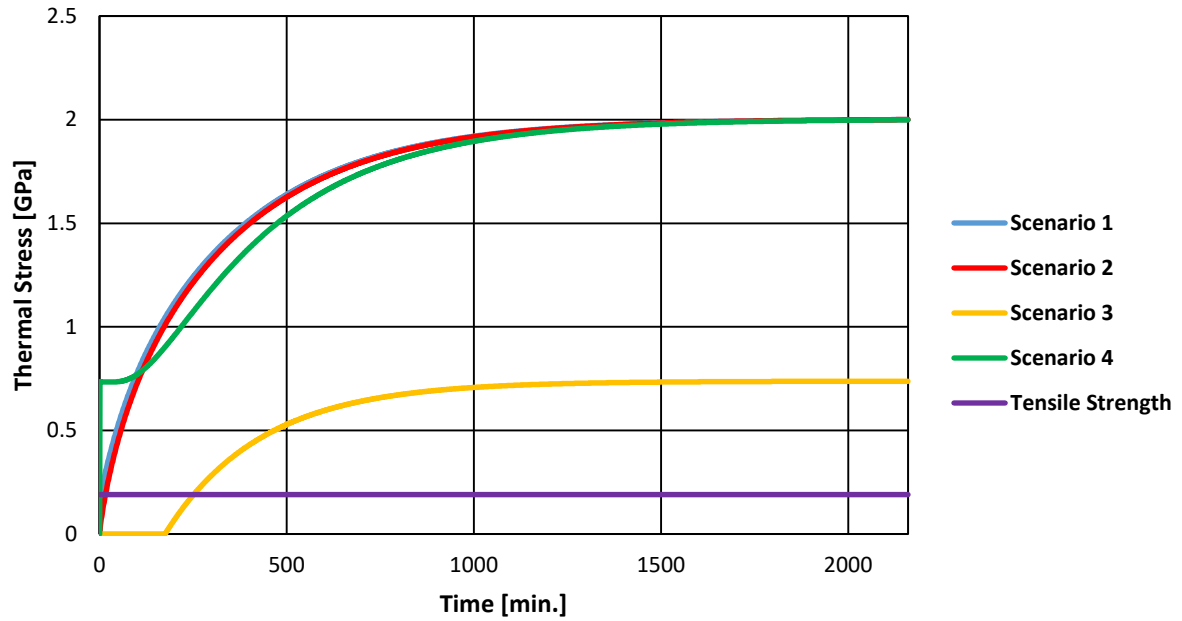

Figure 4.10: Maximum Thermal Stress within the Uranium
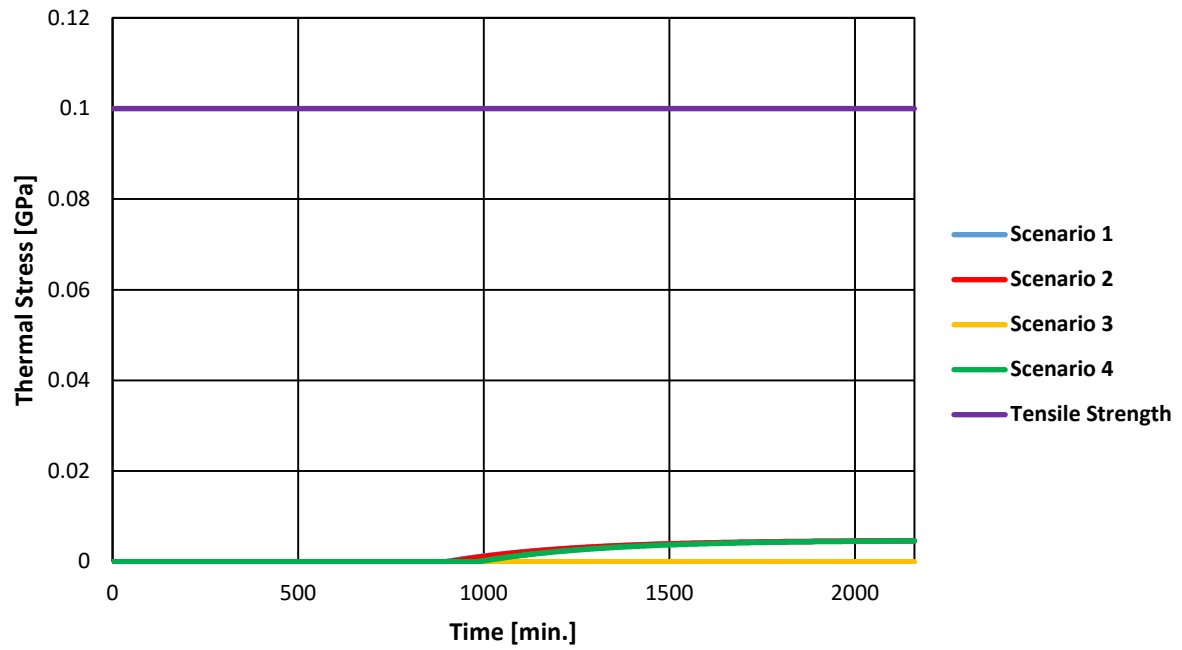
73

Figure 4.11: Maximum Thermal Stress within the Beryllium

Figure 4.12: Maximum Thermal Stress in the Plutonium

74

4.1.2. Figure of Merit Analysis

In order to calculate the FOM_1 and FOM_2 values, each of the components must first be calculated. Table 4.3 shows the FOM components: bare critical mass (M), heat decay (h), spontaneous fission neutron generation rate (S), and the dose rate (D), for the plutonium vectors from the Lightbridge fuel inspired design (LB), the light water reactor used fuel (LWR), and the mixed oxide used fuel (MOX). The uncertainty in the bare critical mass was found by repeating the k-code simulations using three different data libraries in MCNP6: .60c, .65c, and .80c. Although the bare critical mass of the Lightbridge vector is slightly lower than the LWR and MOX, the heat decay and spontaneous fission neutron generation rate are notably higher. As expected, the dose rate is relatively low.

Table 4.3: FOM Components

	LB	LWR	MOX
M [kg]	22.6 ± 0.5	24.2 ± 0.2	24.0 ± 0.3
h [W/kg]	104.6 ± 1.3	14.6 ± 0.2	24.1 ± 0.3
S [n/s·kg]·10^5	8.91 ± 0.11	5.06 ± 0.01	5.94 ± 0.01
D [rem/h]	0.0751 ± 0.0015	0.0088 ± 0.0001	0.0138 ± 0.0001

Table 4.4 shows the FOM values for the three plutonium vectors. As a review, FOM_1 applies to less technically advanced states and FOM_2 applies to technically advanced states. In the case of less technically advanced states, all three plutonium vectors are unattractive for weapons purposes. In the case of the technically advanced states, all three plutonium vectors are attractive. When comparing the LB plutonium vector to the other two (LWR and MOX), both FOM_1 and FOM_2 are notably lower. However, considering they still fall within the same range, the significance of the difference between the values is debatable and can't give any real conclusion as to which vector is more or less attractive.

Table 4.4: FOM Values

	LB	LWR	MOX
FOM_1	0.457 ± 0.010	0.720 ± 0.005	0.647 ± 0.005
FOM_2	1.260 ± 0.023	1.964 ± 0.002	1.801 ± 0.002

4.2. Uranium Analysis

4.2.1. Model Based Analysis

This section analyzes the steady state and transient heat transfer within the updated model described in Table 3.8. The weapons grade (90%) uranium vector from Table 3.6 is used. Considering Table 4.1 and Table 4.2 show that all other sources of heat are negligible, only the heat generation from the α decay within the uranium weapons pit will be included. In addition to the heat transfer, the dose rate to the high explosives will also be calculated.

Figure 4.13 shows the total heat generation in units of Watts over time. As the ^{232}U decays, its daughter products contribute additional decay heat which greatly increases the total heat generation. This value reaches a maximum after approximately 10 years.
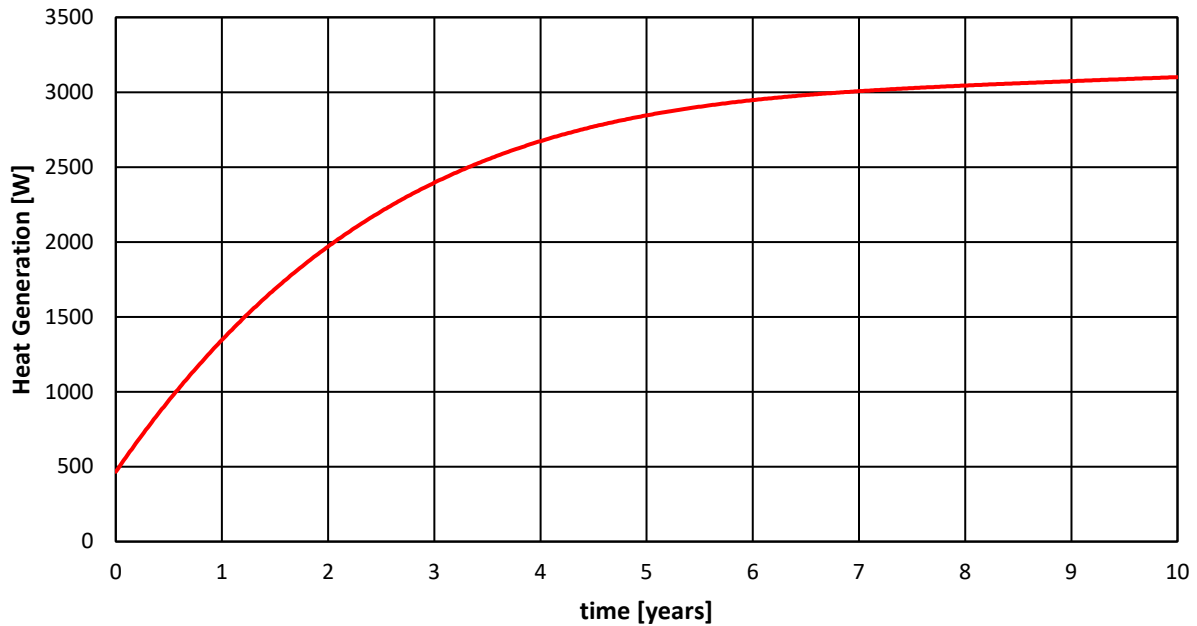
Figure 4.13: Heat Generation of Weapons Pit over Time

Although the decay heat increases over time, the rate of increase is on the order of months. As shown in the transient plutonium analysis, steady state is reached after approximately a day, so we shall assume steady state is reached at each of the time intervals of 0, 0.25, 0.5, 1, 5, and 10 years.

Figure 4.14 through Figure 4.20 show the steady state temperature profiles at the various time intervals. Even when the uranium is fresh (t=0), the temperature within the high explosives reaches its "self-explosion" temperature. Over time, the temperature within the model increase significantly to the point of exceeding the "self-explosion" temperature within the high explosives by 100's of degrees. These results show the heat generation produced is well above what is required to render the HNED useless.
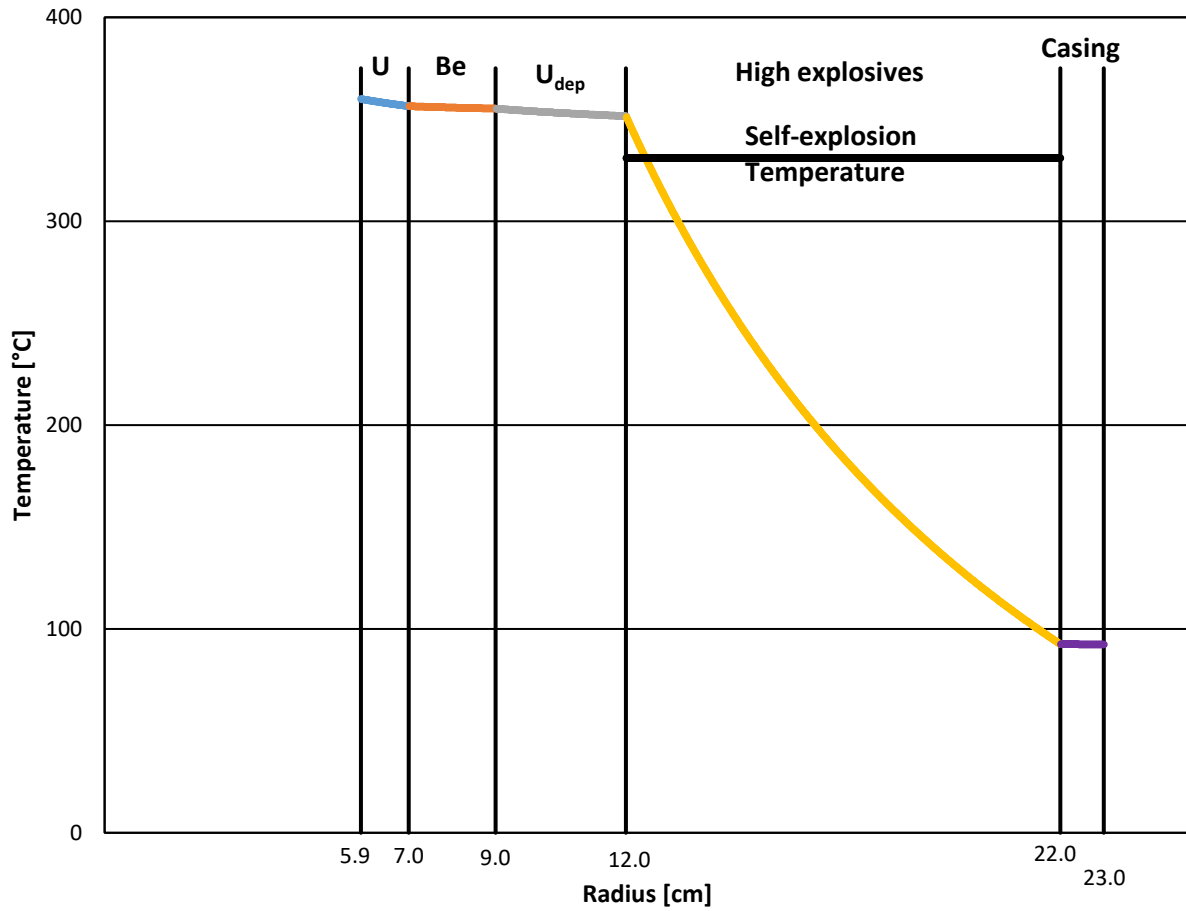
Figure 4.14: Steady State Temperature Profile at Time Interval t = 0
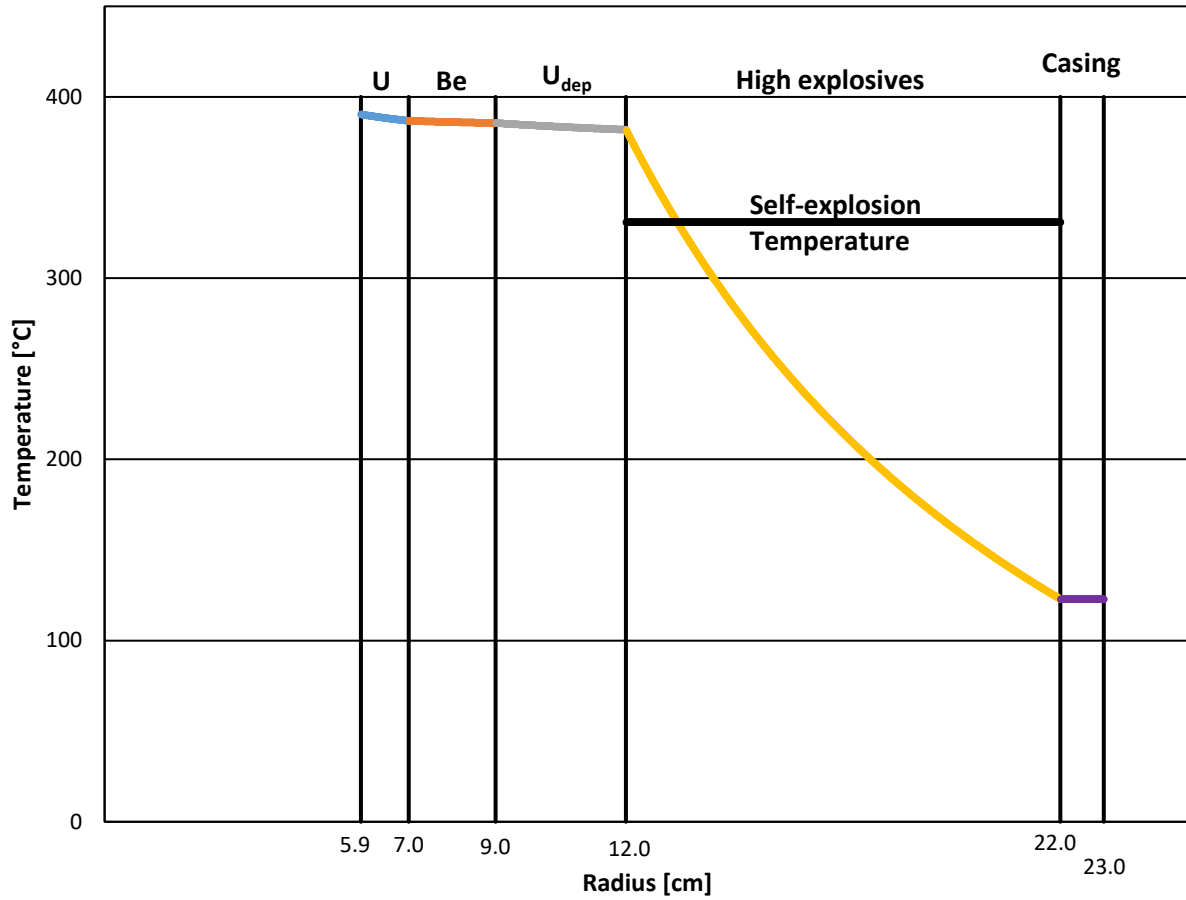
Figure 4.15: Steady State Temperature Profile at Time Interval t = 0.25 year
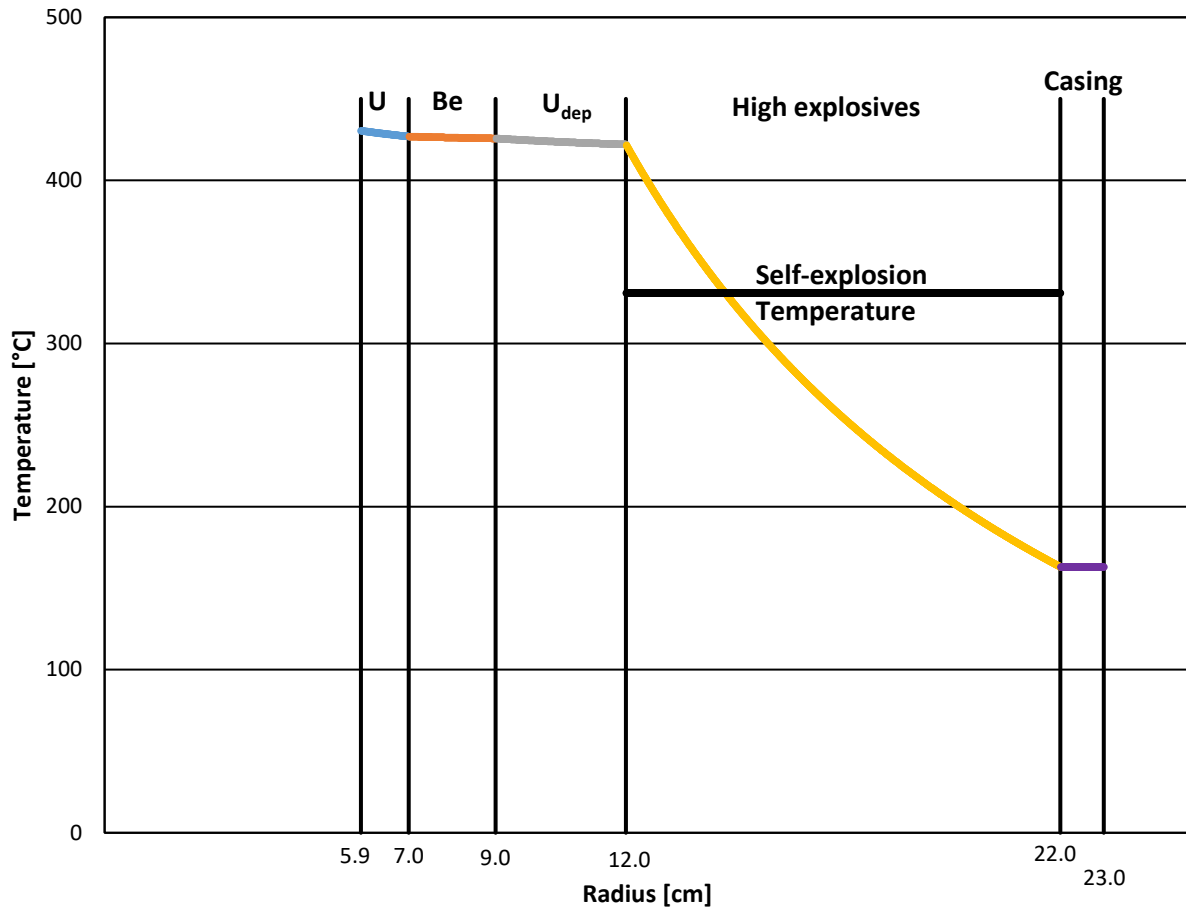
Figure 4.16: Steady State Temperature Profile at Time Interval t = 0.5 year
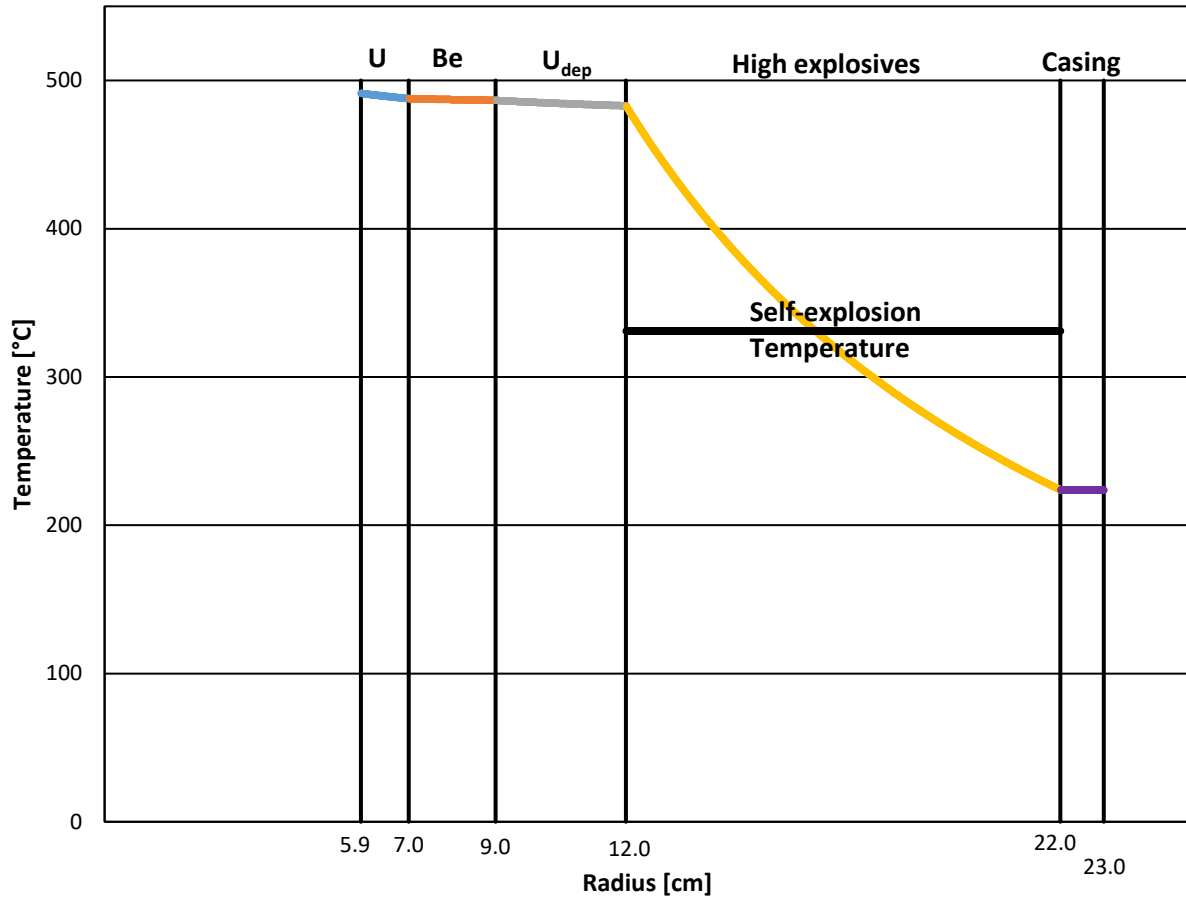
Figure 4.17: Steady State Temperature Profile at Time Interval t = 1 year
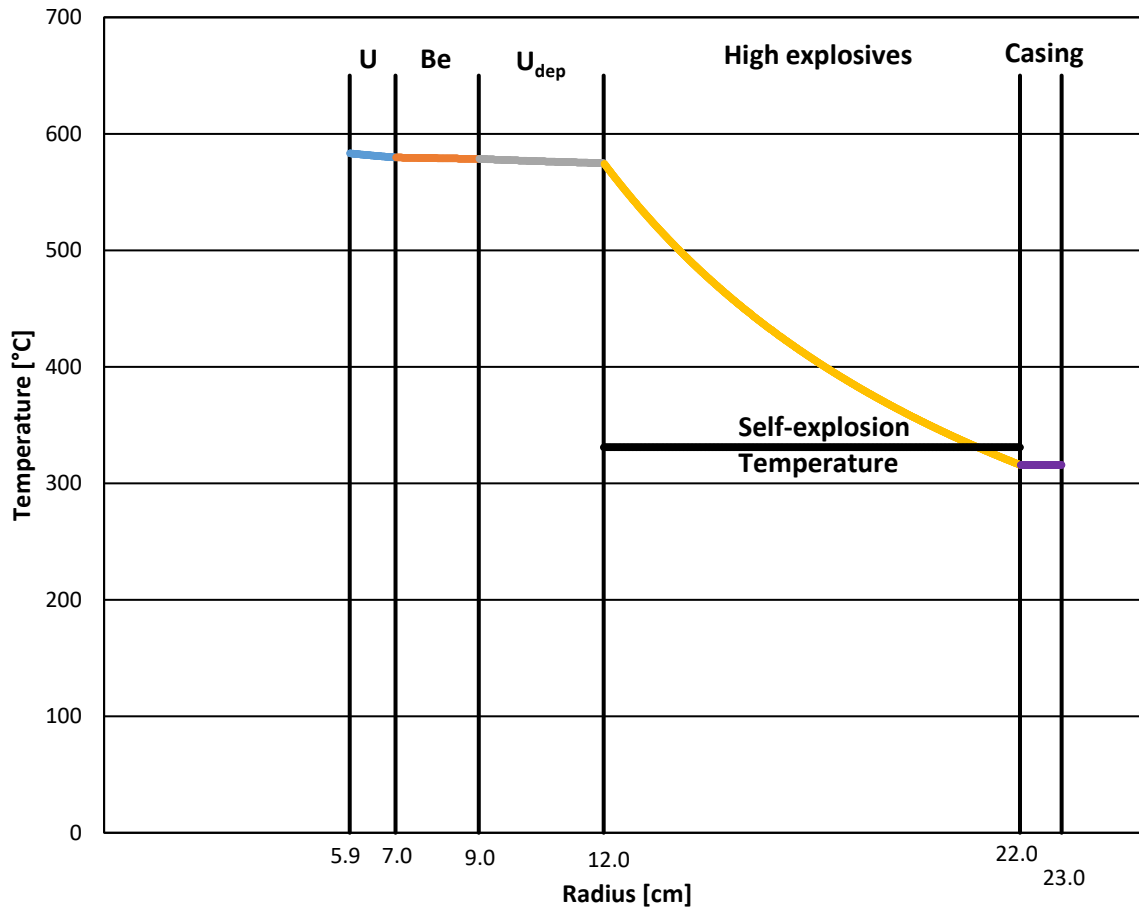
Figure 4.18: Steady State Temperature Profile at Time Interval t = 2 years
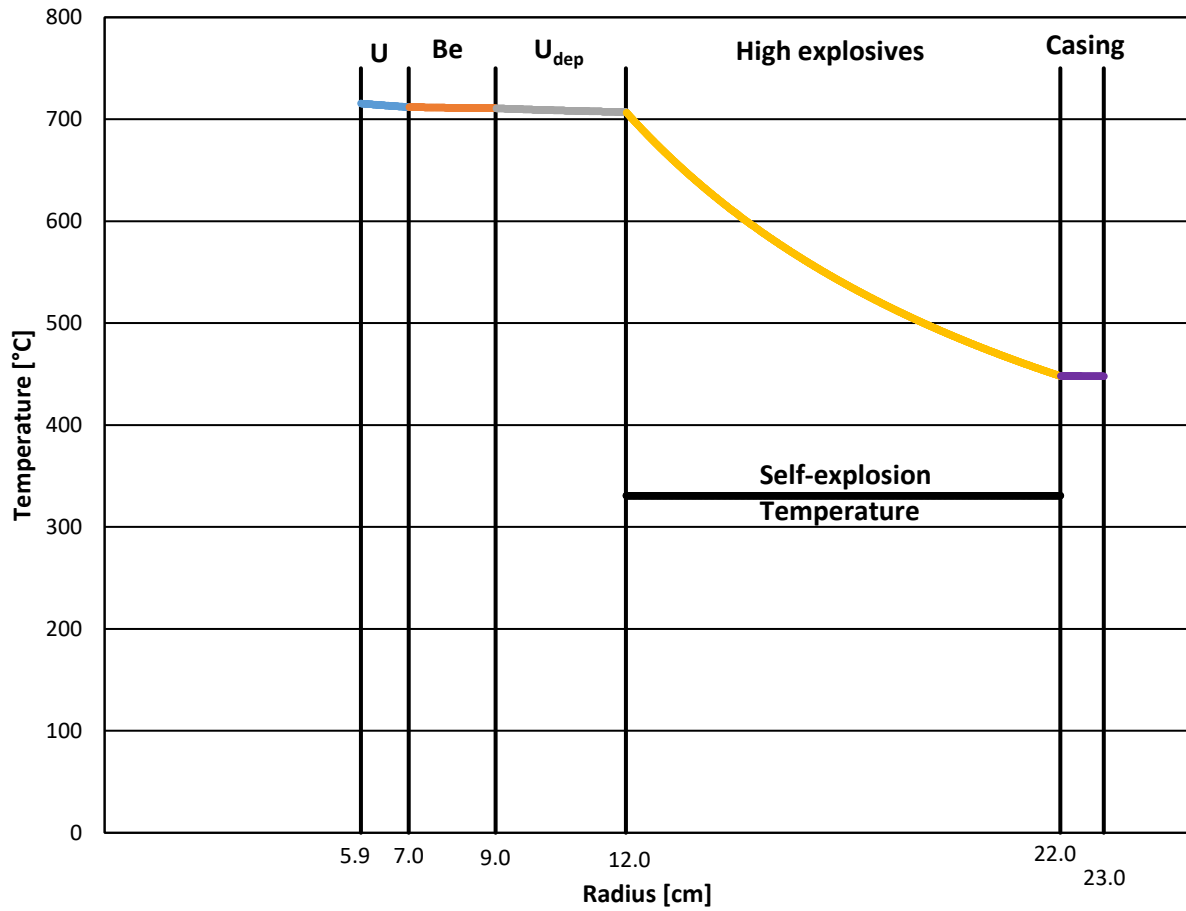
Figure 4.19: Steady State Temperature Profile at Time Interval t = 5 years
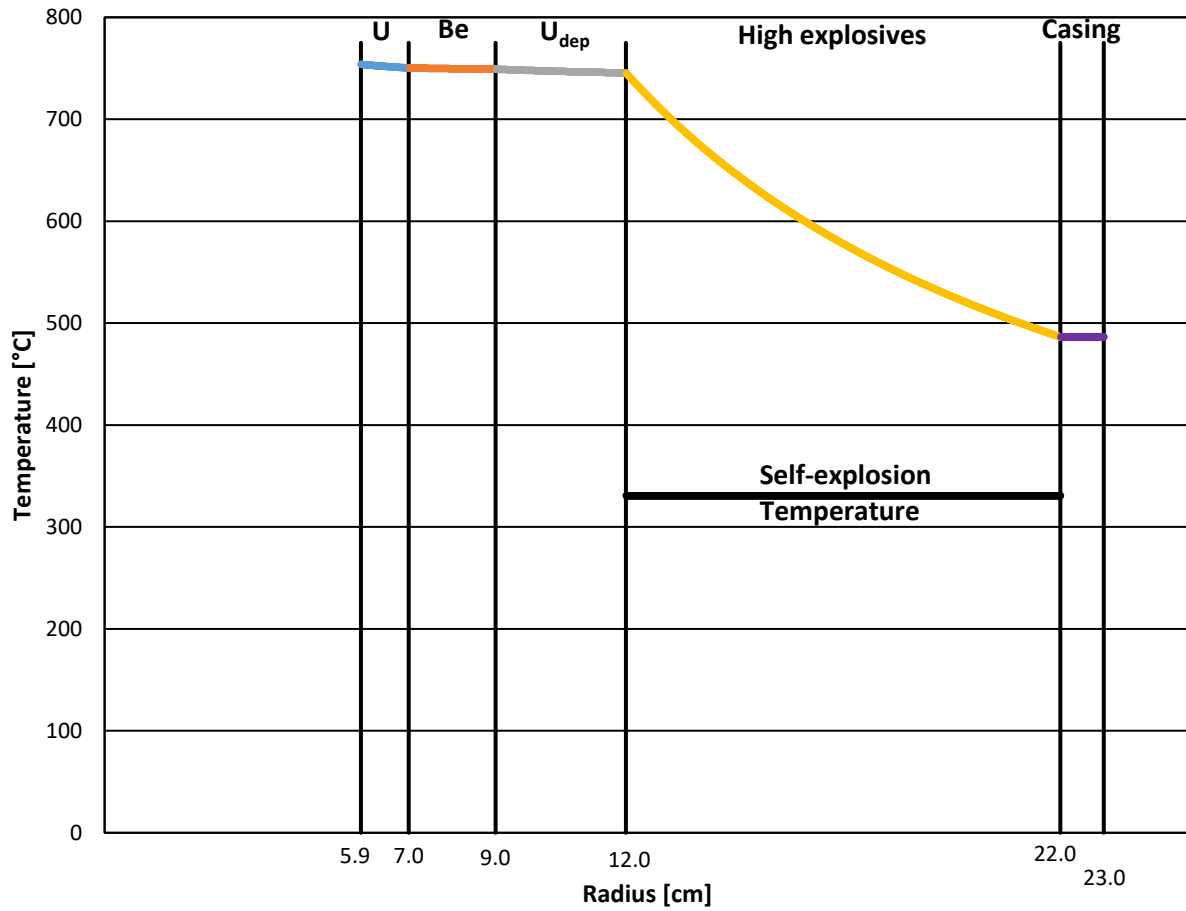
Figure 4.20: Steady State Temperature Profile at Time Interval t = 10 years

In addition to the effects of the heat generation on the high explosives, the dose rate from the decay of ^{232}U also damages the high explosives. Figure 4.21 shows the dose rate to the high explosives over time.
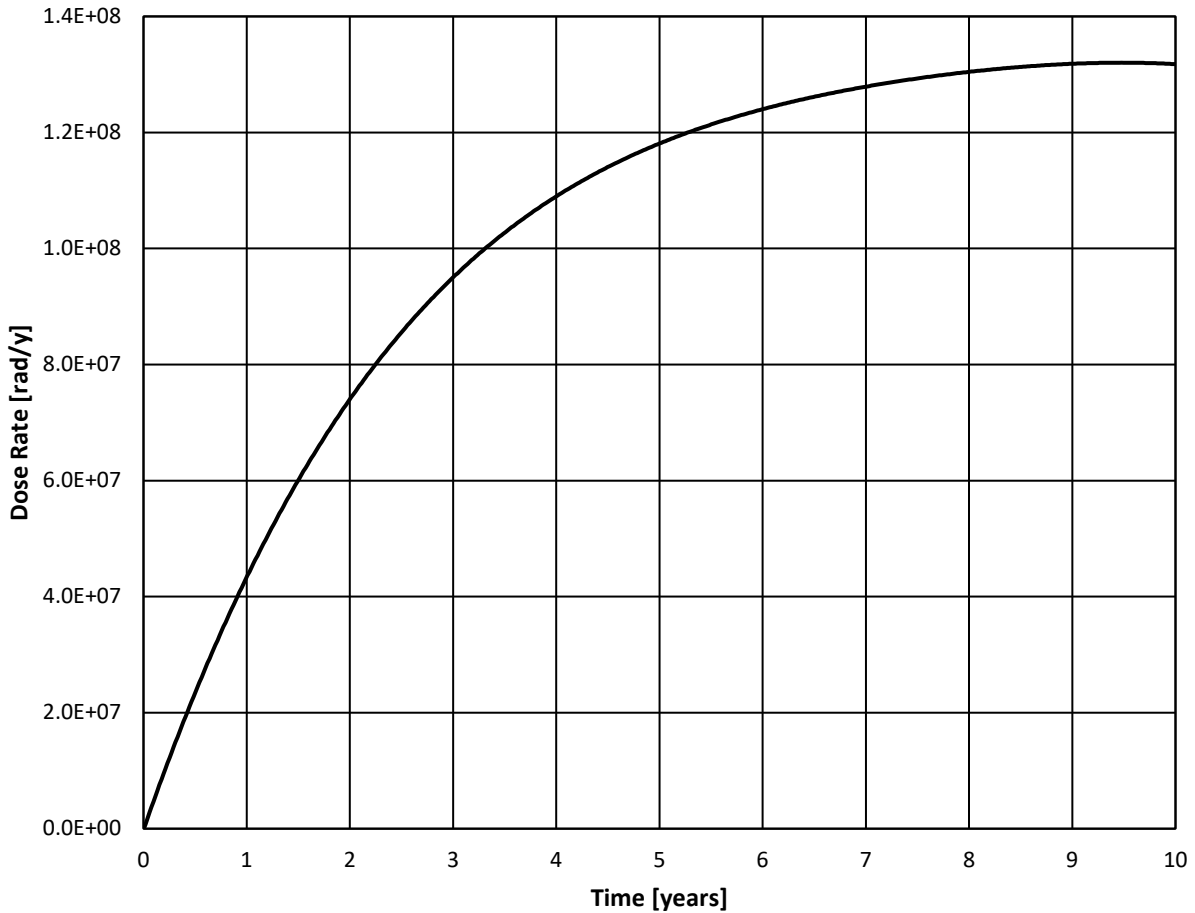
Figure 4.21: Dose Rate to the High Explosives over time

In order to obtain the total dose to the high explosives, the dose rate over time must be integrated. Figure 4.22 shows the dose rate to the high explosives over time and the 100 MR ($8.77 \cdot 10^7$ rad) degradation limit. The degradation limit is reach after approximately 2.1 years. Thus, the high explosives would begin to degrade 2.1 years after the full assembly of the weapon. The fully assembled weapon must not be stored for longer than 2.1 years

because the degradation of the high explosives would lead to a significant reduction of the

performance of the implosion eventually leading to total ineffectiveness of the weapon.
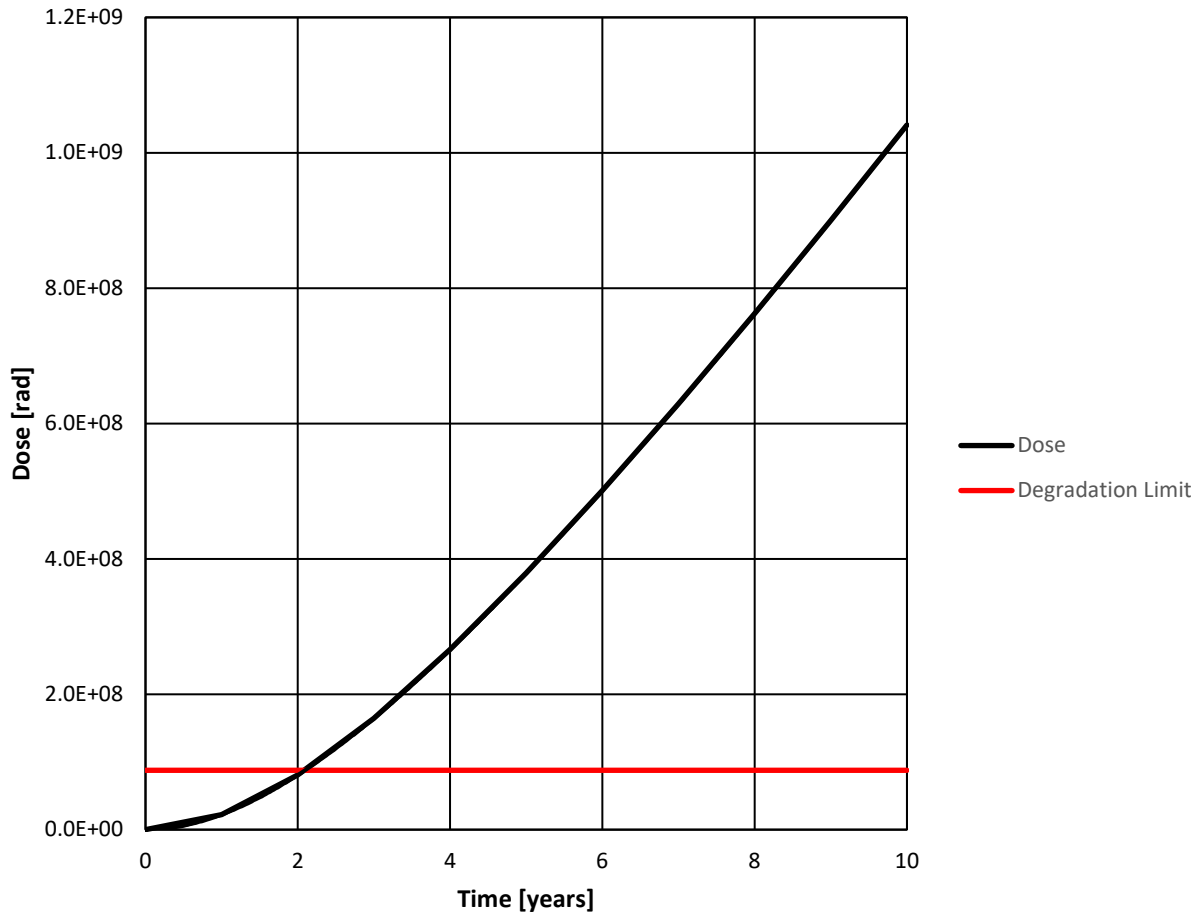
Figure 4.22: Dose to the High Explosives over time

The transient heat transfer analysis will include the 4 scenarios briefly described

below. Only the fresh uranium vector (t = 0) will be analyzed, rather than include every

time interval.

- Scenario 1: the uranium pit reaches thermal equilibrium with surrounding room

  then inserted into the Model

- Scenario 2: the uranium pit is externally cooled in liquid nitrogen then inserted into

  the Model

- Scenario 3: the uranium pit is inserted into an externally cooled Model

- Scenario 4: the fully assembled Model in thermal equilibrium with liquid nitrogen is removed and placed into a large room

Figure 4.23 shows the transient temperature profile from scenario 1. The temperature within the high explosives reaches its self-explosion temperature after approximately one day. This is a relatively small time frame and would require the weapon be used the same day of the insertion of the weapons pit. For deterrence purposes, the time frame is too short and storing the weapons pit separately would likely be impractical and reduces the level of readiness.
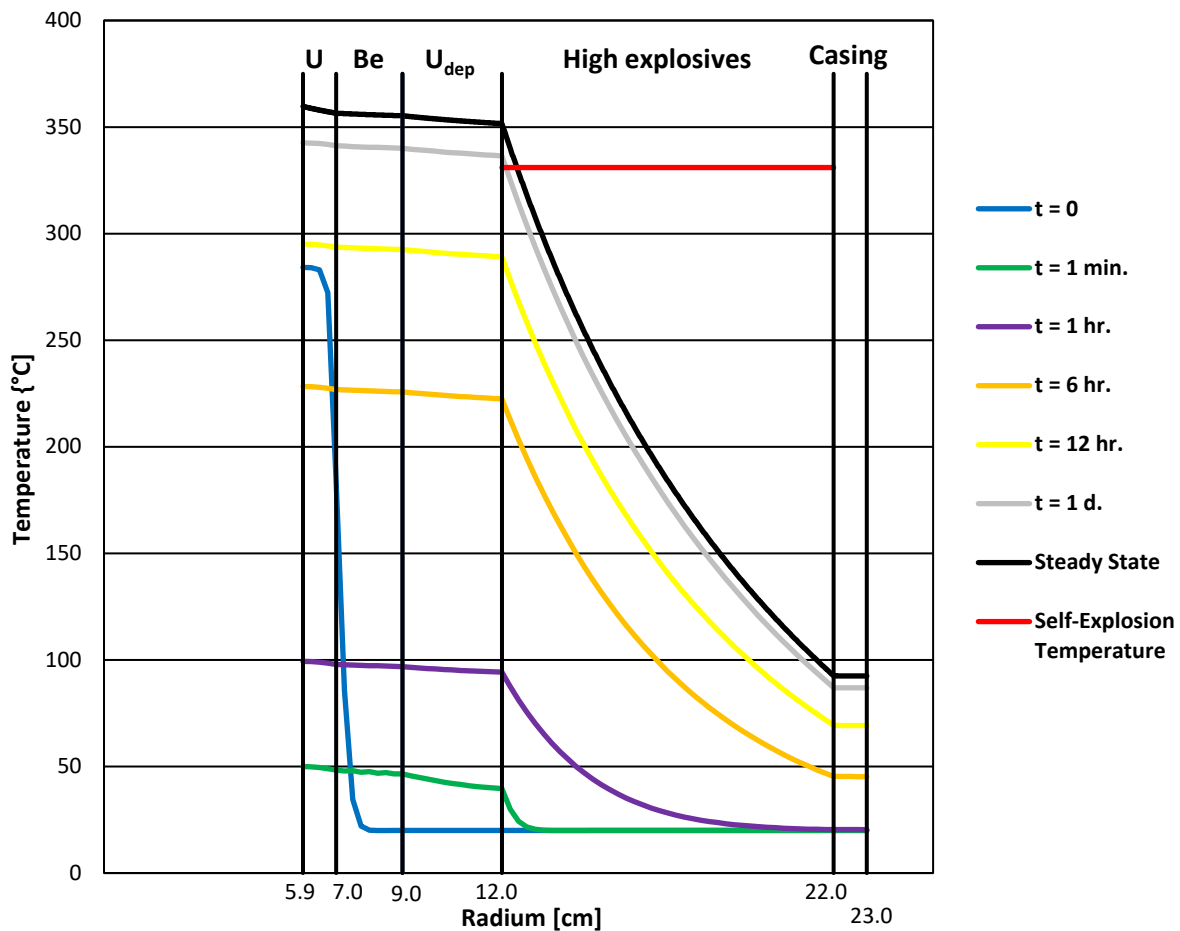
Figure 4.23: Transient Temperature Profile from Scenario 1

87

Figure 4.24 shows the transient temperature profile from scenario 2. As in scenario 1, the temperature within the high explosives reaches its self-explosion temperature after approximately one day. The lower initial temperature profile of the weapons pit only reduces the time taken to reach the self-explosion temperature by minutes. The final conclusion is the same as in scenario 1.
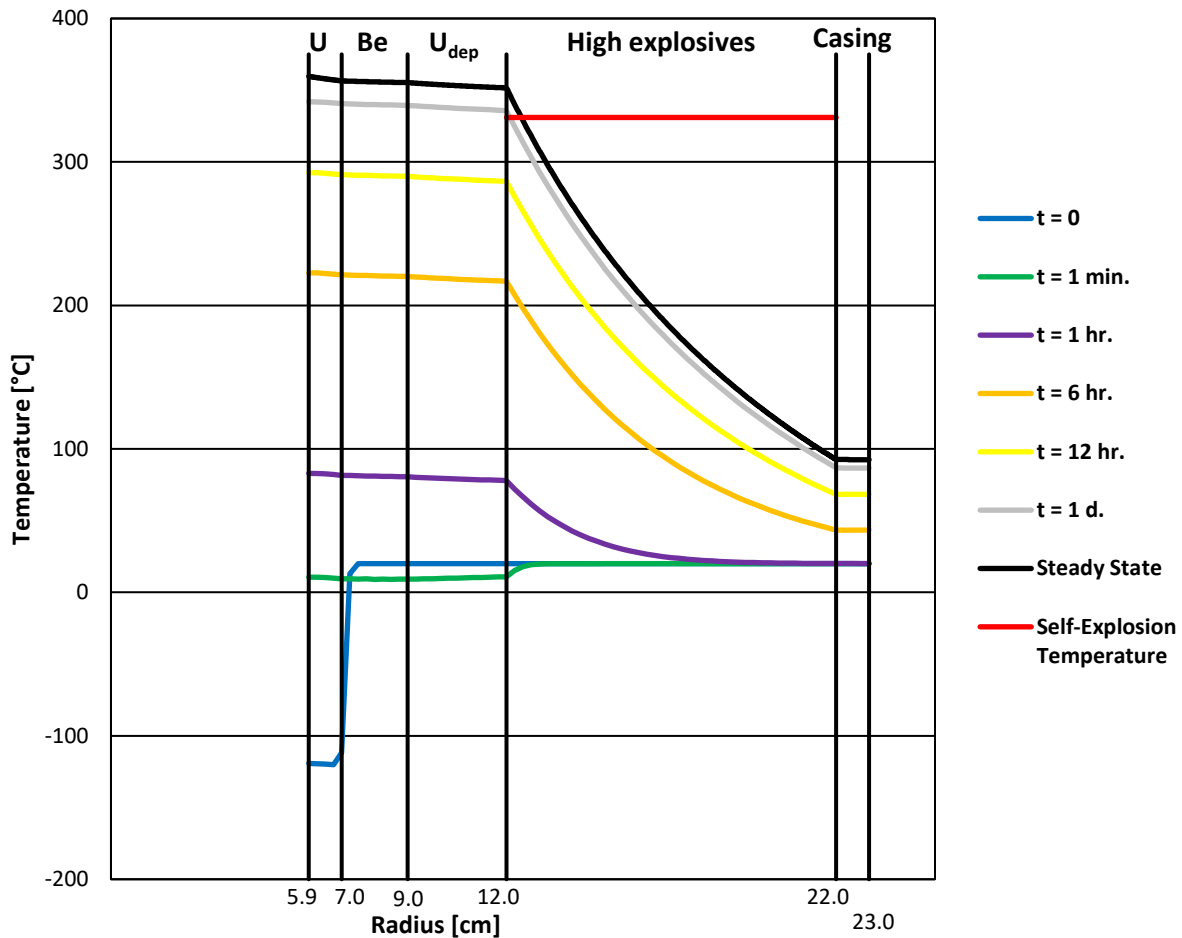
Figure 4.24: Transient Temperature Profile from Scenario 2

Figure 4.25 shows the transient temperature profile from scenario 3. The external cooling of the liquid nitrogen prevents the temperature within the high explosives from reaching its self-explosive temperature. Although this technique is effective, continually cooling the HNED with liquid nitrogen would be expensive and impractical.
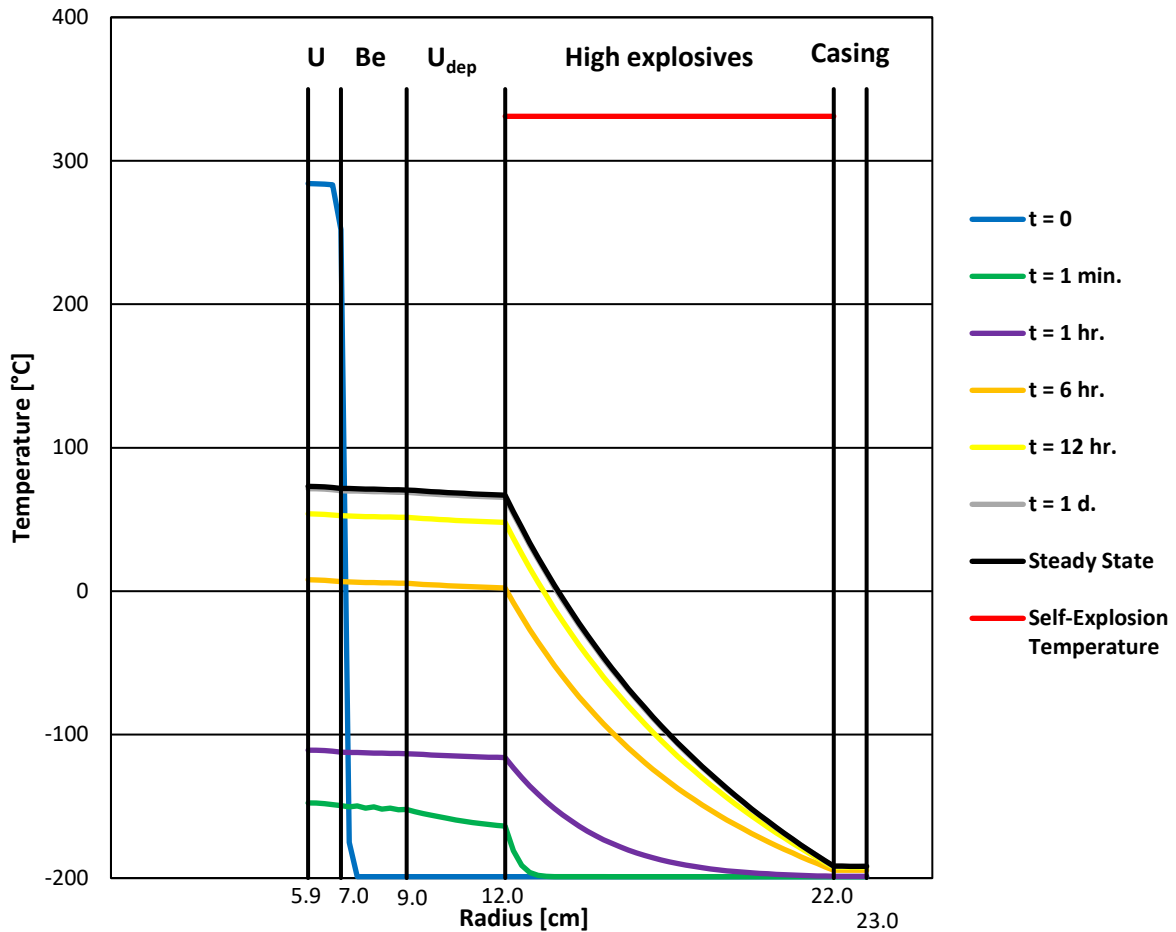
Figure 4.25: Transient Temperature Profile from Scenario 3

Figure 4.26 shows the transient temperature profile from scenario 4. As in scenario 1 and 2, the temperature within the high explosives reaches its self-explosion temperature after approximately one day. Although Figure 4.25 shows that continually cooling the HNED with liquid nitrogen will prevent self-explosion, once removed from the liquid nitrogen, the HNED must be used within one day in order to avoid self-explosion. Considering how expensive and complicated liquid nitrogen storage would be and the limited time frame, scenario 4 would be impractical.
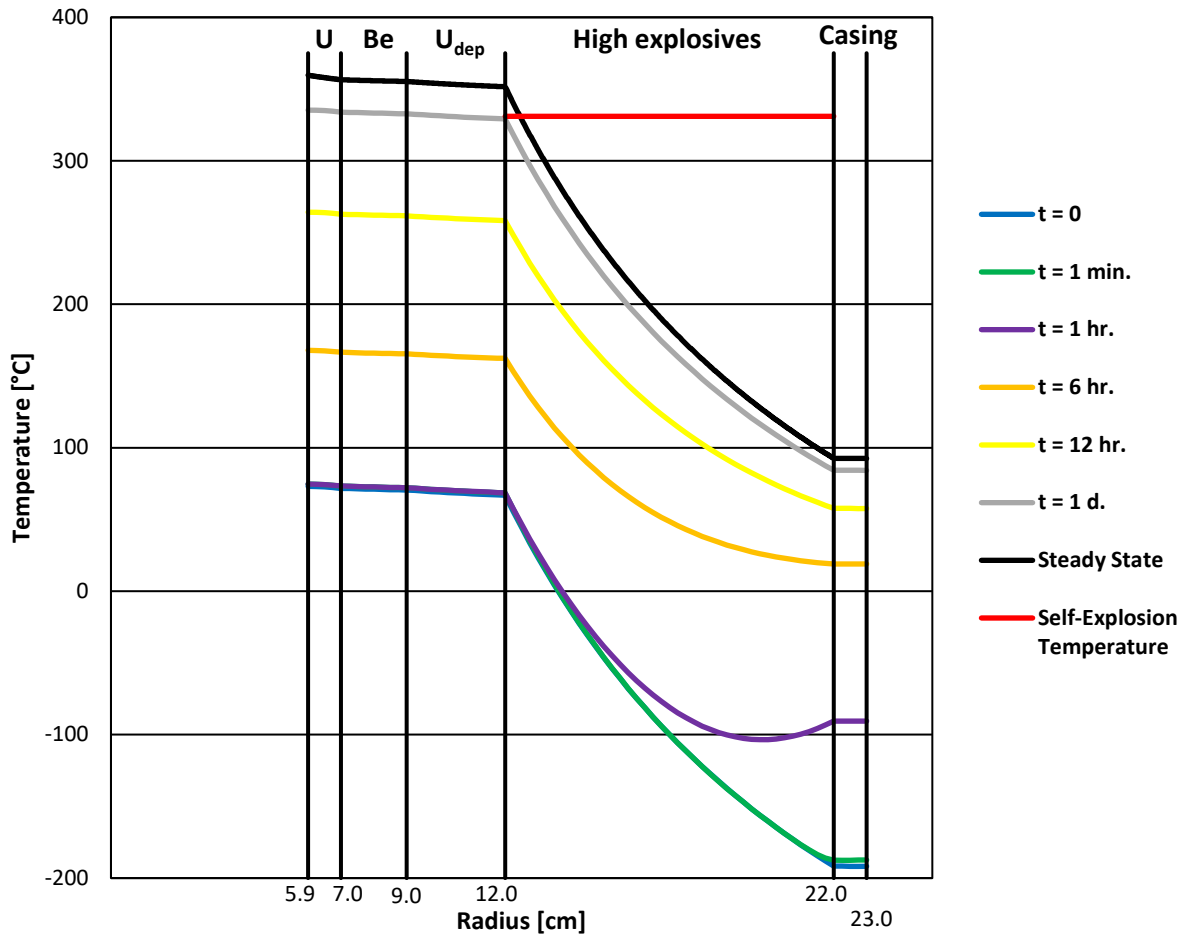
Figure 4.26: Transient Temperature Profile from Scenario 4

Figure 4.27 through Figure 4.31 shows the maximum thermal stress over time and tensile strength of each material in the HNED model. The thermal stress in the aluminum and weapons grade uranium do not reach their tensile strength in any of the scenarios, thus no plastic deformation will occur. The thermal stress in the high explosives and depleted uranium reach their tensile strength within approximately an hour in scenarios 1, 2, and 3. Plastic deformation will occur in these materials causing asymmetries in the implosion and reducing the yield. The maximum thermal stress in the beryllium reaches its tensile strength in all four scenarios. In scenarios 1, 2, and 3, the tensile strength is reached within an hour. In scenario 4, the tensile strength is reached within a day. In all four

90

scenarios, plastic deformation will occur in at least one shell of the HNED. This plastic

deformation will reduce the yield of the HNED. The underperformance of a nuclear weapon

may discourage its use by a state entity.
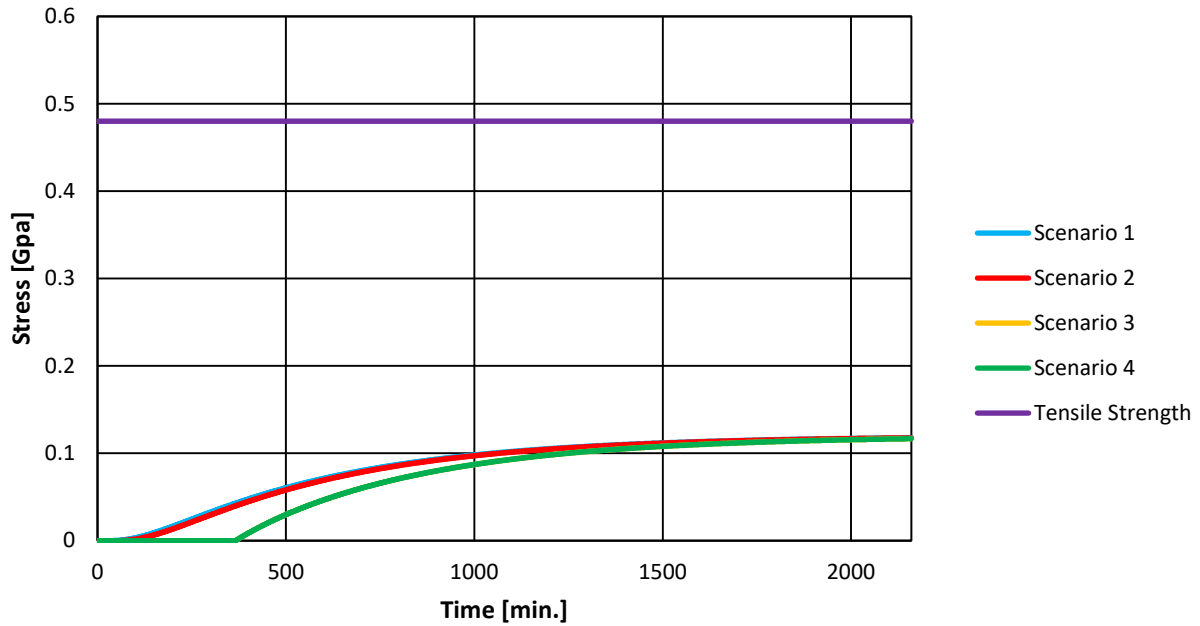
Figure 4.27: Maximum Thermal Stress in the Aluminum
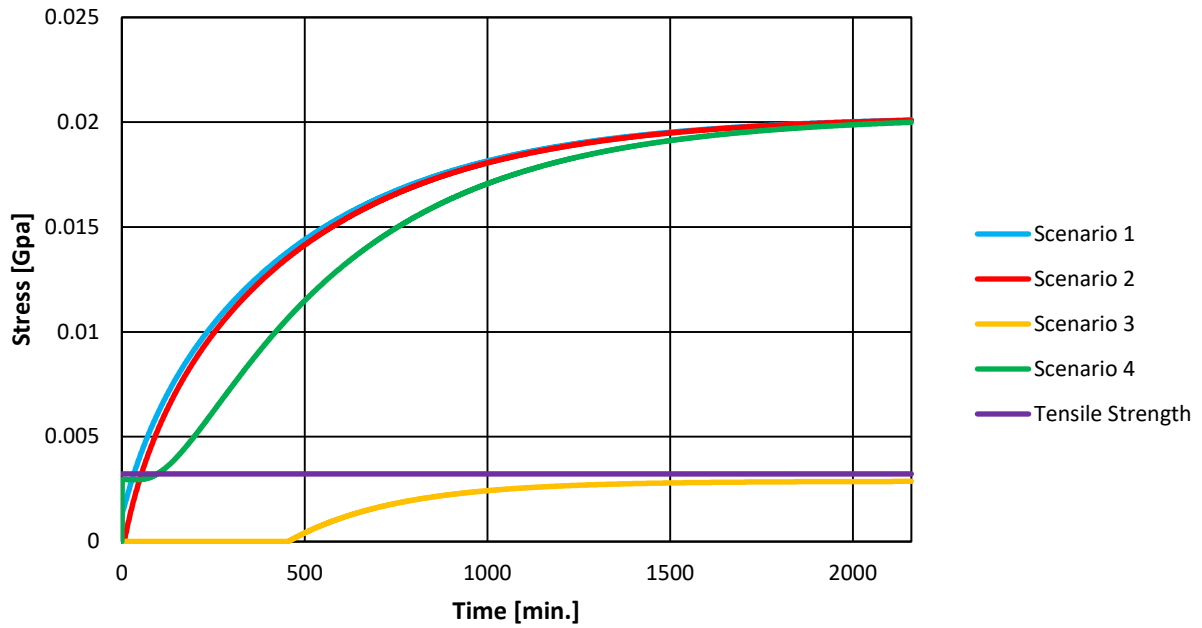
Figure 4.28: Maximum Thermal Stress in the High Explosives
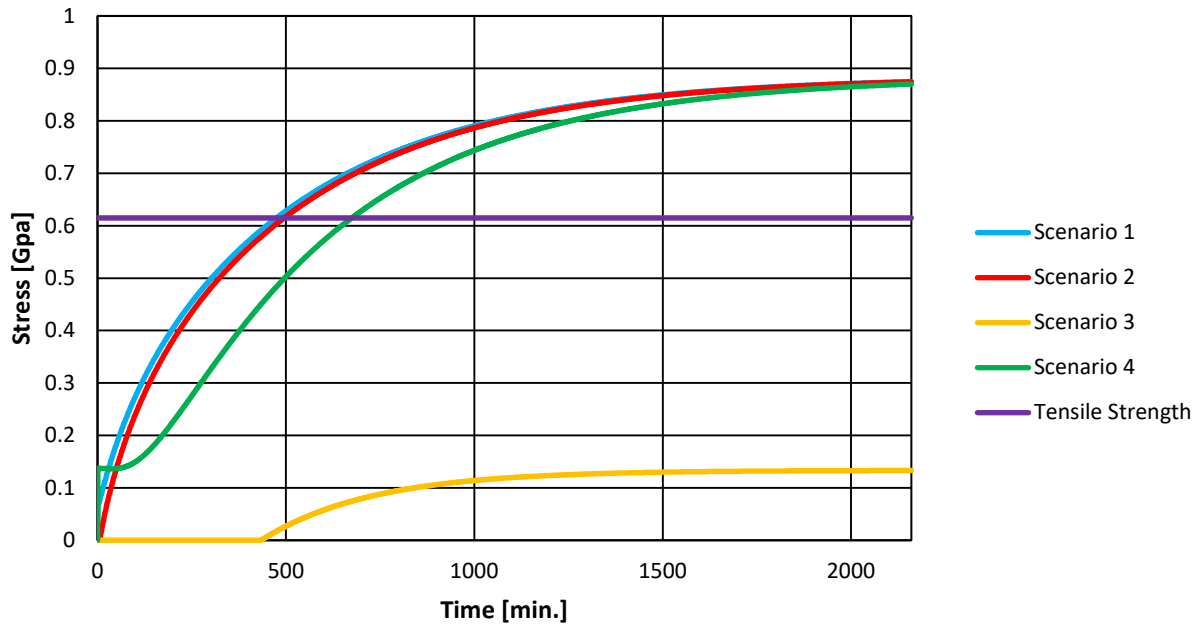
Figure 4.29: Maximum Thermal Stress in the Depleted Uranium
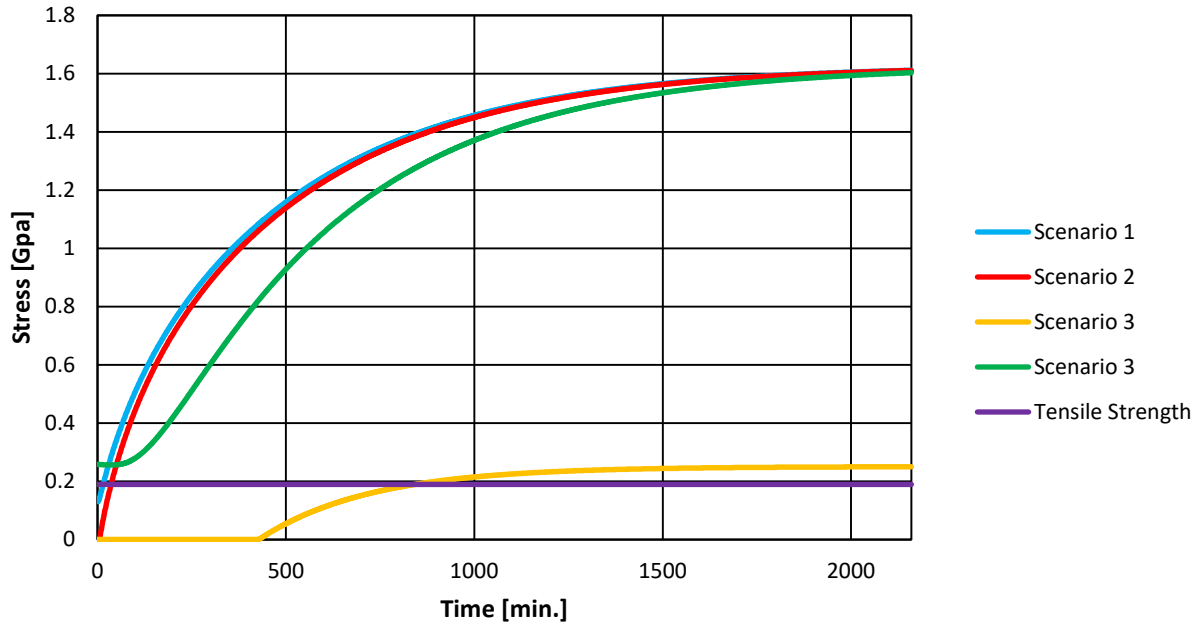
Figure 4.30: Maximum Thermal Stress in the Beryllium
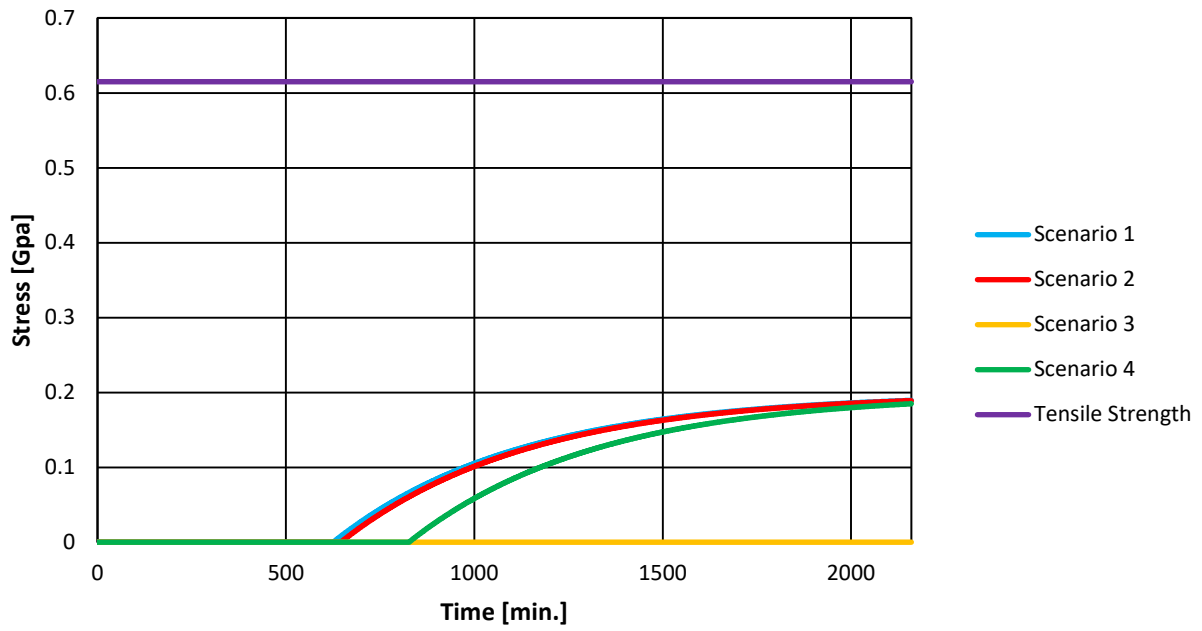
Figure 4.31: Maximum Thermal Stress in the Weapons Grade Uranium

4.2.2. Figure of Merit Analysis

In order to calculate the Figure of Merit values for the "90%" uranium isotopic vector including ^{232}U, each factor must be calculated. The bare critical mass is 39.0 ± 1.6 kg. The spontaneous fission neutron generation rate is 81.7 ± 1.5 neutrons/s·kg. This value is too low to produce a significant difference between the FOM$_1$ and FOM$_2$ equations, therefor spontaneous fission neutron generation rate will be excluded from the calculation of the Figure of Merit and the results are assumed to be applicable to both less technically advanced and technically advanced states. Figure 4.32 shows the heat generation per mass of the uranium material over time. As shown, the heat generation increases by more than a factor of five over the ten year time interval. Due to limits in the available nuclear data, the uncertainty of the heat generation is not included.
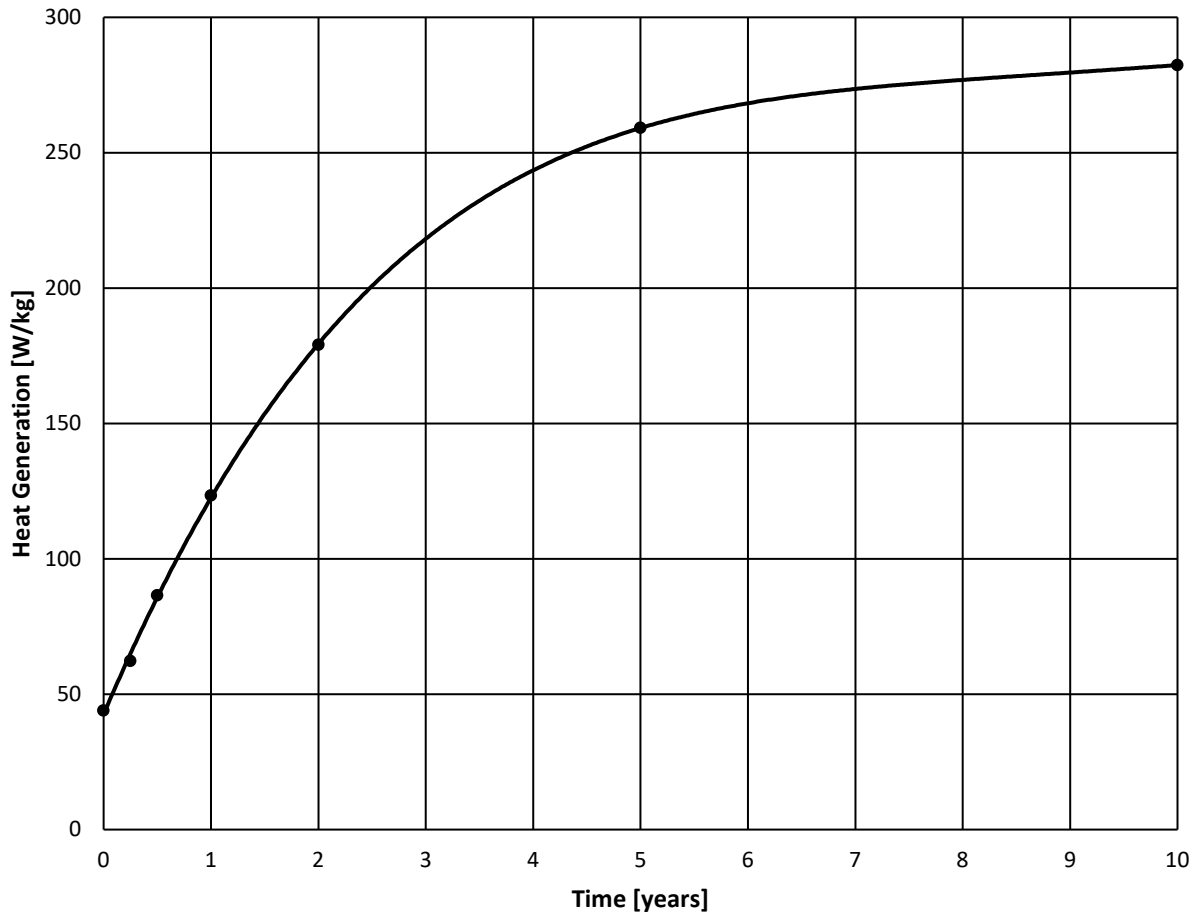
Figure 4.32: Heat Generation per Mass vs. Time

Figure 4.33 shows the dose rate from 1 meter of 0.2 times the bare critical mass over time. The dose rate initially increases from approximately zero rem/h to nearly 1000 rem/h over the ten year time interval. The "self-protection" dose rate of 500 rem/h is reached after approximately 1.5 years.

95
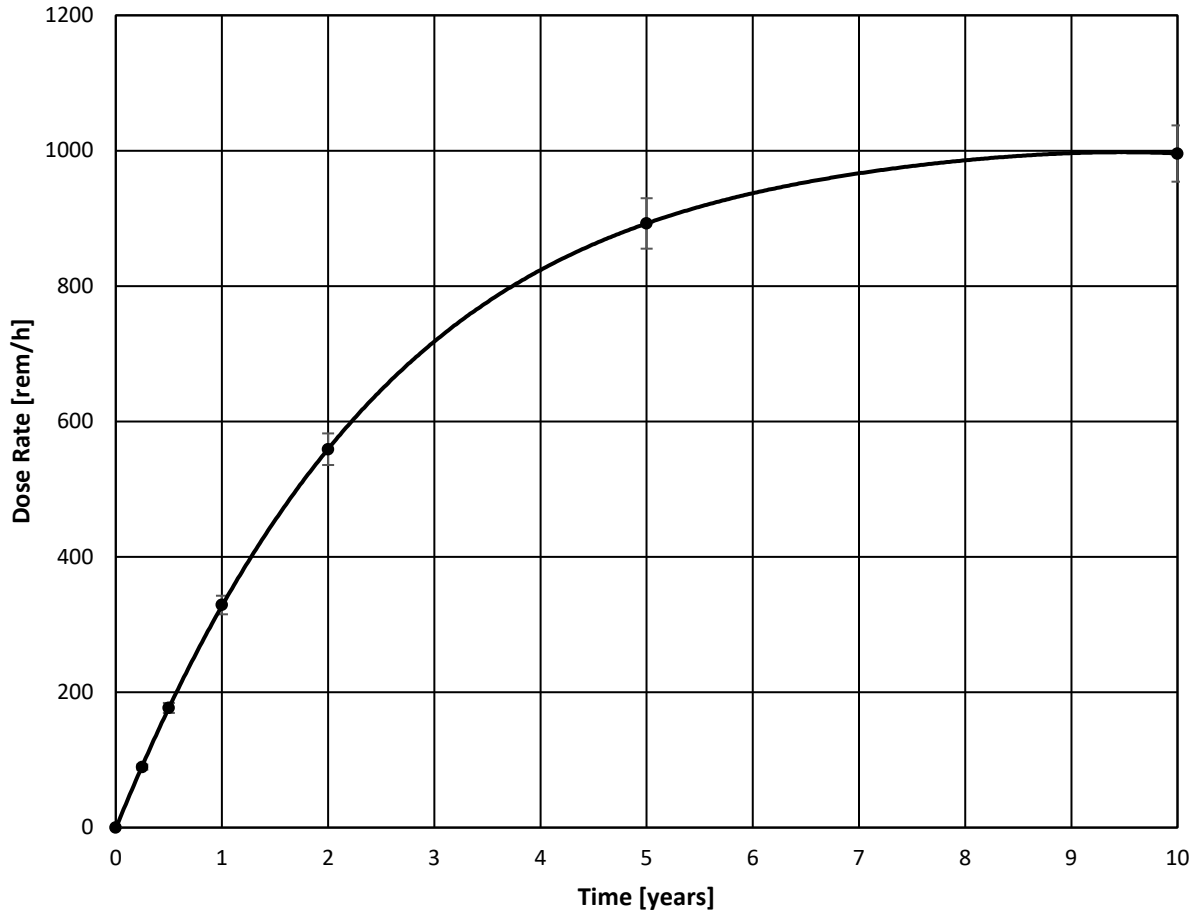
Figure 4.33: Dose Rate from 1 meter of 2/10 the Bare Critical Mass vs. Time

Figure 4.34 shows the Figure of Merit values over time. The increase in dose rate

and heat generation cause a significant decrease in the Figure of Merit value and therefor

the material attractiveness over time. After approximately 6 to 9 months, the uranium

material becomes unattractive for weapons purposes to both less technically advanced

states and technically advanced states. After 10 years, the Figure of Merit value is nearly

below one and thus the material is nearly very unattractive. This essential creates a time

limit for the weapons utility of the material. Although the material is certainly usable for

weapons purposes within the first 6 to 9 months, once the material becomes unattractive,

the [232]U daughter products must be removed in order to renew the material's weapons

utility. The burden of semi-annually refurbishing the uranium material in order to maintain a level of readiness would be significant for any state. Considering the primary function of most nuclear weapons arsenals are for deterrence purposes, the level of readiness must be constantly maintained. Although the use of such a material for weapons purposes is not impossible, using this material for deterrence purposes is highly impractical.
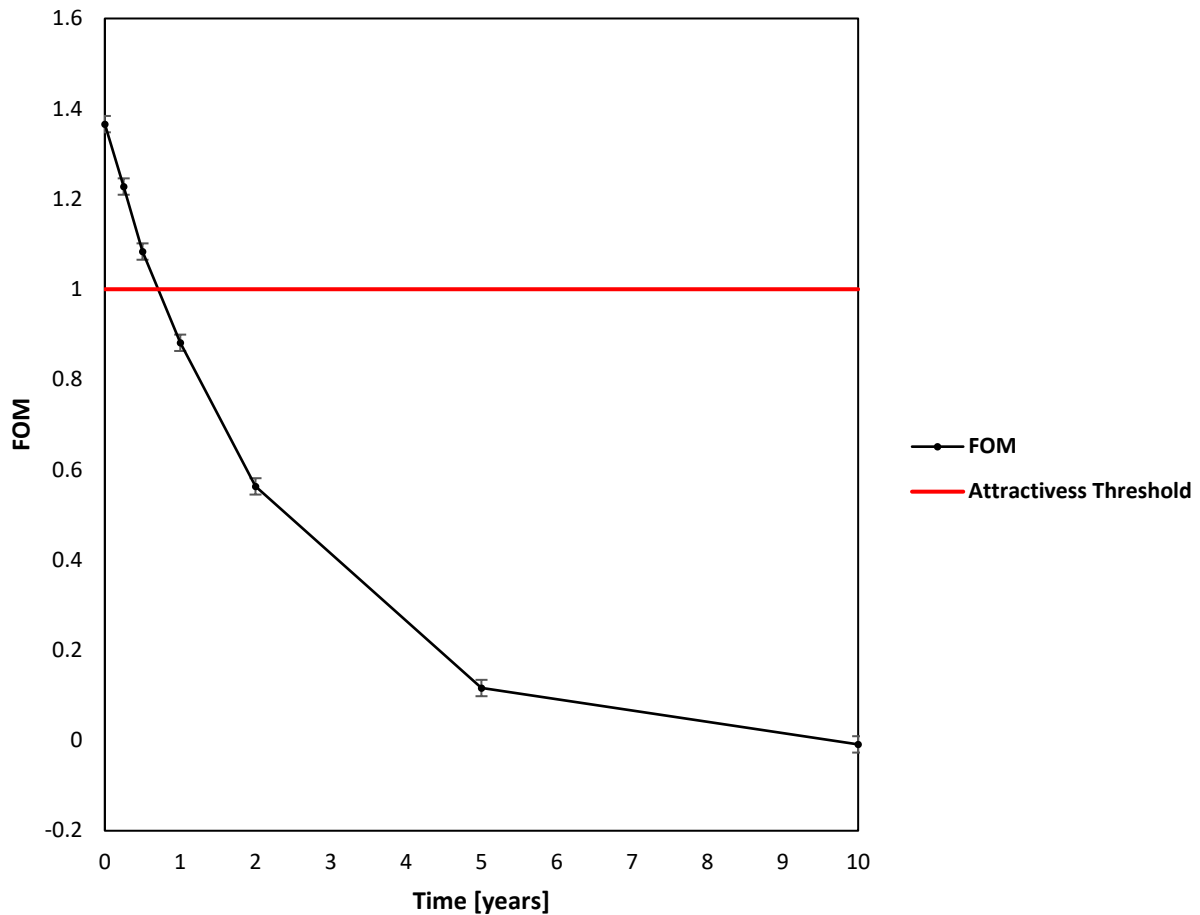
Figure 4.34: Figure of Merit Values vs. Time

4.2.3. Enrichment Issues

Table 4.5 shows the percentage of UF_6 molecules decomposed per second of each of the uranium isotopic vectors containing ^{232}U. Although these values may appear small, the accumulation of UF_6 decomposition over time may be significant.

Table 4.5: Percentage of UF$_6$ Molecules Decomposed per second

Initial	3%	5%	20%	90%
$3.33 \cdot 10^{-7}$	$2.04 \cdot 10^{-6}$	$3.54 \cdot 10^{-6}$	$1.48 \cdot 10^{-5}$	$6.91 \cdot 10^{-5}$

Table 4.6 shows the total percentage of UF$_6$ molecules decomposed over various time intervals from each uranium isotopic vectors containing ^{232}U. These time intervals were chosen as they represent various amounts of time gaseous UF$_6$ may be stored in a civilian nuclear fuel cycle. Even the percentages of UF$_6$ decomposed after only one day would significantly alter the enrichment process. The production of fractions of a percent of molecules having notably lower masses into the enrichment stream would cause these molecules to significantly increase. This would be counterproductive to the primary goal of enrichment: increasing the concentration of ^{235}U.

Table 4.6: Percentage of UF$_6$ Molecules Decomposed over Various Time Intervals

Time interval	Initial	3%	5%	20%	90%
One day	0.03	0.18	0.31	1.28	5.97
One week	0.20	1.23	2.14	8.93	41.81
One month	0.87	5.34	9.27	38.70	181.18

This analysis is a preliminary simplification of the possible issues ^{232}U may cause in the enrichment process. Although some of the percentages in Table 4.6 are not entirely realistic (such as the 181.18%), these values do indicate that if ^{232}U at the concentrations found here were introduced into the enrichment process, significant UF$_6$ decomposition would occur. This illustrates the magnitude of the impact ^{232}U may have on enrichment. Before ^{232}U could practically be implemented into a civilian nuclear fuel cycle, this impact would need to be more thoroughly explored and additional measures must be taken in order to effectively enrich the uranium materials containing ^{232}U.

4.2.4. Effects on Safety

This section will discuss the dose rate from 1 meter from the gamma ray and neutron emissions of the pellet model shown in Figure 3.1, the rod model shown in Figure 3.2, and the can model shown in Figure 3.3. The initial, 3%, 5%, and 20% uranium isotopic vectors with ^{232}U from Table 3.6. Since the gamma ray emissions change drastically as the daughter products of ^{232}U build-up, the dose rate from the gamma rays are considered at time intervals of 0, 0.5, and 10 years.

Table 4.7 shows the dose rate in units of rem/h from 1 meter from the gamma emissions of the pellet models at time intervals of 0, 0.5, and 10 years.

Table 4.7: Gamm Ray Dose Rate [rem/h] of Pellet Models from 1 meter

Time [years]	Initial	3%	5%	20%
0	$1.095 \cdot 10^{-7}$	$6.709 \cdot 10^{-7}$	$1.159 \cdot 10^{-6}$	$4.839 \cdot 10^{-6}$
0.5	0.001	0.006	0.010	0.040
10	0.005	0.031	0.054	0.225

Table 4.8 shows the dose rate in units of rem/h from 1 meter of the rod models from the gamma emissions at time intervals of 0, 0.5, and 10 years.

Table 4.8: Gamm Ray Dose Rate [rem/h] of the Rod Models from 1 meter

Time [years]	Initial	3%	5%	20%
0	$2.545 \cdot 10^{-6}$	$4.397 \cdot 10^{-6}$	$2.694 \cdot 10^{-5}$	$1.123 \cdot 10^{-4}$
0.5	0.038	0.207	0.405	1.695
10	0.215	1.322	2.285	9.550

Table 4.9 shows the dose rates in units of rem/h from 1 meter of the can models from the gamma emissions at time intervals of 0, 0.5, and 10 years.

Table 4.9: Gamma Ray Dose Rate [rem/h] of Can Models from 1 meter

Time [years]	Initial	3%	5%	20%
0	$1.909 \cdot 10^{-5}$	$1.170 \cdot 10^{-4}$	$2.021 \cdot 10^{-4}$	$8.438 \cdot 10^{-4}$
0.5	0.402	2.464	4.258	17.798
10	2.263	13.881	23.988	100.265

Considering the amount of uranium mass does not change significantly over the 10 year time interval, the neutron emissions are assumed to be constant. Table 4.10 shows the dose rates from the neutron emissions (both spontaneous fission and (α,n)) of the pellet, rod, and can models.

Table 4.10: Neutron Dose Rate of the Models from 1 meter

Model	Initial	3%	5%	20%
Pellet	$8.208 \cdot 10^{-9}$	$5.083 \cdot 10^{-8}$	$8.689 \cdot 10^{-8}$	$7.030 \cdot 10^{-7}$
Rod	$3.863 \cdot 10^{-7}$	$2.229 \cdot 10^{-6}$	$4.091 \cdot 10^{-6}$	$1.718 \cdot 10^{-5}$
Can	$4.634 \cdot 10^{-6}$	$2.840 \cdot 10^{-5}$	$4.909 \cdot 10^{-5}$	$2.066 \cdot 10^{-4}$

In order to compare the dose rates to the 5 rem annual limit of the United States Nuclear Regulatory Commission, the total amount of time an exposed worker would reach this total dose limit is calculated.

Table 4.11 shows the total number of hours a worker exposed to the pellet models would reach the NRC's annual limit of 5 rem.

Table 4.11: Total Time [hours] until Worker Exposed to the Pellet Models would reach 5 rem limit

Time [years]	Initial	3%	5%	20%
0	26,102,530	6,927,959	4,012,805	902,211
0.5	5,539	903	523	125
10	983	160	93	22

Table 4.12 shows the total number of hours a worker exposed to the rod models would reach the NRC's annual limit of 5 rem.

Table 4.12: Total Time [hours] until Worker Exposed to the Rod Models would reach 5 rem limit

Time [years]	Initial	3%	5%	20%
0	1,705,908	754,593	161,097	38,562
0.5	131	24	12	3
10	23	4	2	1

Table 4.13 shows the total number of hours a worker exposed to the can models would reach the NRC's annual limit of 5 rem.

Table 4.13: Total Time [hours] until Worker Exposed to the Can Models would reach 5 rem limit

Time [years]	Initial	3%	5%	20%
0	210,782	34,394	19,905	4,760
0.5	12	2	1	0
10	2	0	0	0

Assuming a 40-hour work week, the total number of hours in an entire work year is 2,080 hours. Although this number does not include possible holidays, such an approximation is adequate for this discussion. In all three models, the dose rates initially could not possibly reach the annual limit. However, after only 0.5 year the 3%, 5%, 20% isotopic vector pellet models could reach the limit within a year. The rod and can models with every isotopic vector considered here pose a significant dose rate threat at both the 0.5 and 10 year time intervals. In some cases, the 5 rem annual limit is reached within only a few hours or even within an hour. This illustrates a significant issue with implementing ^{232}U at the concentrations discussed here in a civilian nuclear fuel cycle. Additional shielding precautions would be essential to handling these materials and would be a

financial burden to any state seeking to utilize these materials. This must be considered before ^{232}U can be utilized to reduce material attractiveness purposes.

4.2.5. Effects on Security

This section will analyze gamma ray and neutron security measurements of the model shown in Figure 3.4 in both its non-shielded and shielded configurations. Measurements of the 90% vector with ^{232}U from Table 3.6 and the 90% vector without ^{232}U from Table 3.7 are compared. Since the scenarios considered here are the detection of a weapon's usable uranium material, the initial, 3%, 5%, and 20% vectors are excluded.

The gamma ray spectra found via the MCNP6 simulations of the security model and the detector shown in Figure 3.5 at time intervals of 0, 0.5, and 10 years of the isotopic vectors with and without ^{232}U are shown below. The measurement time is 5 minutes and the detector is 10 meters from the surface of the model. Figure 4.35 shows the spectra fresh non-shielded geometries. Figure 4.36 shows the spectra from 0.5 year non-shielded geometries. Figure 4.37 shows the spectra from 10 year non-shielded geometries. Even at the initial time interval of 0 years, low energy peaks in the gamma ray spectrum with ^{232}U are clearly visible above the background spectrum. At the 0.5 and 10 year time intervals, the spectra with ^{232}U is several order of magnitudes above both background and the spectra without ^{232}U. The spectra with ^{232}U is clearly visible and distinguishable between that without ^{232}U. This illustrates a significant increase in the detectability of the weaponized uranium material via the introduction of ^{232}U.
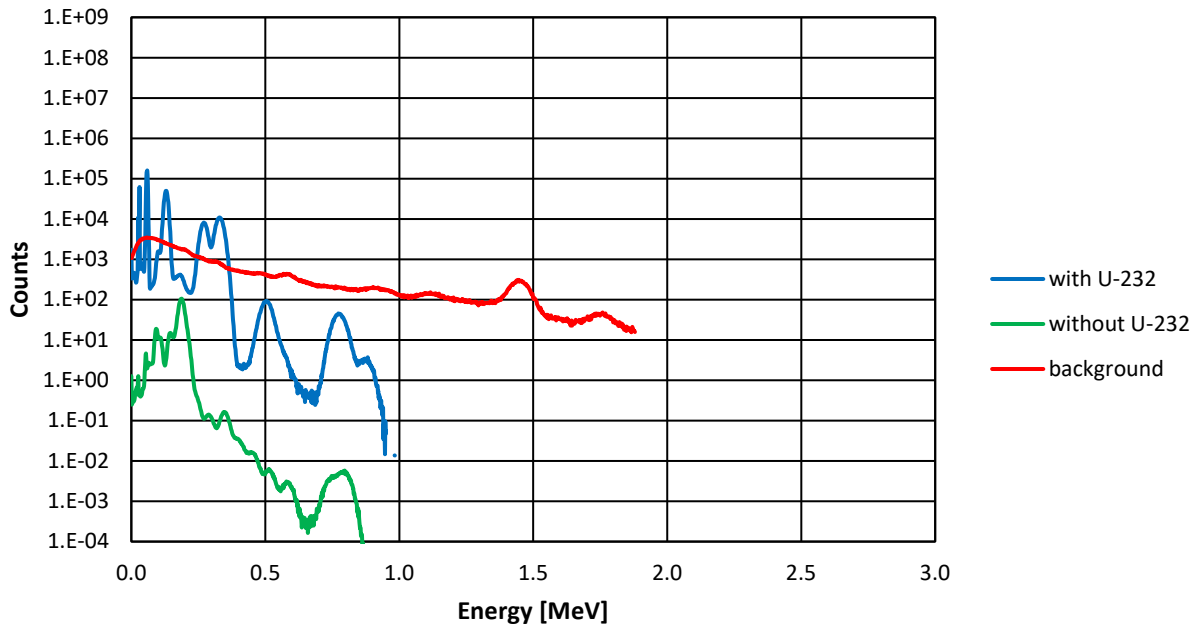
Figure 4.35: Fresh non-shielded geometry
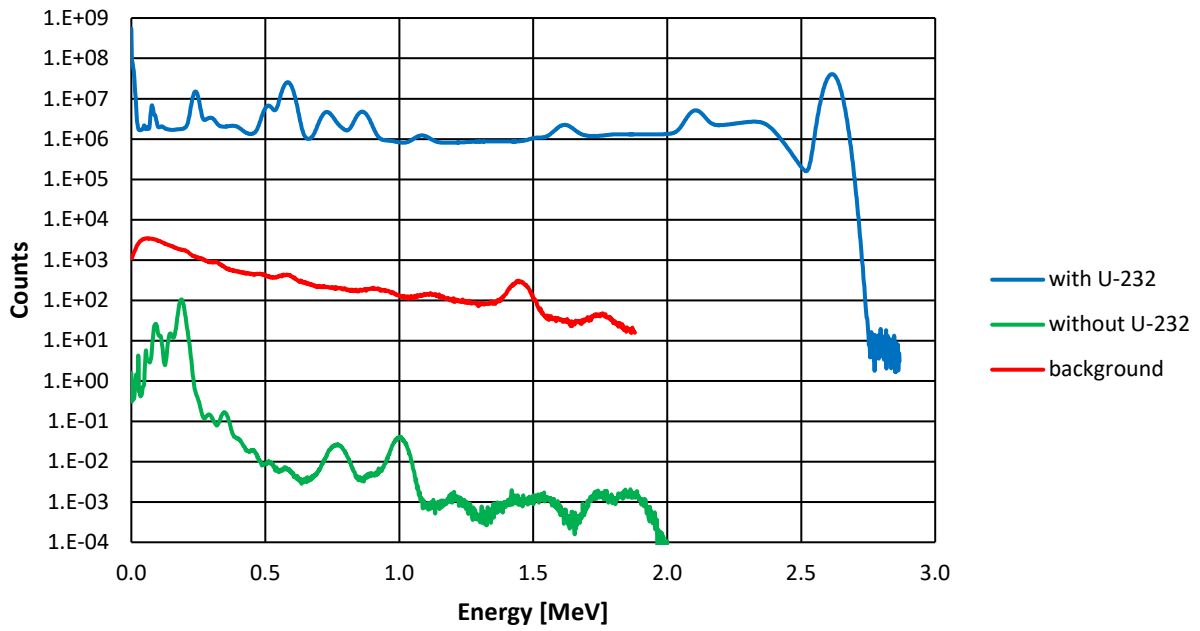
Figure 4.36: 0.5 year non-shielded geometry

103
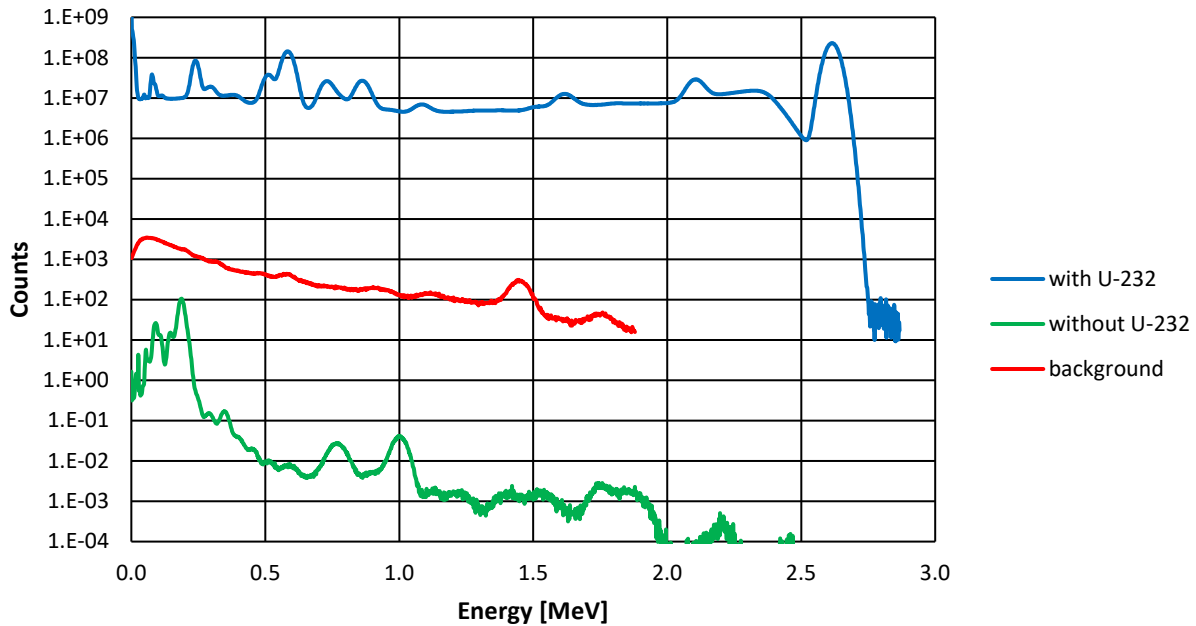
Figure 4.37: 10 year non-shielded geometry

The results from the shielded geometries are similar to that of the non-shielded cases. Figure 4.38 shows the spectra from the fresh shielded geometries. Figure 4.39 shows the spectra from the 0.5 year shielded geometries. Figure 4.40 shows the spectra from 10 year shielded geometries. The lead shielding proves effective at significantly reducing the low energy peaks in both the spectrum with and without ^{232}U. As a result, the fresh spectra are well below background and would be difficult to detect. However, the spectra with ^{232}U at 0.5 and 10 years is clearly visible above the spectra without ^{232}U and background. The shielding has a minimal effect on the spectra with ^{232}U, particularly at higher energies, as can be seen by the intensity of the 2.6 MeV ^{208}Tl peak. This illustrates the significant increase in detectability after the build-up of ^{232}U daughter products is present even when lead shielding is utilized.
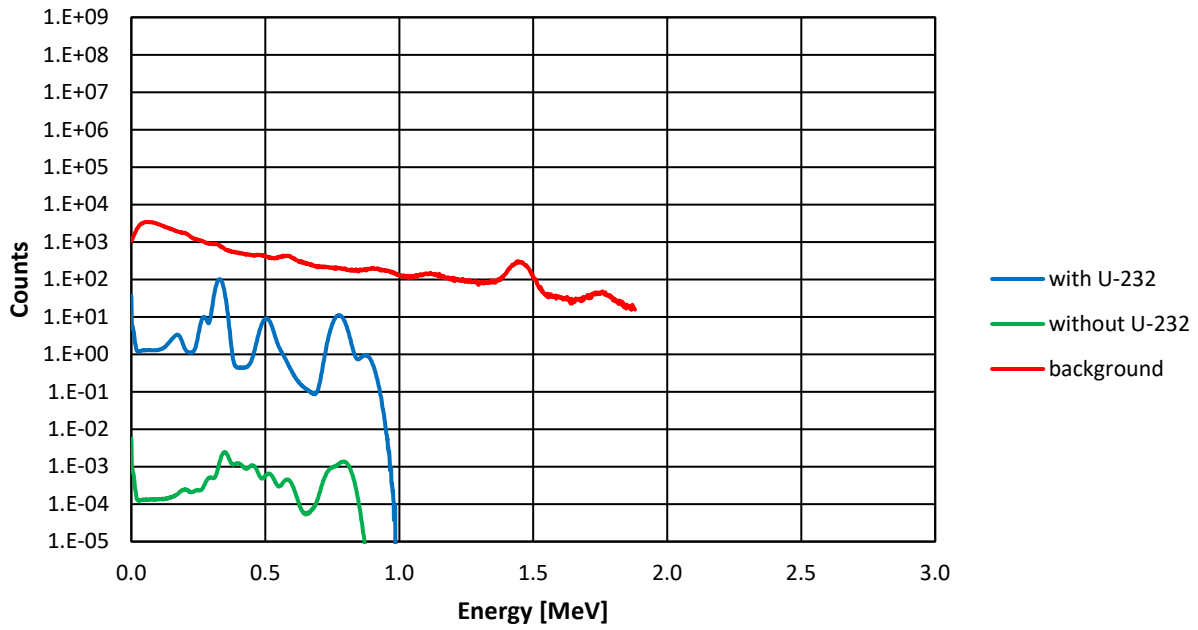
Figure 4.38: Fresh shielded geometry
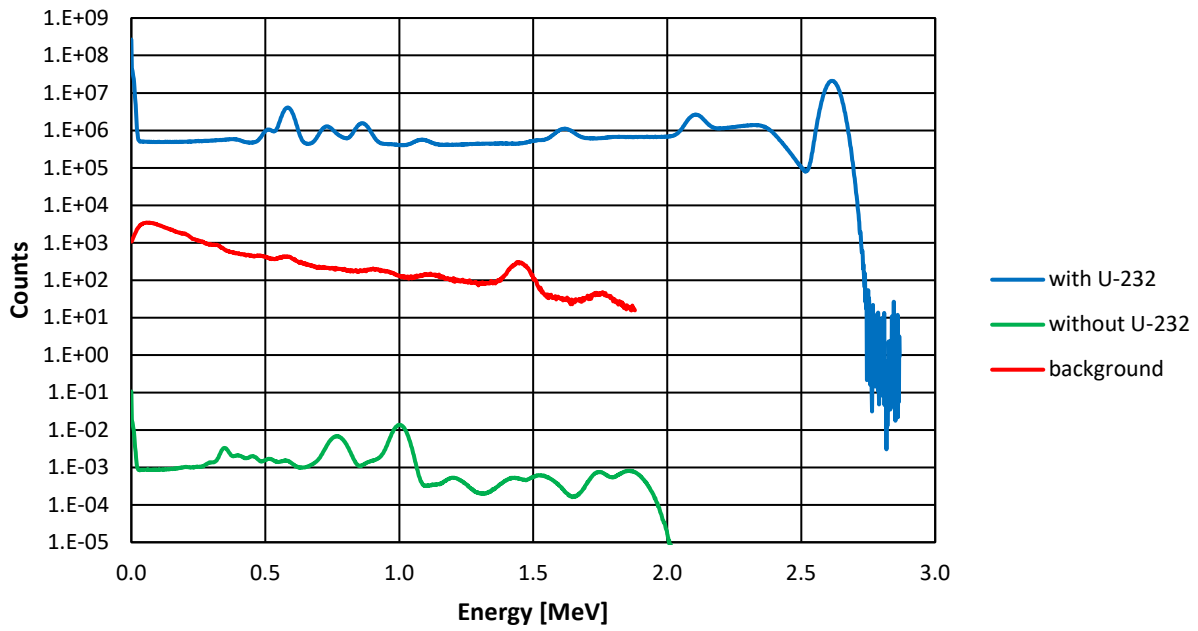
Figure 4.39: 0.5 years shielded geometry

105
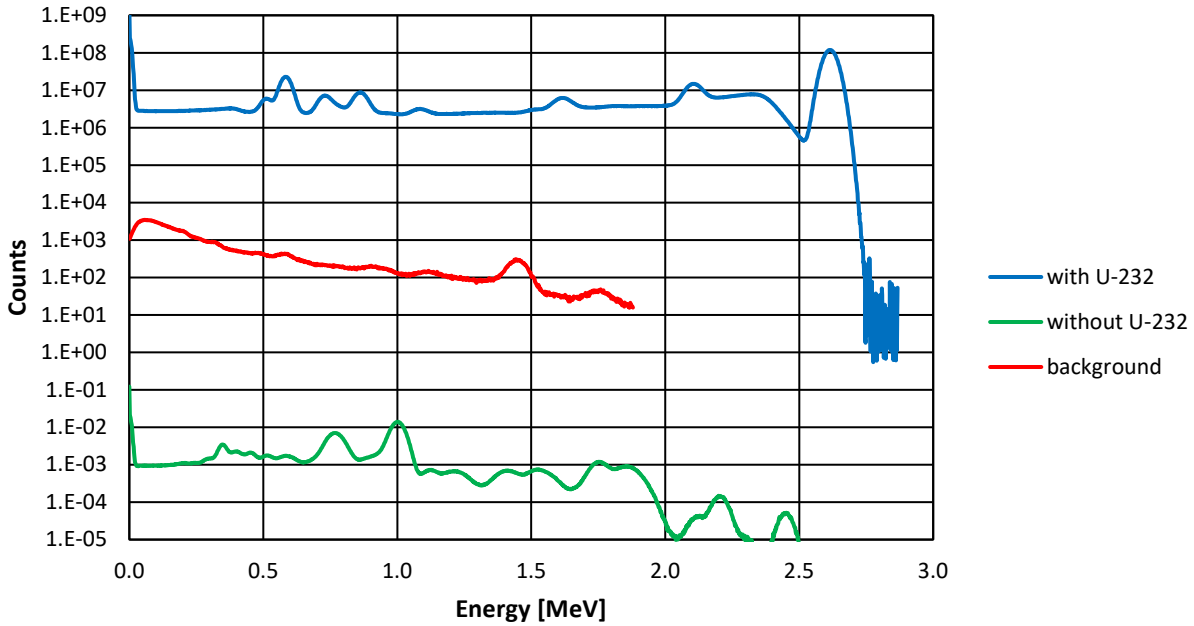
Figure 4.40: 10 years shielded geometry

Although the above spectra show an improvement in detectability, misidentification of this material is possible. ^{228}Th is found in both the ^{232}U and ^{232}Th decay chain. As a result, the proceeding daughter products of ^{228}Th are found in both the ^{232}U materials considered here and in nature. The detection of these daughter products from nature could lead to a possible misidentification. In order to evaluate the impact of misidentification, additional background measurements would be necessary. Due to the computational nature of this study and inability to access the materials discussed in this section, additional measurements are possibilities for future works.

The following discussion will focus on the total neutron counts from MCNP6 simulations of the neutron detector shown in Figure 3.6 10 meters from the security model. The measurement time is 10 minutes. The 90% isotopic vectors with and without ^{232}U are utilized. Considering the lead shielding in the shielded geometry will have a negligible effect on the neutron emissions, only the shielded geometry is used. The total neutron

106

counts from the security model with ^{232}U is 33 counts. The total neutron counts from the security model without ^{232}U is approximately 0 counts. In order to determine whether this difference in counts is detectable, the background counts must be approximated.

The background counts are approximated by calculating the reaction rate of the background neutrons in the ^{3}He within the detector. Equation 4.1 shows the relationship between the reaction rate (R) and the number of atoms (N), the neutron flux in units of neutrons/cm^2·s (ϕ), and the cross section in units of cm^2 (σ) (6).

Equation 4.1

$$R = N\phi\sigma$$

In this analysis, the reaction rate calculated will be the total neutron count rate from background. The number of atoms is the total number of ^{3}He atoms within the detector: $1.984 \cdot 10^{24}$. The neutron flux is the background neutron flux: approximately 0.015 n/cm^2·s (61). The neutron flux can vary by several percent (62). The value chosen here represents a median approximation of the possible variations in neutron flux based on location. In addition to the flux, the energy spectrum of the background neutrons can vary greatly based on location. The presence of objects such as large concrete structures or variations in altitude can significantly impact the spectrum of background neutrons. The detection efficiency of ^{3}He changes with neutron energy. Figure 4.41 shows the cross sections of various ^{3}He-neutron interactions as a function of neutron energy.
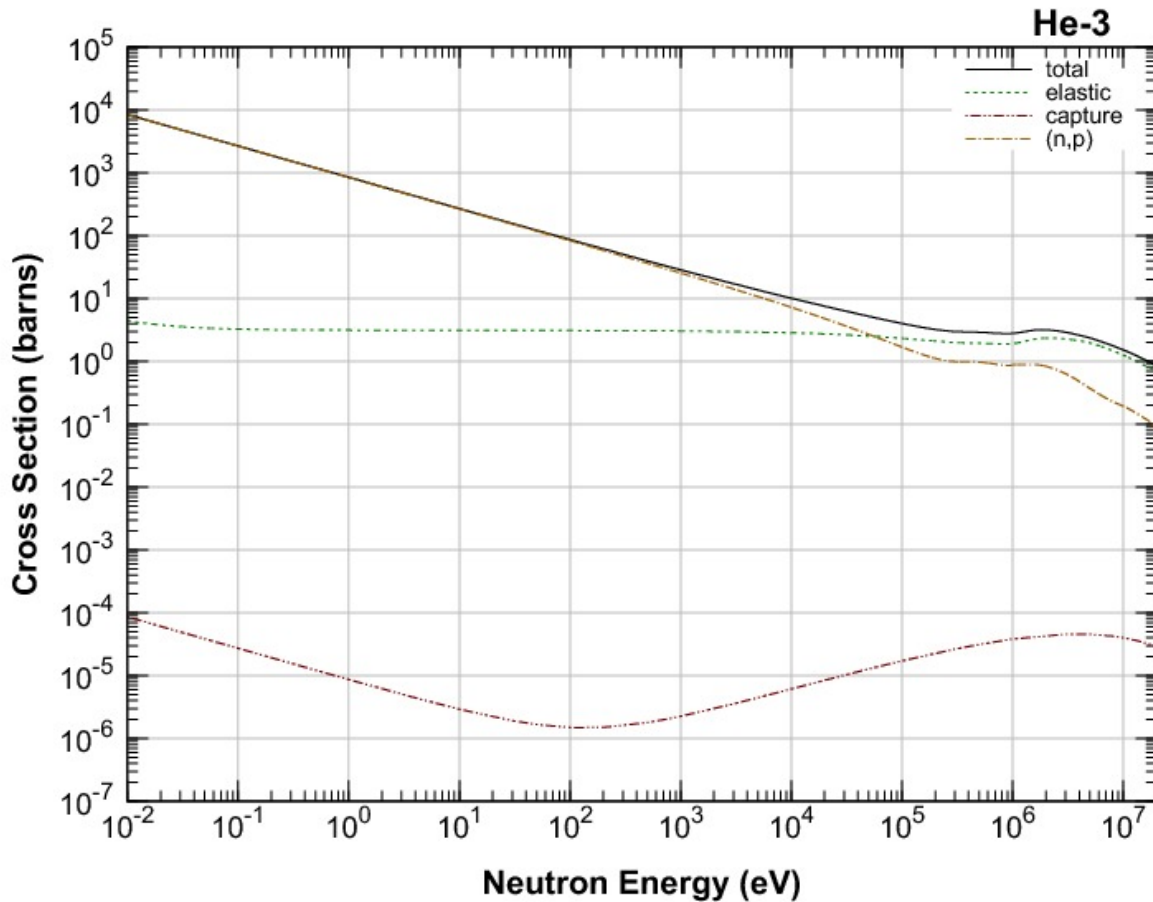
Figure 4.41: ³He cross sections [barns] vs. neutron energy [eV] (63)

In neutron detectors, (n,p) interactions of the ^{3}He produce neutron counts.

Therefore, the (n,p) cross section of ^{3}He should be used in this analysis. Much of the

neutron background energy spectrum falls below 1 MeV. 100 barns (10^{-22} cm^2) is chosen as

this represents the cross section near the highest end of the neutron energy spectrum thus

representing a conservative estimate. Lower energy neutrons would correspond to higher

cross sections and only increase the detection of the background neutrons. The realistic

value would depend heavily on the location of the background measurement. The value

chosen here is intended to be an approximation. Using Equation 4.1, the background count

rate of the detector is 3 counts per second. For a 10 minute measurement, the background

counts is 1786 counts.

Table 4.14 shows the neutron counts after a 10 minute measurement of the 90%

isotopic vectors with and without ^{232}U including background. The values are within a one-

sigma uncertainty and thus are not statistically differentiable. Unfortunately, this indicates

the introductions of ^{232}U did not significantly increase the neutron detectability of the

material. The cross section chosen here assumed high energy background neutrons.

Additional attenuation via structures such as concrete buildings would lower the energy of

the background neutrons and thus increase the detection of these neutrons. An increase in

the detection efficiency of the background neutrons would only strengthen the conclusion

made here that the spontaneous fission of ^{232}U will not significantly increase the neutron

detectability of uranium materials.

Table 4.14: Neutron counts with and without ^{232}U including background

Isotopic Vector	Counts
With ^{232}U	1,819 ± 135
Without ^{232}U	1,786 ± 134

4.2.6. Effects on Safeguards

This section discusses gamma ray and neutron non-destructive assay safeguards

techniques. These techniques are done on the initial, 3%, 5%, and 20% uranium isotopic

vectors with ^{232}U (Table 3.6) and without ^{232}U (Table 3.7) at time intervals of 0.5 and 10

years. The results from the set of isotopic vectors with ^{232}U are compared to that without

[232]U in order to evaluate the effectiveness of the techniques in the presence of [232]U. Only the can model shown in Figure 3.3 is used in this analysis.

First, a non-destructive technique using the [235]U and [238]U gamma ray peaks to quantify [235]U enrichment is analyzed. The set of simulations found here represent a 5 minute gamma ray measurement of the can models by a 2"x2" HPGe detector in MCNP6. The figures include both the spectra with and without [232]U as well as red dashed lines at the 185.7 keV [235]U peak and the 1001 keV [234m]Pa peak (utilized for [238]U).

Figure 4.42 shows the initial uranium isotopic vector spectra with and without [232]U after 0.5 year. Figure 4.43 shows the initial uranium isotopic vector spectra with and without [232]U.
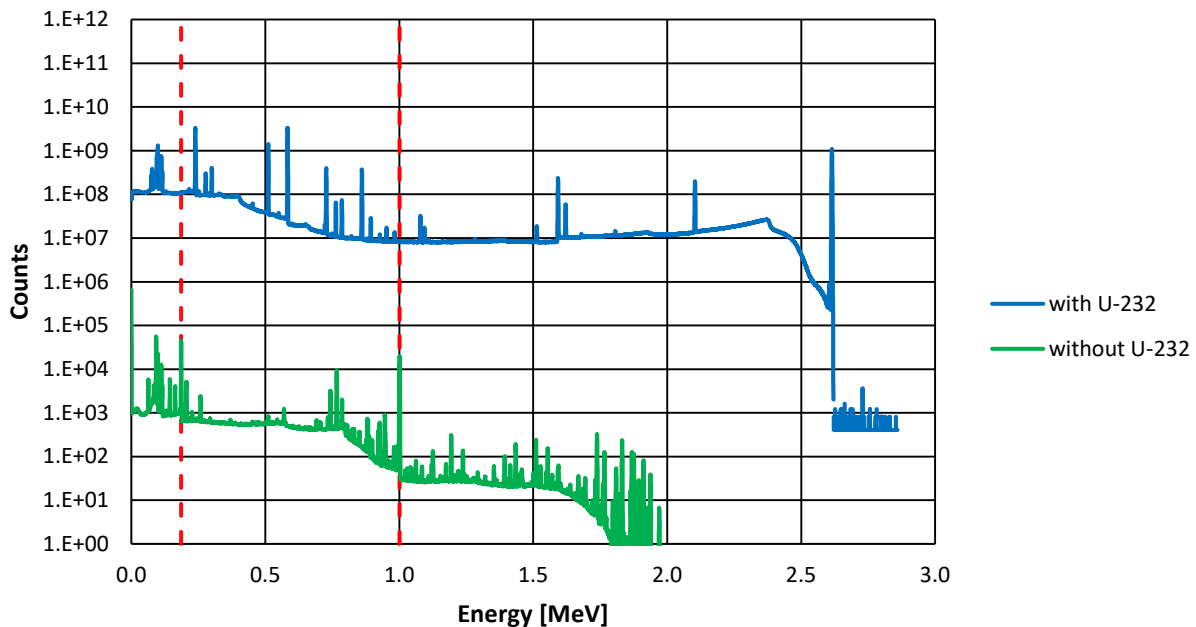
Figure 4.42: Initial uranium isotopic vector spectra at 0.5 year
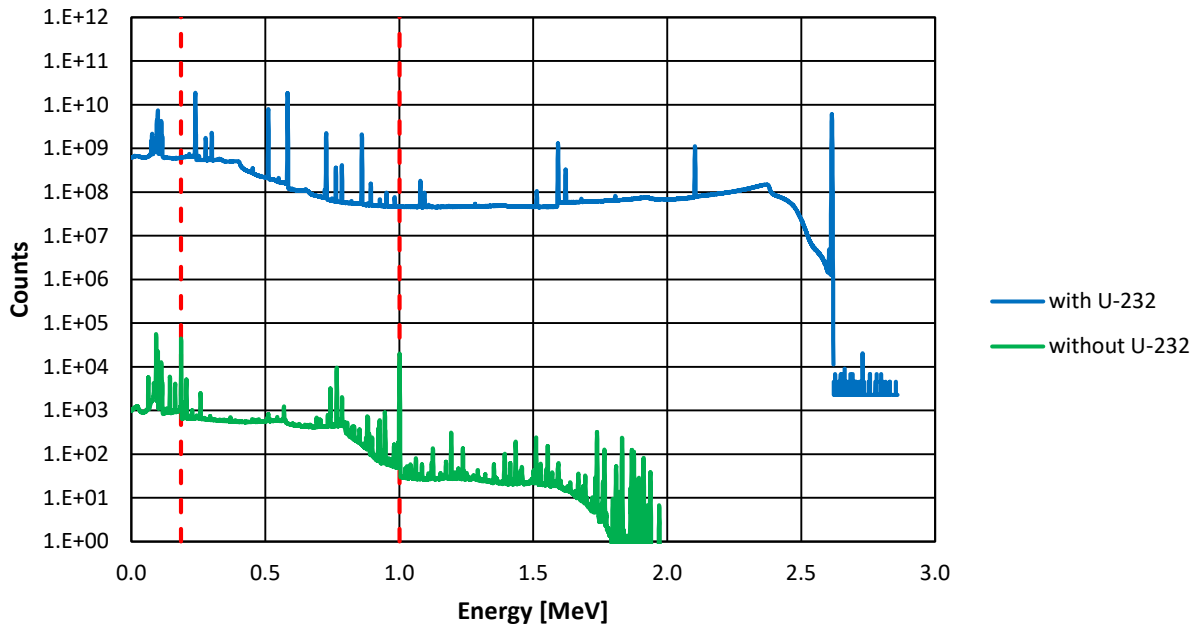
Figure 4.43: Initial uranium isotopic vector spectra at 10 years

Figure 4.44 shows the 3% uranium isotopic vector spectra with and without [232]U

after 0.5 year. Figure 4.45 shows the 3% uranium isotopic vector spectra with and without
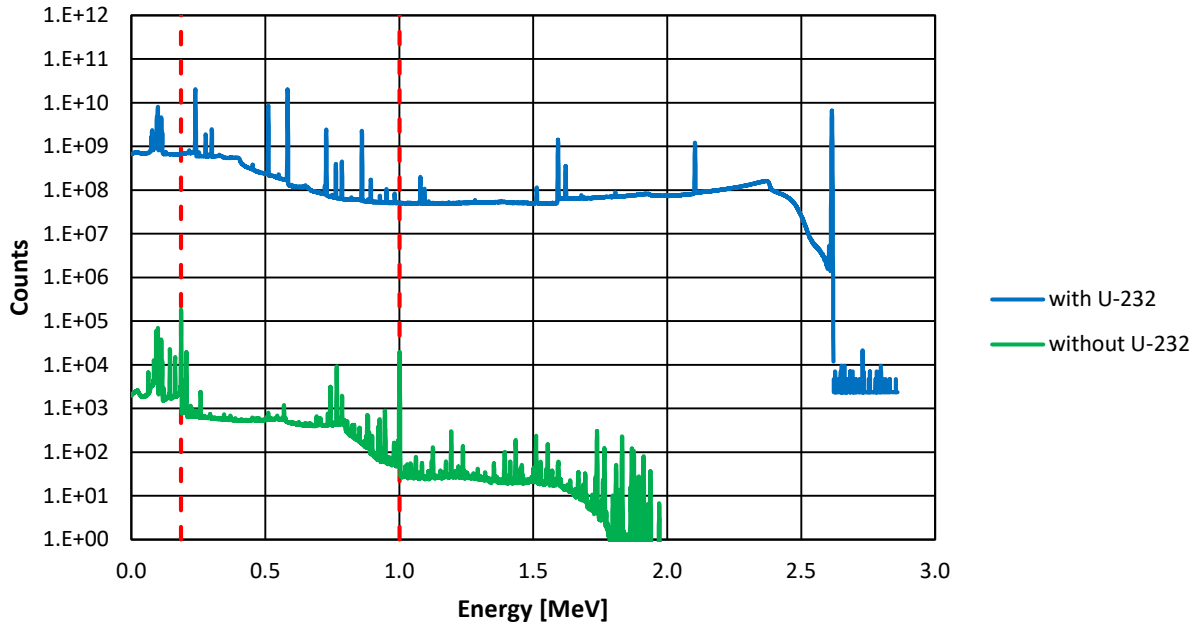
[232]U after 10 years.

Figure 4.44: 3% uranium isotopic vector spectra at 0.5 year
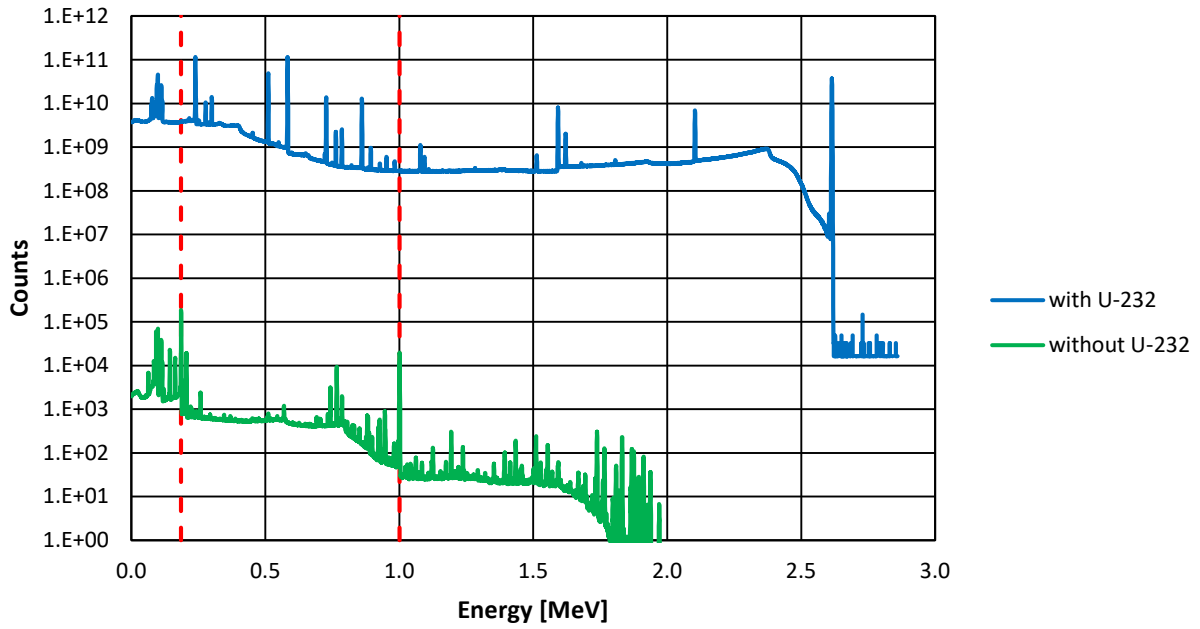
Figure 4.45: 3% uranium isotopic vector spectra at 10 years

112

Figure 4.46 shows the 5% uranium isotopic vector spectra with and without [232]U after 0.5 year. Figure 4.47 shows the 5% uranium isotopic vector spectra with and without [232]U after 10 years.
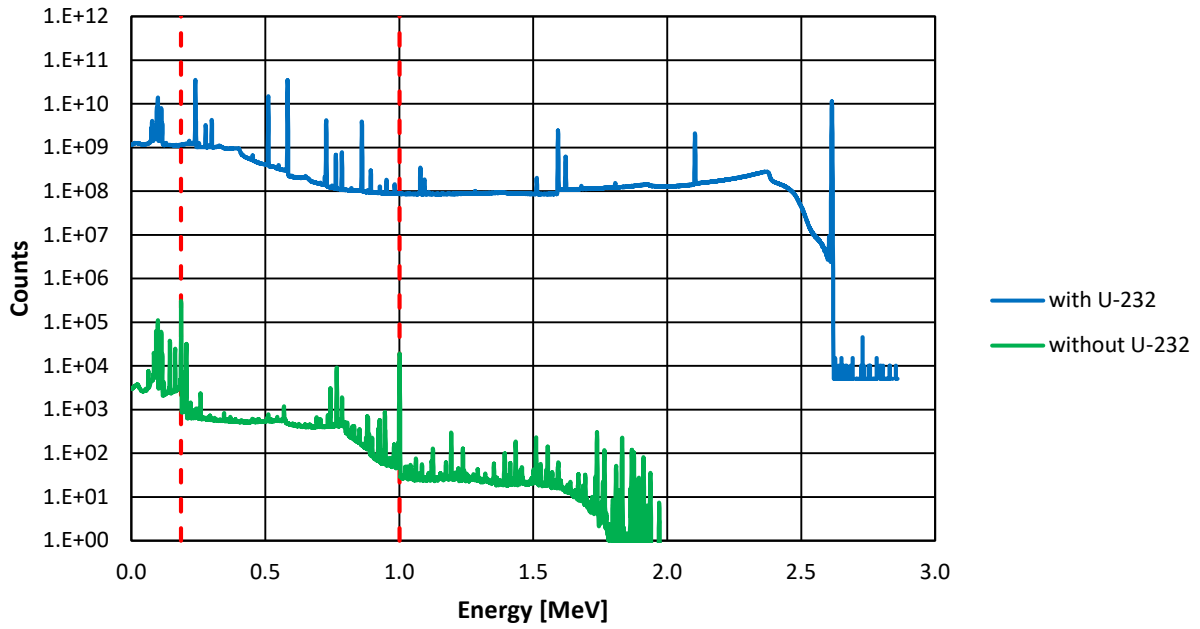
Figure 4.46: 5% uranium isotopic vector spectra at 0.5 year
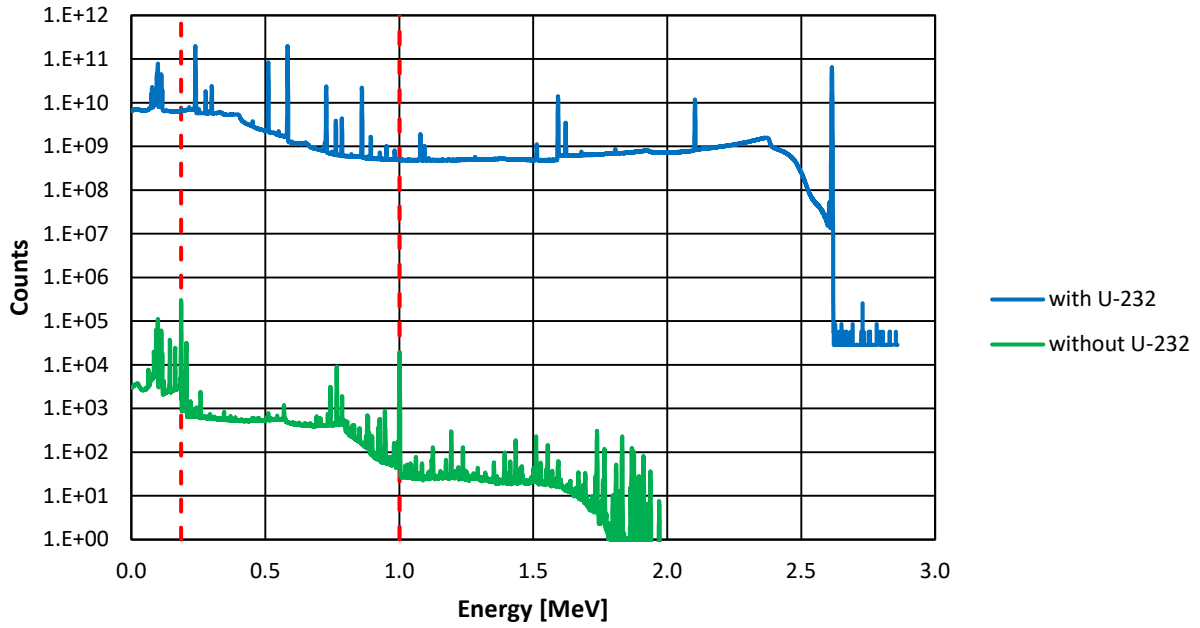
Figure 4.47: 5% uranium isotopic vector spectra at 10 years

Figure 4.48 shows the 20% uranium isotopic vector spectra with and without [232]U after 0.5 year. Figure 4.49 shows the 20% uranium isotopic vector spectra with and without [232]U after 10 years.
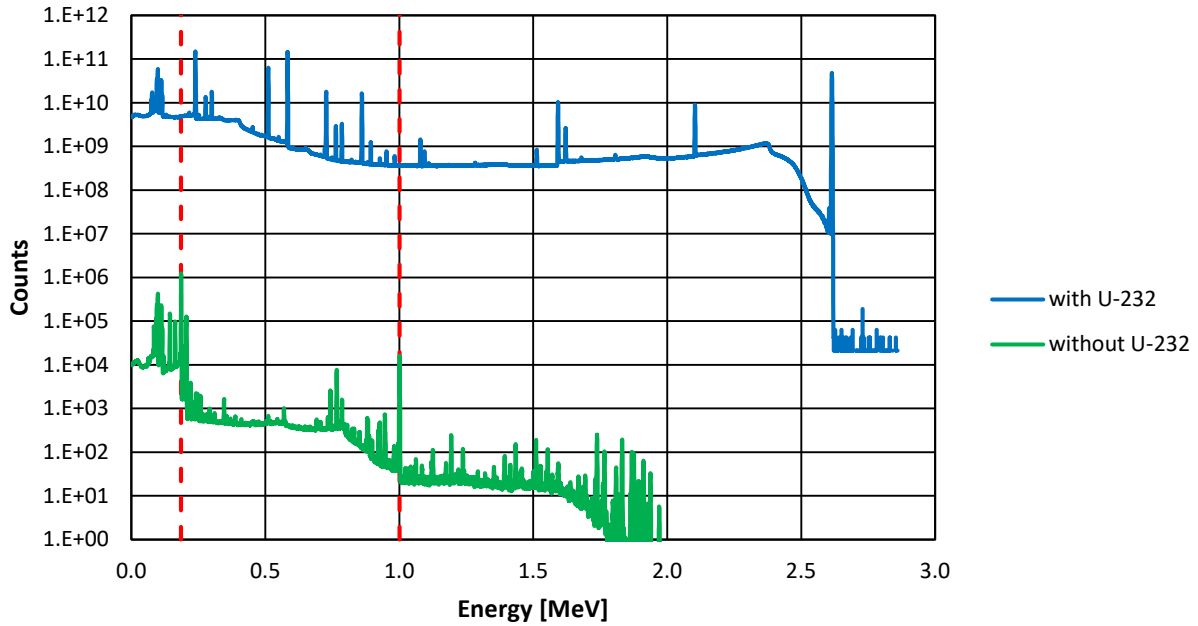
Figure 4.48: 20% uranium isotopic vector spectra at 0.5 year
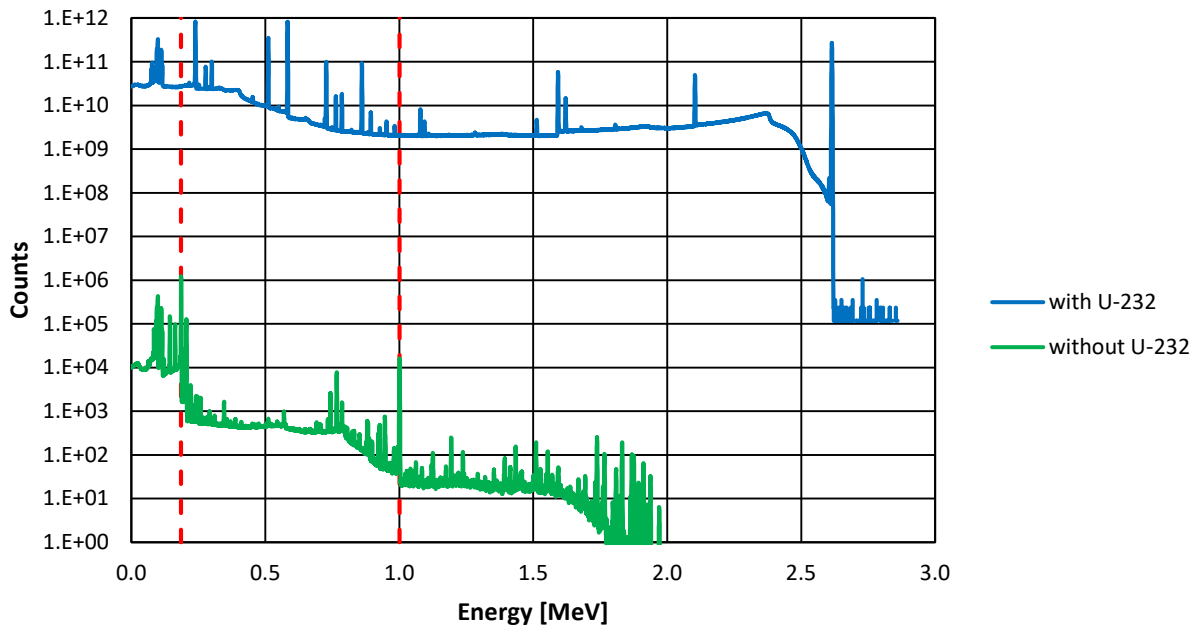
Figure 4.49: 20% uranium isotopic vector spectra at 10 years

As evident in all of the figures, the [235]U and [238]U peaks are clearly visible in the

spectra without [232]U and not visible in the spectra with [232]U. Considering the technique

115

discussed here relies on the calculation of the net peak area of these peaks, this is the first indication that the technique may not be effective. Using Equation 3.19 and Equation 3.20, the net peak areas of the ^{235}U and ^{238}U peaks are calculated using the same regions in all of the spectra shown above. The ratio of the peaks is input into Equation 3.18 to calculate the ratio.

Table 4.15 shows the net peak area and the ratio found from the initial uranium isotopic vectors at time intervals of 0.5 and 10 years.

Table 4.15: Peak ratios from the initial uranium isotopic vectors

			Counts	ratio
0.5 y	without ^{232}U	^{235}U	171,900 ± 508	
		^{238}U	112,700 ± 383	4.752 ± 17.850
	With ^{232}U	^{235}U	426,300 ± 1,592,520	
		^{238}U	1,328,000 ± 520,588	
10 y	without ^{232}U	^{235}U	171,900 ± 508	
		^{238}U	113,300 ± 384	4.406 ± 15.550
	with ^{232}U	^{235}U	2,437,000 ± 8.544.664	
		^{238}U	7,078,000 ± 2,834.231	

Table 4.16 shows the net peak area and the ratio found from the 3% uranium isotopic vectors at time intervals of 0.5 and 10 years.

Table 4.16: Peak ratios from the 3% uranium isotopic vectors

			Counts	ratio
0.5 y	without ^{232}U	^{235}U	717,200± 1,064	
		^{238}U	110,300 ± 404	32.94 ± 232.00
	with ^{232}U	^{235}U	1,304,000 ± 9,166,000	
		^{238}U	6,604,000 ± 3,030,000	
10 y	without ^{232}U	^{235}U	717,300 ± 1,064	
		^{238}U	110,800 ± 405	6.58 ± 8.47
	with ^{232}U	^{235}U	46,370,000 ± 56,780,000	
		^{238}U	47,170,000 ± 18,640,000	

Table 4.17 shows the net peak area and the ratio found from the 5% uranium isotopic vectors at time intervals of 0.5 and 10 years.

Table 4.17: Peak ratios from the 5% uranium isotopic vectors

			Count rate	ratio
0.5 y	without ^{232}U	^{235}U	1,191,000 ± 1,407	
		^{238}U	108,000 ± 412	15.40 ± 27.30
	with ^{232}U	^{235}U	10,230,000 ± 17,660,000	
		^{238}U	14,270,000 ± 5,764,000	
10 y	without ^{232}U	^{235}U	1,191,000 ± 1,407	
		^{238}U	108,600 ± 413	13.34 ± 18.81
	with ^{232}U	^{235}U	72,830,000 ± 99,200,000	
		^{238}U	88,510,000 ± 32,380,000	

Table 4.18 shows the net peak area and the ratio found from the 20% uranium isotopic vectors at time intervals of 0.5 and 10 years.

Table 4.18: Peak ratios from the 20% uranium isotopic vectors

			Count rate	ratio
0.5 y	without ^{232}U	^{235}U	4,819,000 ± 3,214	
		^{238}U	90,600 ± 435	76.34 ± 137.67
	with^{232}U	^{235}U	41,670,000 ± 73,280,000	
		^{238}U	60,110,000 ± 23,940,000	
10 y	without ^{232}U	^{235}U	4,819,000 ± 3,214	
		^{238}U	91,070 ± 437	55.57 ± 73.65
	with ^{232}U	^{235}U	316,500,000 ± 399,700,000	
		^{238}U	332,300,000 ± 133,700,000	

As initially indicated by the spectra, the technique proves to be ineffective. The ratios in each case disagree from unity and have large uncertainties. This is due to the inability to precisely calculate the net peak area of the ^{235}U and ^{238}U peaks in the presence of ^{232}U and its daughter products. The high gamma source strengths of the daughter products of ^{232}U produce a continuum which hides the ^{235}U and ^{238}U peaks making them statistically undetectable. The final ratio found is useless for quantifying ^{235}U enrichment.

This illustrates that this safeguards technique is not useful in the presence of ^{232}U

concentrations discussed here.

The following analysis evaluates a passive neutron multiplicity technique to

calculate uranium mass. The singles, doubles, and triples counts from a passive AWCC 10

minutes measurement of the can models with and without ^{232}U are utilized to calculate the

effective ^{232}U and ^{238}U masses. Table 4.19 shows the passives singles, doubles, and triples

counts from the uranium isotopic vectors with ^{232}U. Table 4.20 shows the singles, doubles,

and triples counts from the uranium isotopic vectors without ^{232}U. The uncertainties shown

are the expected experimental uncertainties calculated using a method developed by Dr.

Croft (57).

Table 4.19: Passive singles, doubles, and triples counts from uranium isotopic vectors with ^{232}U

	Initial	3%	5%	20%
Singles	399,476 ± 637	2,446,709 ± 1,576	4,230,597 ± 2,074	17,825,942 ± 4,272
Doubles	2,070 ± 268	12,581 ± 1,624	23,101 ± 2,807	141,074 ± 11,891
Triples	141 ± 61	857 ± 844	1,614 ± 1,909	10,870 ± 16,527

Table 4.20: Passive singles, doubles, and triples counts from uranium isotopic vectors without ^{232}U

	Initial	3%	5%	20%
Singles	1,365 ± 45	1,404 ± 45	1,396 ± 45	1,643 ± 47
Doubles	214 ± 20	210 ± 19	209 ± 19	182 ± 17
Triples	17 ± 6	17 ± 6	17 ± 6	16 ± 5

The following tables show multiple variables needed to calculate the effective ^{232}U

and ^{238}U masses. These variables are the spontaneous fission factorial moments (v_{s1}, v_{s2},

v_{s3}), doubles gate fraction (f_d), triples gate fraction (f_t), efficiency (ε), and neutron die-away

(τ) time calculated. Each variable was obtained via the same MCNP6 passive simulations

that yielded the singles, doubles, and triples counts above. Table 4.21 shows these values for the uranium isotopic vectors with ^{232}U. Table 4.22 shows these values for the uranium isotopic vectors without ^{232}U.

Table 4.21: Multiplicity analysis variables for uranium isotopic vectors with ^{232}U

	Initial	3%	5%	20%
ν_{s1}	1.98	1.94	1.92	1.81
ν_{s2}	5.72	5.60	5.50	5.16
ν_{s3}	16.92	16.68	16.56	16.90
f_d	0.663	0.663	0.664	0.657
f_t	0.440	0.439	0.441	0.432
ε	0.299	0.299	0.299	0.300
τ [μs]	49.44	49.49	49.27	50.44

Table 4.22: Multiplicity analysis variables for uranium isotopic vectors without ^{232}U

	Initial	3%	5%	20%
ν_{s1}	2.72	2.69	2.68	2.62
ν_{s2}	6.33	6.16	6.05	5.69
ν_{s3}	12.07	11.49	11.12	9.84
f_d	0.659	0.659	0.659	0.662
f_t	0.434	0.434	0.434	0.438
ε	0.325	0.325	0.327	0.325
τ [μs]	50.20	50.21	50.17	49.68

In order to illustrate the technique is effective in uranium materials without ^{232}U, the effective ^{238}U masses ($m_{238\,eff}$) for the uranium isotopic vectors without ^{232}U are calculated using Equation 3.25 with the singles, doubles, and triples counts in Table 4.20 and the values in Table 4.22. The known values are calculated using Equation 3.22. As shown in Table 4.23, the calculated effective ^{238}U mass agrees well with the known values. This shows the technique works well when not in the presence of ^{232}U

Table 4.23: Calculated and known effective ^{238}U masses from the uranium isotopic vectors without ^{232}U

	m$_{238\ eff}$ [g]		
	Calculated	Known	Percent difference
Initial	983	983	0.00
3%	961	961	0.00
5%	945	941	0.43
20%	796	790	0.76

Table 4.24 shows the calculated and known effective ^{238}U masses ($m_{238\ eff}$) and ^{232}U masses ($m_{232\ eff}$) from the uranium isotopic vectors with ^{232}U. The effective ^{232}U masses were calculated using Equation 3.26 and the effective ^{238}U masses were calculated using Equation 3.25 with the singles, doubles, and triples counts in Table 4.19 and the values in Table 4.21. The known effective ^{232}U masses were found using Equation 3.24 and the known effective ^{238}U masses were found using Equation 3.22. The calculated and known values disagree considerably.

Table 4.24: Calculated and known effective ^{238}U and ^{232}U masses from the uranium isotopic vectors with ^{232}U

	m$_{232\ eff}$ [g]			m$_{238\ eff}$ [g]		
	Calculated	Known	Percent difference	Calculated	Known	Percent difference
Initial	26	13	100	11,131	1,005	1,007
3%	195	14	1,293	67,864	1,095	6,097
5%	239	15	1,493	122,491	1,172	10,351
20%	337	23	1,365	689,192	1,761	39,036

In order to attempt to correct the disagreement between the calculate and known values, rather than use the leakage multiplication found via Equation 3.28, the net multiplication (M_{net}) from the MCNP6 simulations is used instead. This net multiplication is a weighted average of the net multiplications found via the (α,n) and spontaneous fission

MCNP6 simulations. Table 4.25 shows the calculated and known effective ^{238}U masses ($m_{238\ eff}$) and ^{232}U masses ($m_{232\ eff}$). Although this percent difference is less using M_{net}, the disagreement is still too significant to accurately and effectively quantify the uranium mass.

Table 4.25: Calculated and known effective ^{238}U and ^{232}U masses from the uranium isotopic vectors with ^{232}U using M_{net}

| | $\mathbf{m_{232\ eff}}$ [g] | | | $\mathbf{m_{238\ eff}}$ [g] | | |
	Calculated	Known	Percent difference	Calculated	Known	Percent difference
Initial	16	13	23.08	1,685	1,005	67.66
3%	45	14	221.43	4,798	1,095	338.17
5%	76	15	406.67	7,977	1,172	580.63
20%	567	23	2,365.22	55,525	1,761	3,053.04

The major difference between the neutron emissions of the uranium isotopic vectors with ^{232}U and without ^{232}U is the significant difference in their (α,n) emission rates. Table 4.26 shows the (α,n) and spontaneous fission neutron emission rates of the uranium isotopic vectors with ^{232}U. Table 4.27 shows the (α,n) and spontaneous fission neutron emission rates of the uranium isotopic vectors without ^{232}U. As shown in the tables below, the α decay of ^{232}U in the UO_2 produces significantly more (α,n) neutrons than those found in the uranium isotopic vectors without ^{232}U.

Table 4.26: (α,n) and spontaneous fission neutron emission rates of uranium isotopic vectors with ^{232}U [n/s]

	(α,n)	Spontaneous Fission	Total
Initial	4,365	14	4,379
3%	26,785	16	26,801
5%	46,274	17	46,291
20%	193,633	28	193,661

Table 4.27: (α,n) and spontaneous fission neutron emission rates of uranium isotopic vectors without ^{232}U [n/s]

	(α,n)	Spontaneous Fission	Total
Initial	0	14	14
3%	1	13	14
5%	1	13	14
20%	6	11	17

The significantly larger (α,n) source strength in the uranium isotopic vectors with ^{232}U cause a notable increase in the sensitivity of the relationship between the effective masses and the leakage multiplication. Figure 4.50 shows the effective ^{238}U mass ($m_{238\,eff}$) as a function of the leakage multiplication (M_L). Slight variations in the leakage multiplication will produce only slight variations in the effective ^{238}U mass. For example, a 1% difference in the leakage multiplication will produce only a difference of approximately 10 grams in the effective ^{238}U masses.
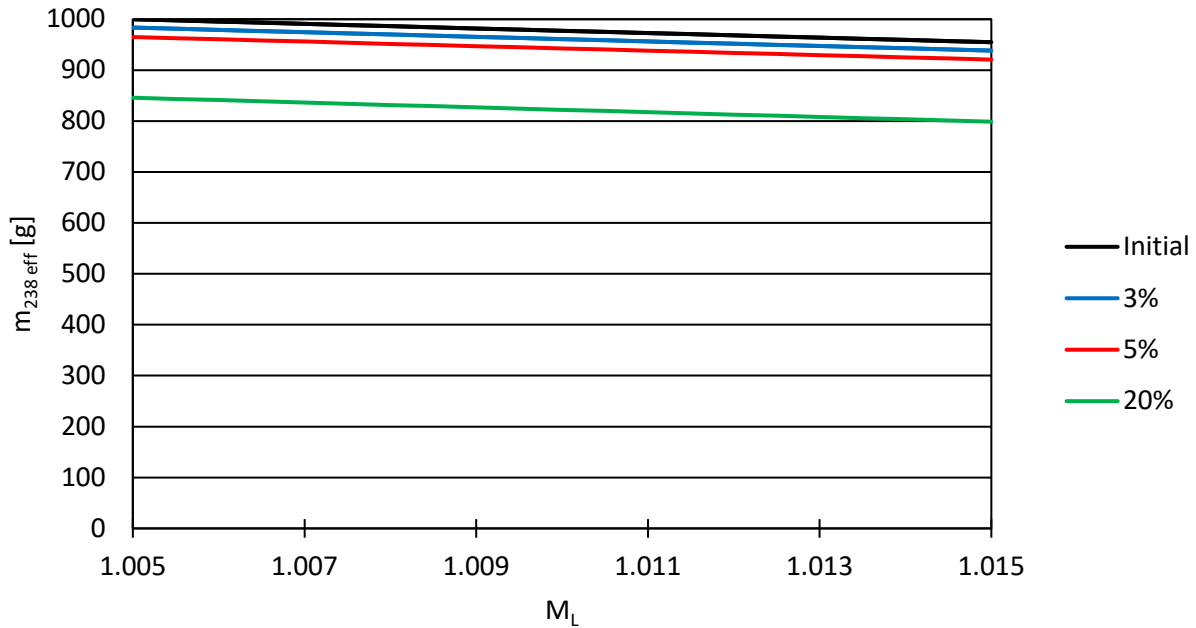
Figure 4.50: Effective ^{238}U mass vs. leakage multiplication from uranium isotopic vectors without ^{232}U

Figure 4.51 shows the effective ^{232}U mass ($m_{232\ eff}$) as a function of the leakage

multiplication (M_L) from the uranium isotopic vectors with ^{232}U. Unlike the relationship

shown in Figure 4.50, the relationship between the effective ^{232}U mass and the leakage

multiplication is significantly sensitive. Slight variations in the leakage multiplication

produces significantly different ^{232}U mass values (on the order of 100s to 1000s of grams).

This impact increases with higher concentrations of ^{232}U. Minor errors in the nuclear data

used will produce significantly erroneous effective ^{232}U masses. The limited nuclear data of

^{232}U produces significant issues with the use of this technique to quantify uranium mass. In

order to effectively calculate the uranium mass via passive neutron interrogation in the

presence of ^{232}U, further investigation must be done to produce accurate nuclear data for

^{232}U in real world measurements.
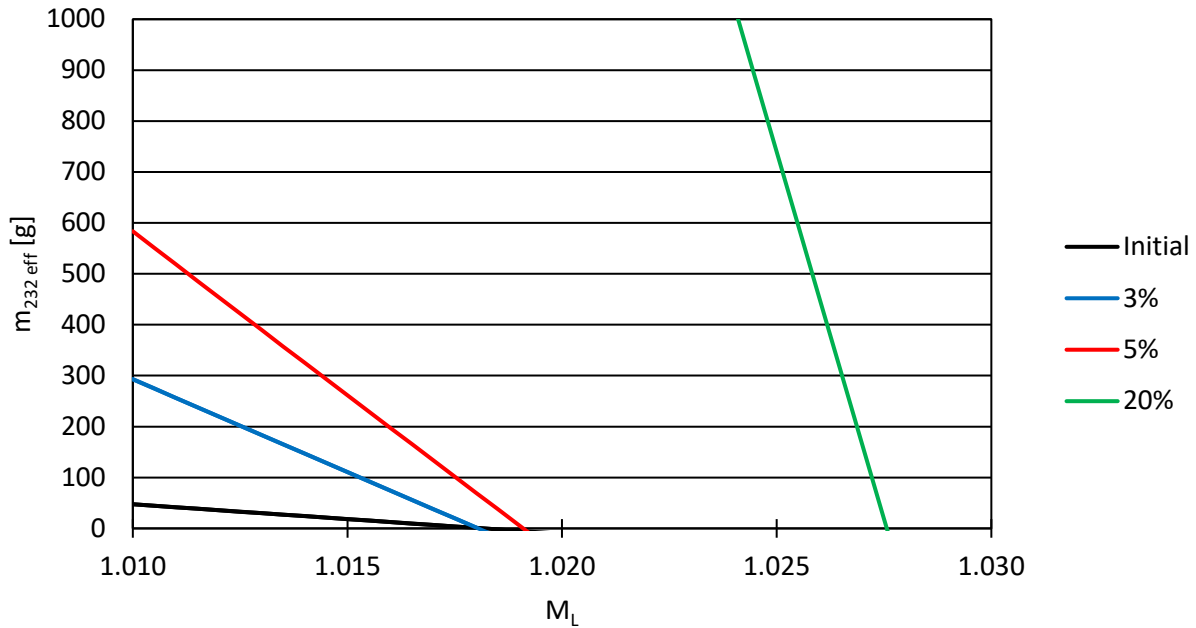
Figure 4.51: Effective ^{232}U mass vs. leakage multiplication from uranium isotopic vectors with ^{232}U

In addition to the passive neutron interrogation discussed here, an active analysis is also done. The AWCC is utilized in its active configuration in MCNP6 to produce active doubles count rates from the uranium isotopic vectors with and without ^{232}U. Figure 4.52 shows the active doubles count rates graphed as a function of the ^{235}U mass from the uranium isotopic vectors with and without ^{232}U. The relationship between the active doubles count rate and the ^{235}U mass are similar both with and without ^{232}U. There is a slight contribution in the active doubles count rate from the ^{232}U mass. If the passive doubles count rate can be removed from the active measurement, then this active interrogation could possibly be used to quantify the ^{235}U mass.
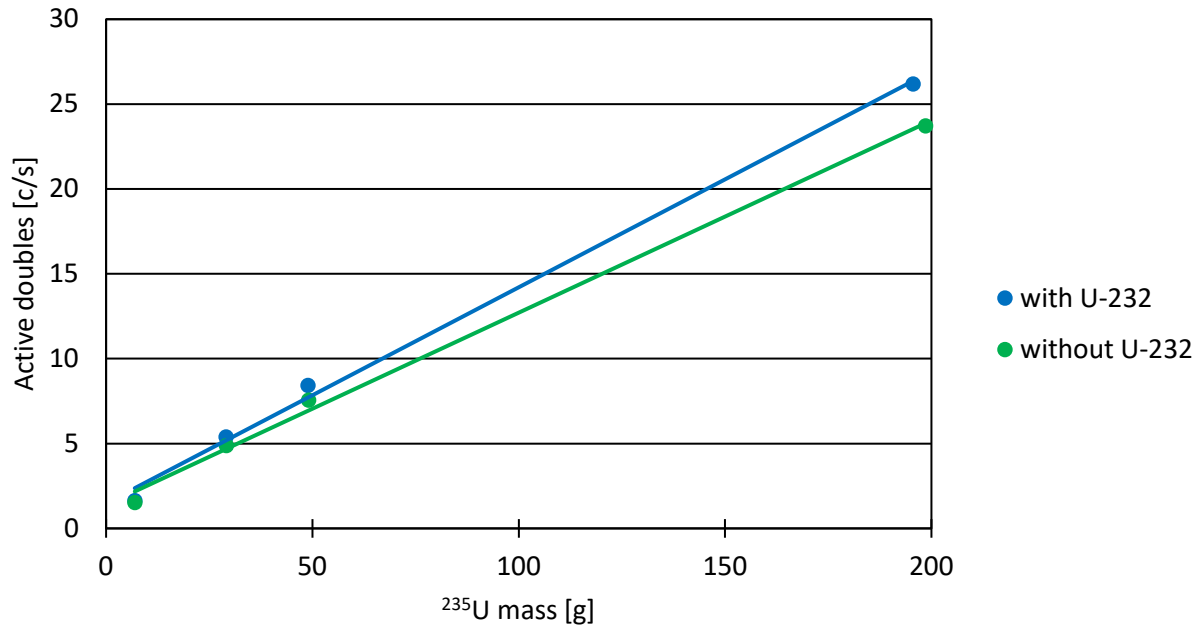
Figure 4.52: Active doubles count rate vs. ^{235}U mass

5. CONCLUSIONS AND FUTURE WORKS

5.1. Plutonium Conclusions

The analyses in this study illustrate the value of increasing the concentration of ^{238}Pu in used fuel for reducing the material attractiveness. However, the magnitude of this decrease in material attractiveness is not significant enough to warrant the label of "proliferation proof" or even unattractive for weapons purposes. Although the model based analysis was promising, the Figure of Merit analysis showed the difficulty in reaching the unattractive limit via increased ^{238}Pu concentrations.

The model based approach concluded the concentration of ^{238}Pu in the plutonium isotopic vector shown in Table 3.1 was high enough to render the HNED models described in Table 3.3 and Table 3.4 useless. In the time dependent analysis of the more realistic model (Table 3.4), the self-explosion temperature in the high explosives was reached after approximately 7.5 hours from the initial insertion of the weapons pit into the model. However, external cooling with liquid nitrogen prevented the self-explosion temperature from being reached. The tensile strength in the high explosives and beryllium was reached in all four scenarios, likely producing plastic deformation. The possibility of the weapon being rendered totally useless or a significant reduction in the yield represent major obstacles to proliferation. These results show the impractically and difficulty in weaponizing this plutonium vector for these simple implosion models.

The application of the Figure of Merit equations shown in Equation 2.1 and Equation 2 to the plutonium vector yielded significantly fewer positive results regarding its material attractiveness. In comparison to the additional plutonium vectors from Table 3.5, the material attractiveness was lower. However, all three fell within the same range for both

126

FOM equations. For less technically advanced states, all three plutonium vectors are unattractive according to FOM_1 (Equation 2.1). For technically advanced states, all three plutonium vectors are attractive according to FOM_2 (Equation 2.2). This conclusion is to be expected as the heat generation factor in FOM equations is normalized to 80% ^{238}Pu and the spontaneous fission neutron generation rate is normalized to reactor grade. Thus, any plutonium isotopic vector from used reactor fuel with less than 80% ^{238}Pu will be unattractive for less technically advanced states and attractive for technically advanced states. Currently, surpassing these limits in used fuel is in most cases impractical or even unattainable given current reactor designs. Therefor as long as the Figure of Merit approach discussed here in its present form is used to analyze plutonium vectors from used fuel, these conclusions will be the same.

5.2. Uranium Conclusions

This study successfully illustrated the reduction of material attractiveness in uranium materials via the introduction of ^{232}U and the build-up of its daughter products. Unlike the case of the plutonium analysis, this reduction of material attractiveness proved successful in both the model based and Figure of Merit analyses. However, the introduction of ^{232}U poses additional obstacles to its implementation in a civilian nuclear fuel cycle.

The model based analysis showed the concentration of ^{232}U in the weapons grade uranium vector (90%) from Table 3.6 in the model shown in Table 3.8 sufficient to reduce the material attractiveness. As shown in Figure 4.14 through Figure 4.20, the temperature in the high explosives exceeds its self-explosion temperature rendering the weapon useless. In addition, the high explosives begin to degrade after 2.1 years as a result of radiation dose. The transient heat transfer analysis showed that the self-explosion

temperature within the high explosives is reached after approximately 1 day, unless the model is continuously externally cooled by liquid nitrogen. Similarly, to the plutonium model based results, the strength of the high explosives and beryllium is surpassed in all four scenarios. This will likely produce plastic deformation in those materials and a possible reduction in the yield. The model based analysis illustrates the impracticality of utilizing this uranium material in simple implosion type fission weapons.

The Figure of Merit results also show a significant decrease in material attractiveness. Considering the spontaneous fission neutron generation rate of the weapons grade uranium vector is relatively low, the FOM equations for less technically advanced states (Equation 2.1) and for technically advanced states (Equation 2.2) yield the same results. Thus, these conclusions are valid for both less technically advanced and technically advanced states. As shown in Figure 4.34, the build-up of ^{232}U's daughter products causes the material to become unattractive for weapons purposes within the first 6 to 9 months after separation. In order to maintain the weapons usability of the material, the daughter products must be removed approximately semi-annually. This poses a significant burden on the proliferating state and would be impractical.

Although the merits of utilizing ^{232}U to decrease material attractiveness are clear, implementing ^{232}U in civilian nuclear fuel cycles would be difficult. At the ^{232}U concentrations shown in Table 3.6, the dose rate from the pellet (Figure 3.1), rod (Figure 3.2), and can (Figure 3.3) pose a significant safety risk. The 5 rem annual limit imposed by the U.S. Nuclear Regulatory Commission would be reached far too quickly and thus significant shielding would be required. In addition, both gamma ray and neutron non-destructive assay techniques proved ineffective in the presence of ^{232}U. Although,

quantifying ^{235}U mass via active neutron interrogation may be possible. Considering both the safety and safeguards concerns, the decrease in material attractiveness is currently not sufficient to justify the implementation of ^{232}U at these concentrations in a civilian nuclear fuel cycle. The burden of increasing shielding throughout the handling of the material as well as the need for new non-destructive assay safeguards techniques would likely outweigh the obstacles to proliferation from most state's perspectives.

One of the most beneficial conclusions of this study is the increase in detectability with the addition of ^{232}U. Although the security neutron analysis showed no increase in detectability, the security gamma ray analysis showed a significant increase in detectability. When comparing gamma ray measurements of the 90% vector with ^{232}U (Table 3.6) and that without ^{232}U (Table 3.7), the spectra with ^{232}U are clearly distinguishable between background and the spectra without ^{232}U, in particularly at the 6 month and 10 year time intervals. The intensity of the spectra with ^{232}U indicates the possibility of producing an increase in detectability even at a lower concentration of ^{232}U. Although the concentrations of ^{232}U discussed here are likely too high to implement within a civilian nuclear fuel cycle, the possibility of implementing lower concentrations of ^{232}U exists. This possibility could come to fruition if the safety and safeguards impacts of ^{232}U are minimized while its impact on gamma ray detectability is further evaluated. Combing computational and experimental efforts to explore gamma ray measurements of uranium materials with significantly lower concentrations of ^{232}U than those discussed here would be useful to determine the minimum amount of ^{232}U that would produce a notable increase in detectability.

5.3. Conclusions on the Effectiveness of Material Attractiveness Analyses

This study utilized two different techniques to evaluate material attractiveness that represent both a specific evaluation and a more broad evaluation. The model based analysis is likely the most restrictive analysis in terms of overall material attractiveness conclusions. Although it is impossible to evaluate the material attractiveness for specific HNED models, a comprehensive determination must involve all the possible permutations of nuclear weapons designs. Currently this is not possible, because the vast majority of these possible designs fall within the classified space. The Figure of Merit analysis discussed in this study allows for a more comprehensives evaluation while still relying on open source information for the analysis. However, these techniques are just two of the many possible techniques utilized to quantify material attractiveness or proliferation resistance.

As mentioned in this study, the most significant shortcoming of the FOM equations shown in Equation 2.1 and Equation 2.2 is its inability to account for processes such as enrichment or reprocessing. In the uranium analysis, this study evaluated several isotopic vectors at various ^{235}U concentrations originating from the same initial uranium isotopic vector. Due to limits of the FOM equations, the material attractiveness of only the weapons grade (90%) isotopic vector could be considered. Therefor the entire enrichment process is neglected in the final determination of this material attractiveness. Ideally, the material attractiveness of the specific material initially possessed by the state would be useful rather than the material attractiveness of the weaponized version of this material. Similarly, the plutonium analysis only considers the plutonium isotopic vector in its final

metallic state rather than present in the used fuel. This doesn't account for the processing required to remove plutonium from the used fuel.

A public workshop preformed at the request of the U.S. Department of Energy known as the "Proliferation Risk in Nuclear Fuel Cycles" discussed several aspects of proliferation risk assessments (64). This workshop not only discussed the Figure of Merit analysis used here, but also more comprehensive methods of evaluating proliferation resistance. These more comprehensive methods not only consider the material attractiveness, but also many factors that contribute to proliferation risk such as characteristics of the entire fuel cycle or the proliferant state. Perhaps the most comprehensive of these methods is the Proliferation Resistance Analysis and Evaluation Tool for Observed Risk (PRAETOR) that was developed at Texas A&M (65). PRAETOR uses what is known as a multi attribute utility analysis methodology to consider many possible attributes to the proliferation of nuclear material to quantify the associated proliferation risk (66). Although useful, this method is most useful in analyzing a larger aspect of a nuclear fuel cycle rather than a specific material.

Another specific illustration of the shortcomings of the Figure of Merit analysis can also be found in the literature. A group at LLNL applied the figure of merit equation to a specific material but made additional considerations (66). Although the figure of merit conclusions showed the material was attractive, the group recognized the following attributes were not evaluated in the FOM analysis: the difficulty of stealing, diverting, or transporting the material and the number of significant quantities available. The group concluded that combining the figure of merit with these additional considerations proves useful although they concede that it may be "impossible to come up with absolute

131

quantitative measures of proliferation resistance." This final conclusion serves as the main justification for only utilizing the FOM equations to quantify the material attractiveness.

If the techniques described in this study (utilizing ^{238}Pu and ^{232}U for decreasing material attractiveness) were to be expanded, the use of a tool such as PRAETOR would be useful. In the case of the plutonium material, the final conclusions would not likely change, because the current obstacles of reprocessing and handling of similar plutonium materials are not considered significant to justify a reduction in safeguards. However, in the case of uranium, the final conclusions may possibly differ. The decay of ^{232}U poses significant handling and reprocessing issues. If the safety and safeguards issues shown here were overcame and ^{232}U were implemented into a civilian nuclear fuel cycle, applying a PRAETOR would be necessary as a compliment to the FOM analysis. Analysis this hypothetical fuel cycle that included ^{232}U might shed additional light on ^{232}U's comprehensive effect at reducing the proliferation risk. However, this is outside of the scope of this study and would require additional considerations to limit the burden of ^{232}U on the state seeking to use the material for peaceful purposes.

VITA

CODY LEE LLOYD

lloydcl2@vcu.edu

Education

- **Ph.D. Candidate in Mechanical and Nuclear Engineering (December, 2020)**
  Virginia Commonwealth University, Richmond, VA, USA

- **Bachelor of Science in Physics (July, 2015)**
  Longwood University, Farmville, VA, USA

Publications

- Shah, M., Goddard, B., **Lloyd, C**., Witherspoon, R., Britt, T., Investigation Material Attractiveness for an Innovative Metallic Fuel Design, Nuclear Engineering and Design 357, doi:10.1016/j.nucengdes.2019.110385 2020.
- Hua, M., Goddard, B., **Lloyd, C.**, Leppink, E., Abraham, S., Noey, J., Clarke, S., and Pozzi, S., Simulation of the Nondestructive Assay of 237Np using Active Neutron Multiplicity Counting, Nuclear Science and Engineering, Vol. 194(2), pp. 154-162, 2020.
- Dodd, B., Britt, T., **Lloyd, C.**, Shah, M., Goddard, B., Novel Homogeneous Burnable Poisons in Pressurized Water Reactor Ceramic Fuel, Nuclear Engineering and Technology, doi:10.1016/j.net.2020.05.021 2020.
- **Lloyd, C.**, Goddard, B., The effects of U-232 on Enrichment and Material Attractiveness over Time. Nuclear Engineering and Design, Volume 352, Pages 1-6, 2019.
- **Lloyd, C.**, Hadimani, R., Goddard, B., Time Dependent Heat Transfer of Proliferation Resistant Plutonium. Nuclear Engineering and Technology, Volume 51, Pages 510-517, 2019.
- Goddard, B., Bosc, E., Al Hasani, S., **Lloyd, C.**, Evaluation of Background Dose Contributions in the United Arab Emirates, Journal of Environmental Radioactivity, Volume 189, Pages 191-196, 2018.
- **Lloyd, C.**, Goddard, B., Proliferation resistant plutonium: An updated analysis. Nuclear Engineering and Design, Volume 330, Pages 297-302, 2018

Conference Proceedings

- **Lloyd, C.**, Goddard, B., Figure of Merit Analysis of Proliferation Resistant Plutonium and Uranium. 60th INMM Annual Meeting, 2019.

- **Lloyd, C.,**Goddard, B., "Proliferation Resistant Uranium by way of 232U," Proc. 27th International Conference on Nuclear Engineering, Tsukuba, Ibaraki, Japan May 19-24, 2019.
- **Lloyd, C.**, Goddard, B., Quantifying the Proliferation Resistance of a Plutonium Vector. ANS Student Conference, 2019.
- **Lloyd, C.**, Goddard, B., Proliferation Resistant Plutonium and Uranium by way of Decay Heat. 59th INMM Annual Meeting, 2018.
- **Lloyd, C.**, Goddard, B. 2018. A Hybrid School of Thought: Physics to Nuclear Engineering. ANS Student Conference, 2018.
- **Lloyd, C.**, Effectively Shielding a Pion Detector, Louisiana Academy of Science Meeting, 2016.
- **Lloyd, C.**, Geometric Probabilities of Three Points in a Sphere, Cook College of Arts and Sciences Showcase, Longwood University, 2015.

Bibliography

1. *20th Annual Reference Issue.* **News, Nuclear.** March 2018, pp. 39-71.

2. **Initiative, Nuclear Threat.** IRAN. *NTI.* [Online] January 2020.

https://www.nti.org/learn/countries/iran/.

3. NORTH KOREA. *NTI.* [Online] August 2019. https://www.nti.org/learn/countries/north-

korea/.

4. **Coster-Mullen, John.** *Atom Bombs: The Top Secret Inside Story of Little Boy and Fat Man.*

Waukesha : Coster Mullen, 2012.

5. **School, Yale Law.** The Atomic Bombings of Hiroshima and Nagasaki: Chapter 10- Total

Casualties. *The Avalon Project.* [Online] 2008.

https://avalon.law.yale.edu/20th_century/mp10.asp.

6. **Shultis, J. Kenneth and Faw, Richard E.** *Fundamentals of Nuclear Science and*

Engineering. Boca Raton, FL : CRC Press, 2017.

7. **The United Nations.** *Treaty on the Non-Proliferation of Nuclear Weapons.* 1970.

8. **IAEA.** The Structure and Content of Agreements Between the Agency and States

Required in Connection with the Treaty on the Non-Proliferation of Nuclear Weapons. June

1972.

9. **The United Nations.** UNODA. *Treaty on the Non-Proliferation of Nuclear Weapons (NPT).*

[Online] 2019. https://www.un.org/disarmament/wmd/nuclear/npt/.

10. **IAEA.** *IAEA Department of Safeguards: Long-Term Strategic Plan (2012-2023).* Vienna :

IAEA, 2012.

11. *IAEA Safeguards Glossary: 2001 Edition.* Vienna : s.n., 2002.

12. **Beller, Denis E. and Krakowski, Robert A.** *Burnup Dependence of Proliferation Attributes of Plutonium from Spent LWR Fuel.* s.l. : Los Alamos National Laboratory, 1999.

13. *Predetonation probability of a fission-bomb core.* **Reed, B. Cameron.** s.l. : American Journal of Physics, 2010, Vol. 78, pp. 804-808.

14. **Avrami, Louis.** *Radiation-Induced Changes in Explosive Materials.* Springfield : National Technical Information Service U.S. Department of Commerce, 1973.

15. **Nias, A. H. W.** *An Introduction to Radiobiology 2nd Edition.* Chichester : John Wiley & Sons, 1998.

16. **CDC.** Acute Radiation Syndrome: A Fact Sheet for Clinicians. *Centers for Disease Control and Prevention.* [Online] 2018.

https://emergency.cdc.gov/radiation/arsphysicianfactsheet.asp.

17. **NRC, U.S.** Subpart C - Occupational Dose Limits. *United States Nuclear Regulatory Commission Web site.* [Online] August 24, 2018. [Cited: December 18, 2019.]

https://www.nrc.gov/reading-rm/doc-collections/cfr/part020/part020-1201.html.

18. *The Attractiveness of Materials in Advanced Nuclear Fuel Cycles for Various Proliferation and Theft Scenarios.* **Bathke, Charles G., et al.** Paris : s.n., 2009. Proceeding of Global.

19. *Evaluation of Proliferation Resistance of Plutonium Based on Decay Heat.* **Kimura, Yoshiki, Saito, Masaki and Sagara, Hiroshi.** 5, 2011, Journal of Nuclear Science and Technology, Vol. 48, pp. 715-723.

20. *Plutonium Denaturing by 238-Pu.* **Kessler, G.** 2007, Nuclear Science and Engineering, Vol. 155, pp. 53-73.

21. **KAERI.** Nuclear Data Center at KAERI. *Table of Nuclides.* [Online] 2000.

http://atom.kaeri.re.kr:8080/ton/index.html.

22. *Evaluation of proliferation resistance of plutonium based on spontaneous fission neutron emission rate.* **Kimura, Yoshiki, Saito, Masaki and Hiroshi Sagara, Chi Young Han.** 2012, Annals of Nuclear Energy, Vol. 46, pp. 152-159.

23. **Reiley, D., et al.** *Passive Nondestructive Assay of Nuclear Materials.* s.l. : United States Nuclear Regulatory Commission, 1991.

24. *Denaturing of Plutonium by Tranmutation of Minor-Actinides for Enhancement of Proliferation Resistance.* **Sagara, Hiroshi, et al.** 2, 2005, Journal of Nuclear Science and Technology, Vol. 42, pp. 161-168.

25. **Moir, R.** *U232 Nonproliferation Features.* s.l. : Lawrence Livermore National Laboratory, 2010.

26. *Evaluation of Self- Protectiong of 20% Uranium Denatured with U-232 Against Unauthorized Reenrichment.* **Kryuchkov, E. F., Apse, V. A. and V. A. Yufereva, V. B. Glebov, A. N. Shmelev.** 2009, Nuclear Science and Engineering, Vol. 162, pp. 208-213.

27. *Radiation Effect of Alpha Particles on Uranium Hexaflouride.* **Bernhardt, H. A., Jr., W. Davis and Shiflett, C. H.** 1958. Second United Nations International Conference on the USES of Atomic Energy.

28. **IAEA.** *Thorium fuel cycle- Potential Benefits and Challenges.* Vienna : International Atomic Energy Agency, 2005.

29. *The Preparation of Carrier-Free U-232 and the Estimation of Various Nuclides Produced by the Neutron Irradiation of Pa-231.* **Sakanoue, M. and Komura, K.** 6, 1966, Nuclear Science and Technology, Vol. 3, pp. 249-255.

30. *Thermophysical Properties of Materials for Nuclear Engineering: A Tutorial and Collection of Data.* **IAEA.** Vienna : International Atomic Energy Agency, 2008.

31. *Plutonium and Its Alloys: From Atoms to Microstructure.* **Hecker, S. S.** 2000.

32. *Atomic, Crystal, Elastic, Thermal, Nuclear, and Other Properties of Beryllium.* **Goldberg, A.** s.l. : LLNL, 2006, Vols. UCRL-TR-223850.

33. **J. M. Gere, B. J. Goodno.** *Mechanics of Materials SI ed.* Stanford : Cengage Learning, 2012.

34. *On Predicting the Effective Elastic Properties of Polymer Bonded Explosives Using Recursive Cell Method.* **B. Banerjee, D. O. Adams.** 2, s.l. : International Journal of Solids and Structures, 2004, Vol. 41.

35. *Deformation, Strengths, and Strains to Failure of Polymer Bonded Explosives.* **Palmer, S. J. P., Field, J. E. and Huntley, J. M.** s.l. : Proceedings of the Royal Socienty A, 1993. Vol. 440.

36. *Thermal Expansion of PBX 9501 and PBX 9502 Plastic-Bonded Explosives.* **Thompson, D. G.; Brown, G. W.; Deluca, R.; Giambra, A. M.; Sandstrom, M. M.** Lubbock, TX : s.n., 2009. 37th Meeting of the North American Thermal Analysis Society.

37. **Çengel, Yunus A.** *Heat Transfer: A Practical Approach 2nd Edition.* New York : McGraw-Hill, 2003.

38. *Thermal Properties and Heat Transfer Coefficients in Cryogenic Cooling.* **Biddulph, M. W. and Burford, R. P.** 6, s.l. : Cryogenics, 1982, Vol. 22, pp. 283-286.

39. **Chapra, S. C. and Canale, R. P.** *Numerical Methods for Engineers 7th ed.* New York : McGraw-Hill, 2015.

40. *Lightbridge Corporation's Advanced Metallic Fuel for Light Water Reactors.* **Malone, J., et al.** 2012, Materials for Nuclear Systems, Vol. 180, pp. 437-442.

41. **Global, Pace.** *Lightbridge Metallic PWR Fuel Evaluation of Proliferation Resistance Properties.* 2013.

42. *Time dependent heat transfer of proliferation resistant plutonium.* **Lloyd, Cody, Hadimani, Ravi and Goddard, Braden.** 2, s.l. : Nuclear Engineering and Technology, 2019, Vol. 51, pp. 510-517.

43. *MCNP6 User's Manual.* **LANL.** 2008.

44. *Detecting Nuclear Warheads.* **Fetter, S., et al.** 1990, Science & Global Security, Vol. 1, pp. 225-302.

45. **Hiller, L., et al.** *RadSrc Library and Application Manual.* s.l. : Lawrence Livermore National Laboratory, 2013.

46. *Systematics of fission fragment total kinetic energy release.* **Viola, V. E., Kwiatkowski, K. and Walker, M.** 4, s.l. : Physical Review C., 1985, Vol. 31, pp. 1550-1552.

47. *Novel homogeneous buranable poisons in pressurized water reactor ceramic fuel.* **Dodd, B., et al.** s.l. : Nuclear Engineering and Technology, 2020.

48. *242 Pu Critical Mass.* **Brewer, R. W.** s.l. : Los Alamos National Laboratory, 1996. LA-UR-99-3509.

49. *Generalized Modeling of Enrichment Cascades That Include Minor Isotopes.* **Weber, Charles.** Orlando, FL : s.n., 2012. INMM 53rd Annual Meeting.

50. *Sources 4C: A Code for Calculating (alpha,n), Spontaneous Fission, and Delayed Neutron Sources and Spectra.* **Wilson, W. B., et al.** Sante Fe, NM : American Nuclear Society: Radiation Protection and Sgielding Division 12th Biennial Topical Meeting, 2002.

51. *The effects of U-232 on enrichment and material attractiveness over time.* **Lloyd, Cody, Goddard, Braden and Witherspoon, Raven.** s.l. : Nuclear Engineering and Design, 2019, Vol. 352.

52. *Energy Engineering and Systems Analysis: Nuclear Fuel.* **Argonne National Laboratory.** 2011.

53. *Corrosion of Zirconium Alloys Used for Nuclear Fuel Cladding.* **Motta, A. T., Couet, A. and Comstock, R. J.** Pittsburg, PA : Westinghouse Electric Company, 2015.

54. *The Epithermal Neutron Multiplicity Counter Design and Performance Manual: More Rapid Plutonium and Uranium Inventory Verifications by Factors of 5-20.* **Stewart, J. E., et al.** s.l. : Los Alamos National Laboratory, 2000. LA-13743-M.

55. *Genie 2000 Gamma Analysis Foundations and Optimization.* **Sharp, Cathey.** College Park, MD : A Day on the Beltway with Canberra, Canberra Seminar, 2017.

56. *High-Fidelity Passive Neutron Multiplicity Measurements and Simulations of Uranium Oxide.* **Goddard, B. and Croft, S.** s.l. : Nuclear Instruments and Methods in Physics Research A, 2013, Vol. 712, pp. 147-156.

57. *A priori precision estimation for neutron triples counting.* **Croft, S., Swinhoe, M. T. and Henzl, V.** Ghent : 2nd International Conference on Advancements in Nuclear Instrumentation, Measurement Methods and their Applications, 2011.

58. *Safeguards Techniques and Equipment 2011 Edition.* **IAEA.** Vienna : International Nuclear Verification Series No. 1, 2011.

59. *Description and Operations Manual for the Active Well Coincidence Counter.* **LANL.** s.l. : Los Alamos Scientific Laboratory, 1979, Vols. LA-7823-M.

60. *Proliferation Resistant Plutonium: An Updated Analysis.* **Lloyd, C. and Goddard, B.** s.l. : Nuclear Engineering and Design, 2018, Vol. 330, pp. 297-302.

61. *Cosmic Coincidences: Investigations for Neutron Bacground Supression.* **Heimback, Craig R.** s.l. : Journal of Research of the National Institute of Standards and Technology, 2007, Vol. 112, pp. 95-105.

62. *Measurement of the flux and energy spectrum of cosmic-ray induced neutrons on the ground.* **Gordon, M. S., et al.** 6, s.l. : IEEE Trnsactions on Nuclear Science, Dec. 2004, Vol. 51, pp. 3427-3434.

63. **JAEA.** JENDL - 4.0. [Online] https://wwwndc.jaea.go.jp/j40fig/jpeg/he003_f1.jpg.

64. *Proliferation Risk in Nuclear Fuel Cycles: Workshop Summary.* **Academies, National Research Council of the National.** 2011.

65. *Proliferation Resistance Analysis and Evaluation Tool for Observed Risk (PRAETOR) Methodology.* **Chirayath, S. S., et al.** 2, s.l. : Journal of Nuclear Materials Management, 2015, Vol. 43.

66. *The application of a figure of merit for nuclear explosive utiliy as a metric for material attractiveness in a nuclear material theft scenario.* **King, W. E., et al.** 11, s.l. : Nuclear Engineering and Design, 2011, Vol. 240, pp. 3699-3707.